General Disclaimer

One or more of the Following Statements may affect this Document

- This document has been reproduced from the best copy furnished by the organizational source. It is being released in the interest of making available as much information as possible.

- This document may contain data, which exceeds the sheet parameters. It was furnished in this condition by the organizational source and is the best copy available.

- This document may contain tone-on-tone or color graphs, charts and/or pictures, which have been reproduced in black and white.

- This document is paginated as submitted by the original source.

- Portions of this document are not fully legible due to the historical nature of some of the material. However, it is the best reproduction available from the original submission.

Produced by the NASA Center for Aerospace Information (CASI)

NASA CR-120215

cy 1

NASA CR 120215

ELECTRICAL

(NASA-CR-120215) COMPARISON OF THRUSTER CONFIGURATIONS IN ATTITUDE CONTROL SYSTEMS M.S. Thesis. Progress Report (Auburn Univ.) 141 p HC $5.75 CSCL 22B

N76-10213

Unclas

G3/18 42590

PROPERTY OF
MARSHALL LIBRARY
A&TS-MS-IL

ENGINEERING EXPERIMENT STATION

AUBURN UNIVERSITY

AUBURN, ALABAMA

COMPARISON OF THRUSTER CONFIGURATIONS IN ATTITUDE CONTROL SYSTEMS

Prepared By

GUIDANCE AND CONTROL STUDY GROUP

JOSEPH S. BOLAND, III, PROJECT LEADER

FOURTH TECHNICAL REPORT

SEPTEMBER 14, 1973

CONTRACT NAS8-26580
GEORGE C. MARSHALL SPACE FLIGHT CENTER
NATIONAL AERONAUTICS AND SPACE ADMINISTRATION
HUNTSVILLE, ALABAMA

APPROVED BY:

J. David Irwin
Associate Professor and Head
Electrical Engineering

SUBMITTED BY:

Joseph S. Boland, III
Associate Professor
Electrical Engineering

FOREWARD

The Auburn University Engineering Experiment Station submitted a proposal which resulted in Contract NAS8-26580 being awarded on November 15, 1970. The contract was awarded to the Engineering Experiment Station by the George C. Marshall Space Flight Center, National Aeronautics and Space Administration, Huntsville, Alabama, and was active until September 15, 1973.

This report is a technical summary of the progress made by the Electrical Engineering Department, Auburn, Alabama in the performance of this contract.

ACKNOWLEDGEMENT

A thesis to be submitted by Don M. Drinkard, Jr. to the Graduate Faculty of Auburn University in partial fulfillment of the requirements for the degree of Master of Science is based on the work reported herein.

The research for this thesis was performed under Contract NAS8-26580 awarded to the Auburn Engineering Experiment Station, Auburn, Alabama, by the George C. Marshall Space Flight Center of the National Aeronautics and Space Administration. The Project Leader for this work was Associate Professor Joseph S. Boland, III, of the Electrical Engineering Department, Auburn University.

PERSONNEL

The following staff members of Auburn University are active participants in the work of this contract:

J. S. Boland, III - Associate Professor of Electrical Engineering

D. M. Drinkard, Jr. - Graduate Research Assistant

L. R. White - Graduate Research Assistant

K. R. Chakravarthi - Graduate Research Assistant

SUMMARY

Several aspects concerning reaction control jet systems as used to govern the attitude of a spacecraft are considered. A thruster configuration currently in use is compared to several new configurations developed in this study. The method of determining the error signals which control the firing of the thrusters is also investigated. The current error determination procedure is explained and a new method is presented. Both of these procedures are applied to each of the thruster configurations which are developed and comparisons of the two methods are made.

TABLE OF CONTENTS

LIST OF TABLES . . . . . .

LIST OF FIGURES . . . . . .

I. INTRODUCTION 1

II. DEVELOPMENT OF THE BASIC SIMULATION MODEL. 4

Physical Characteristics of the Vehicle
Attitude Control Loop
Vehicle Attitude Control Law
Rigid Body Dynamics
Transformation Matrix
Inertial Error Measurement System

III. COMPARISONS OF NEW CONFIGURATIONS. 19

Comparisons Via Simulation
Attitude Control Efficiency
The Standard 6 Engine Model
Descriptions of the New Configurations
Simulation Results

IV. ENGINE TORQUE AXES ERROR RESOLUTION. 57

Description of an Engine Torque Axis
Engine Torque Axes For Several Types of Thruster Placements
Error Resolution Into the Engine Torque Axes
Angular Descriptions of the Positions of the Engine Torque Axes
Results of the Simulations With Engine Torque Axes Error Resolution

REFERENCES. 124

APPENDIX A. 125

LIST OF TABLES

III-1. Torque Diagram for the Standard 6 Engine Model 22

III-2. Possible Torque Polarity Combinations. 26

III-3. Torque Diagram for the 4 Engine Model. 28

III-4. Torque Diagram for 8 Engine Model #1 32

III-5. Torque Diagram for 8 Engine Model #2 33

III-6. Torque Diagram for 12 Engine Model #1. 36

III-7. Torque Diagram for 12 Engine Model #2. 37

III-8. Torque Diagram for the 16 Engine Model 38

III-9. Torque Diagram for the 24 Engine Model 40

III-10. Initial Condition Velocity Combinations. 42

III-11. Simulation Results for New Configurations. 43

III-12. Normalized Simulation Results for New Configurations . . . 45

IV-1. Torque Polarities of the 6 Engine Model. 67

IV-2. Torque Polarities of the 24 Engine Model 68

IV-3. Simulation Results for New Configurations With Engine Torque Axes Error Resolution 114

IV-4. Normalized Simulation Results for New Configurations With Engine Torque Axes Error Resolution 115

IV-5. Simulation Results for Each Model Without Transformation Divisions. 120

IV-6. Normalized Simulation Results for Each Model Without Transformation Divisions 121

LIST OF FIGURES

I-1. Vehicle and Inertial Coordinate Systems 3

II-1. Physical Characteristics of the Vehicle 5

II-2. Generalized Block Diagram of the Simulation Attitude Control Loop. 7

II-3. Combination of Vehicle Axes Error Signals for Example Thruster. 8

II-4. Relay Characteristic for Normalized Input 11

III-1. Top View of the Standard 6 Engine Model 22

III-2. Vehicle Attitude Control Law for the Standard 6 Engine Model 23

III-3. Top View of the 4 Engine Model. 28

III-4. Force Resolution for Thruster #3 of the 4 Engine Model 29

III-5. Vehicle Attitude Control Law for the 4 Engine Model 31

III-6. Top View of 8 Engine Model #1 32

III-7. Top View of 8 Engine Model #2 33

III-8. Effect of Skew on the Force Produced By Thruster #5 of 8 Engine Model #2 35

III-9. Top View of 12 Engine Model #1. 36

III-10. Top View of 12 Engine Model #2. 37

III-11. Top View of the 16 Engine Model 38

III-12. Top View of the 24 Engine Model 39

III-13. $ENAVG_N$ vs. Engine $On\text{-}time_N$, the Normalized Results for Each Model. 40

IV-1. General Illustration of an Engine Torque Axis. 59

IV-2. The First Engine Placement and its Corresponding Engine Torque Axis. 61

IV-3. The Second Engine Placement and its Corresponding Engine Torque Axis. 62

IV-4. Angular Relationships of Engine Placements One, Two, and Three. 64

IV-5. The Third Engine Placement and its Corresponding Engine Torque Axis. 66

IV-6. Example Model. 71

IV-7. Parallelogram Law for Vector Addition. 72

IV-8. Resolution of Vehicle Errors Into Engine Torque Axes 74

IV-9. Generalized Block Diagram of the Simulation Attitude Control Loop With the Engine Torque Axes Transformations . . 76

IV-10. Transformation Blocks Included in the Attitude Control Law of the 4 Engine Model. 77

IV-11. The Resolution Plane Perpendicular to the z Axis 80

IV-12. Thruster Placements and Engine Torque Axes for the 6 Engine Model 83

IV-13. Detail of Engine Torque Axis for the 6 Engine Model. 84

IV-14. Engine Torque Axes for the 6 Engine Model. 86

IV-15. Oblique View of the Engine Torque Axes for the 4 Engine Model. 90

IV-16. Effective Moment Arm About the x-Axis of the 4 Engine Model. 91

IV-17. Relationship of the Engine Torque Axes for the 4 Engine Model With the y and z Vehicle Axes. 93

IV-18. Relationship of the Engine Torque Axes for the 4 Engine Model With the y-z Plane 93

IV-19. Engine Torque Axes for the 4 Engine Model. 95

IV-20. Detail View of an Engine Torque Axis. 96

IV-21. Triangle OAD. 97

IV-22. Triangle OCD. 97

IV-23. Triangle OCA. 99

IV-24. Engine Torque Axes for 8 Engine Model #1. 103

IV-25. Engine Torque Axes for Thrusters 4-8 of 8 Engine Model #2. 104

IV-26. Engine Torque Axes for 8 Engine Model #2. 105

IV-27. Engine Torque Axes for Thrusters 7-12 of 12 Engine Model #1. 107

IV-28. Engine Torque Axes for Thrusters 1-6 of 12 Engine Model #1. 107

IV-29. Engine Torque Axes for 12 Engine Model #2 Which Lie in the x-z Plane. 110

IV-30. Engine Torque Axes for 12 Engine Model #2 Which Lie in the y-z Plane. 110

IV-31. Engine Torque Axes 10, 11, 13, and 14 of the 16 Engine Model. 111

IV-32. $ENAVG_N$ vs. Engine $On\text{-}time_N$, the Normalized Results for Each Model With Engine Torque Axes Error Resolution 116

IV-33. $ENAVG_N$ vs. Engine $On\text{-}time_N$, the Normalized Results for Each Model With No Transformation Divisions 122

A- 1. Configuration Used In Determining Gravity Gradient Torques . . . . . .

I. INTRODUCTION

The attitude control system of a space vehicle is concerned with maintaining the vehicle position within certain desired limits about a reference described in a fixed vehicle coordinate system. Reaction control jet systems and control moment gyro systems are two means which have been used in proper combinations for attitude control purposes. This study is concerned with aspects of reaction control jet systems only and does not include any investigation of the factors involved with control moment gyros or combinations of the two systems.

The reaction control jet technique of achieving attitude control involves the use of a set of thrusters strategically placed on the surface of the vehicle and the firing of those thrusters at appropriate times so as to keep the spacecraft within some desired boundaries about a reference attitude. This study is concerned with the placement of the thrusters and with deciding when they are to be fired. The objectives are to position the thrusters and make the firing decision so as to keep the vehicle as close as possible to the reference attitude while expending a minimum amount of fuel.

Simulation is the device used by this study to investigate the features of the reaction control jet system used as the attitude controller. One thruster configuration currently in use in the space program is examined and several new configurations are developed and

compared to the existing system using simulations. One current method of deciding when the individual thrusters are fired is studied and a new procedure is developed for making the firing judgment. The current firing decision method is compared with the new method for each of the configurations which are developed.

Two different reference frames, the vehicle and inertial coordinate systems, are used extensively throughout this study. The characteristics of these two systems which are pertinent to this investigation should be explained before proceeding further. The vehicle coordinate system consists of an orthogonal set of axes with their origin fixed at the center of gravity of the vehicle. For this study it has been decided that the x axis will be the roll axis, the y axis will be the pitch axis and the z axis will be the yaw axis. These axes are fixed with respect to the spacecraft and therefore translate with it everywhere it travels.

Guidance and navigation through outer space are dependent on relations requiring parameters measured with respect to a coordinate frame that is fixed in space. The orientation of the axes of the inertial coordinate system is fixed in space but the origin is not required to be stationary. The origin may be translated freely and is commonly placed at the center of gravity of the spacecraft. So the origin of the inertial coordinate system translates with the vehicle just as the vehicle coordinate system does. Both of these coordinate frames are shown in Figure I-1 [1] with the inertial frame at its original position and translated to certain other important positions.

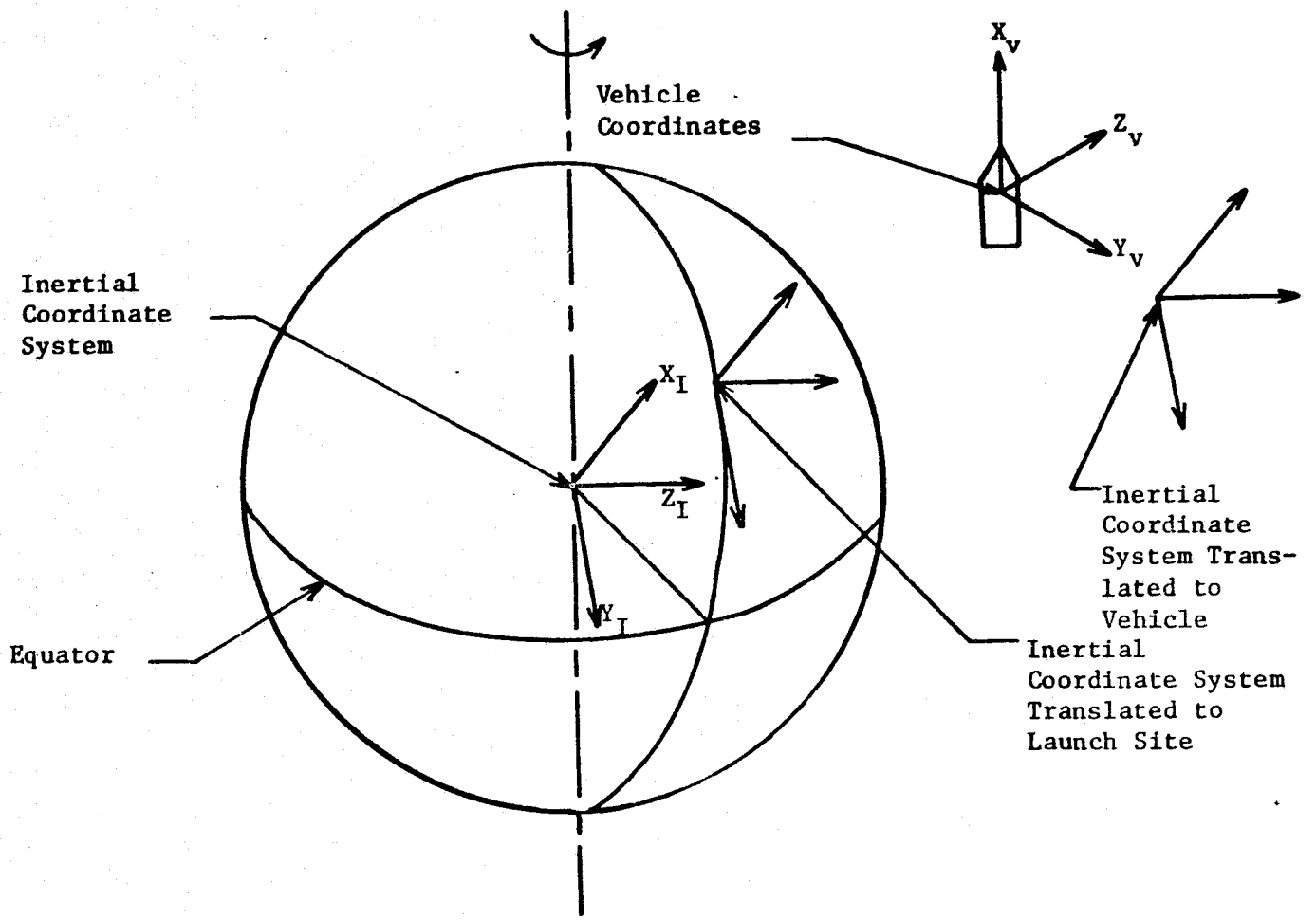

Figure I-1. Vehicle and Inertial Coordinate Systems [1].

II. DEVELOPMENT OF THE BASIC SIMULATION MODEL

A. Physical Characteristics of the Vehicle

Since simulation will be the tool used to provide the data to be utilized in comparisons of the various vehicle engine configurations, a realistic simulation model must be developed in order to give these comparisons value and meaning. A logical first step in the development of a simulation model is the determination of a physical concept of the vehicle. A vehicle with physical size characteristics similar to those of "Skylab I" has been selected but it is hoped that the results of the study will be independent of physical size. The vehicle is constrained to be cylindrical in shape with a center of gravity at the geometric center of the cylinder. The vehicle, as seen in Figure II-1, is 100 ft. in length with a diameter of 20 ft. If the vehicle is assumed to be solid and homogeneous, the moments of inertia are specified in Equations (II-1) and (II-2) where M is the mass of the vehicle, r is the radius of the vehicle, and L is the length of the vehicle [2].

$$I_{xx} = \frac{Mr^2}{2} \tag{II-1}$$

$$I_{yy} = I_{zz} = M(3r^2 + L^2)/12 \tag{II-2}$$

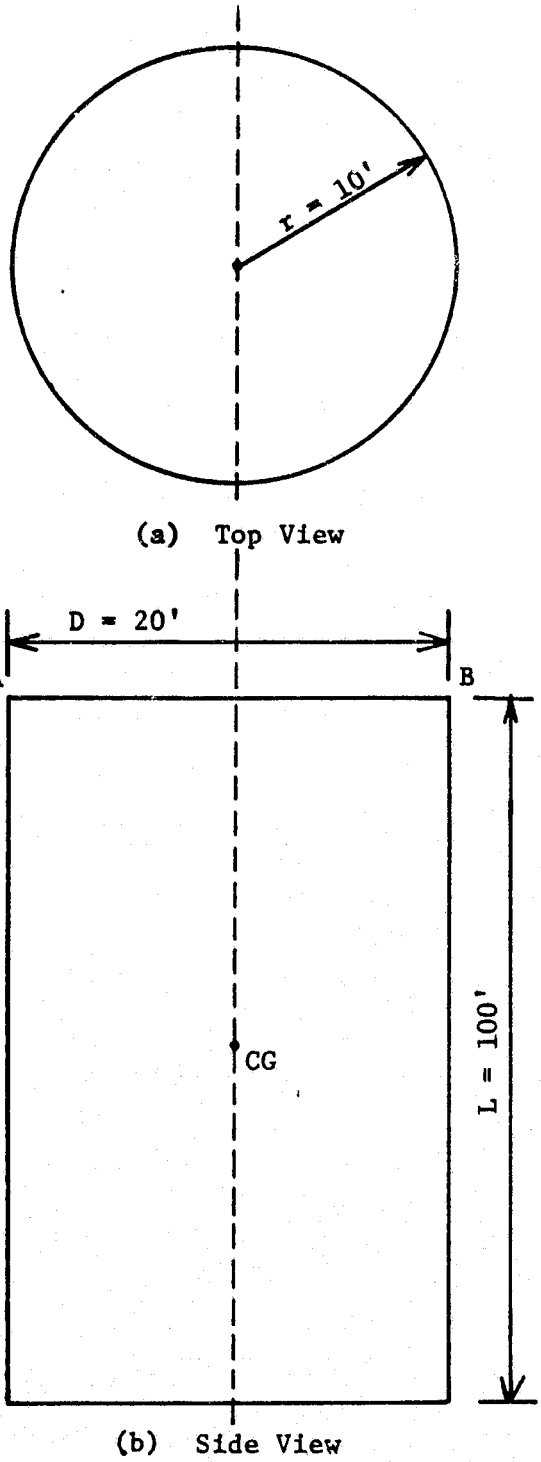

Figure II-1. Physical Characteristics of the Vehicle.

An additional constraint on the vehicle specifies that engines may only be placed on the upper periphery of the cylindrical surface. The upper periphery is intended to mean anywhere on the outer edge of the top of the cylinder as shown in Figure II-1(a.) and indicated in Figure II-1(b.) by letters A-B. This restriction serves to limit the number of different engine placements and consequently, the number of different restoring torques that are available.

B. Attitude Control Loop

The next step in the development of the simulation model is the construction of an attitude control loop. The construction of this loop is taken in several stages with each stage corresponding to one of the blocks in the generalized block diagram shown in Figure II-2. The vehicle control law is concerned with processing attitude error signals to determine the proper torques necessary to maintain a desired attitude. These torques are used in the vehicle dynamics equations which describe the acceleration of the vehicle. The transformation from vehicle coordinates to inertial coordinates is necessary since all inertial navigation must be performed in a space-fixed reference frame. The inertial error measurement system relates the guidance equation requirements to the present vehicle attitude and produces an error signal which is converted to vehicle coordinates for use by the vehicle control law. The sampling operation is necessary since the measured quantities used to form the vehicle axes error signals are only obtained once every second.

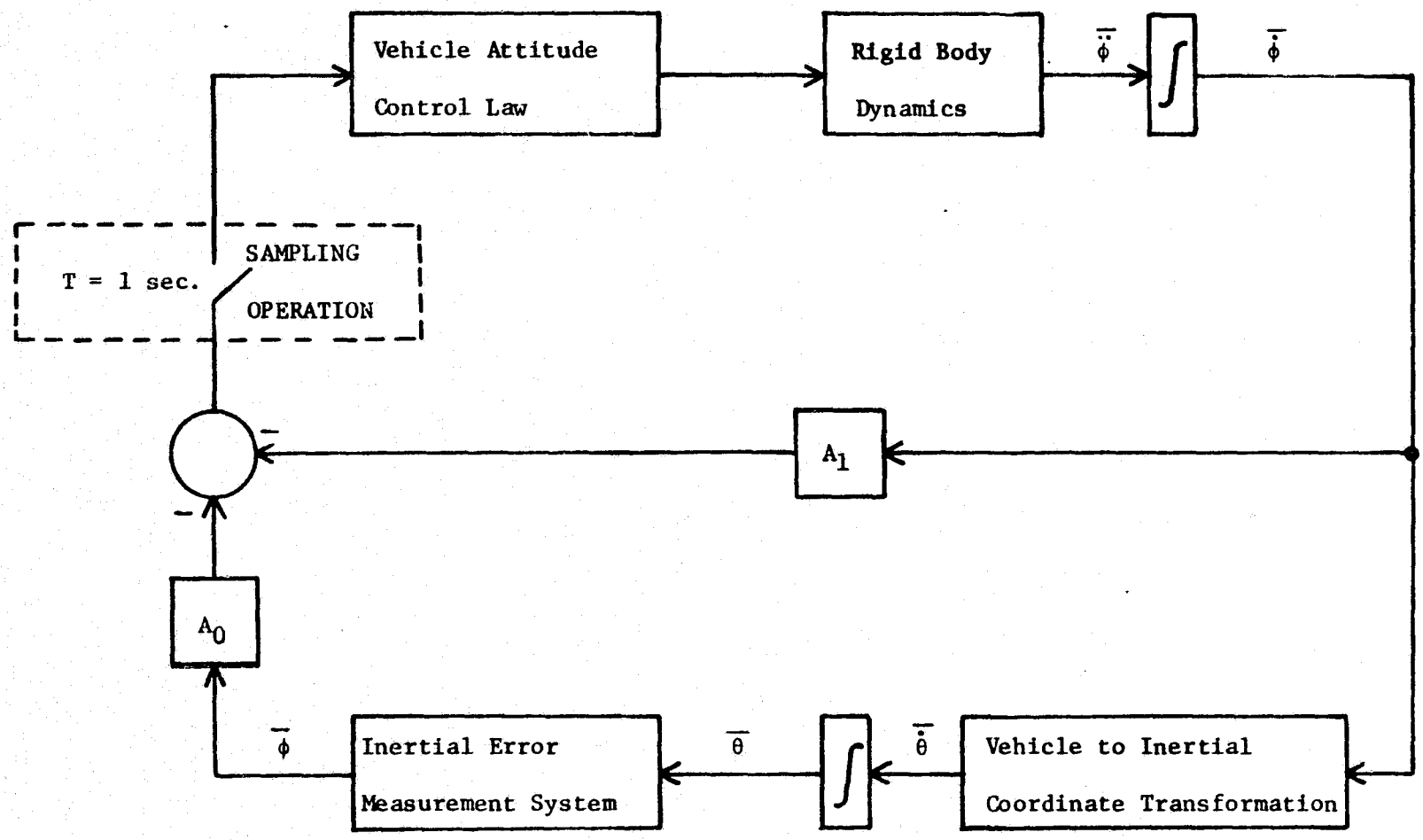

Figure II-2. Generalized Block Diagram of the Simulation Attitude Control Loop.

1. Vehicle Attitude Control Law

The vehicle control law is realized by feeding linear combinations of vehicle axes error signals into relays which control the application of restoring torques. These restoring torques may be produced by appropriate firing of some combination of specially positioned thrusters which expel pressurized cold gas. The linear combinations mentioned are sums and differences of the vehicle axes error signals. The polarities of the torques produced by the thrusters determine these sum and difference combinations.

As an example, suppose a thruster provides positive x axis torque, negative y axis torque, and positive z axis torque. The vehicle axes error signals combined to form the input for the relay which controls the firing of this particular thruster are shown in Figure II-3.

<u>Torque Provided By The Thruster</u>

x	y	z
+	-	+

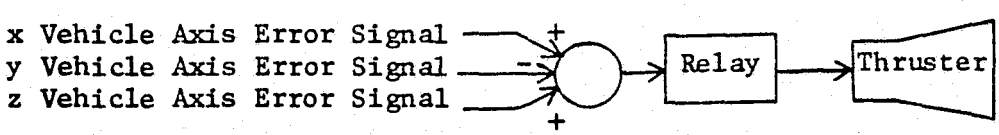

Figure II-3. Combination of Vehicle Axes Error Signals for Example Thruster.

Each of the simulation models to be developed subsequently have vehicle control laws which were constructed in this manner.

As previously mentioned, the restoring torques controlled by the relays utilized in the vehicle control law are provided by cold gas jet thrusters, all producing an equal force. When fired, the thrusters torque the vehicle about its center of gravity. For simplicity it is assumed that each thruster is instantaneously at full force when fired and remains constant at that force level throughout the entire firing interval, i.e., no rise times or delay times are considered. The magnitude of the force provided by each thruster has been set at 200 newtons [3]. These thrusters also have the capability of firing for two different lengths of time. They may fire for a full second or for fifty milliseconds. The latter firing interval is termed a minimum impulse firing.

A certain amount of error is allowed before any corrective action is initiated. This allowable error is sometimes termed deadband or deadzone and is applicable to velocity error as well as position error. The accuracy demanded by the mission dictates the position and rate deadbands allowed. One purpose of velocity or rate deadband is to prevent a velocity of extremely large magnitude from existing without some corrective action being taken. Suppose the vehicle position is within its position deadband limits. If a velocity deadband were not used, a velocity might be present which would force the position from its deadband very quickly. The position and rate deadbands selected for use in this study are commonly used values. The position deadbands are 3° on the roll axis and 2° on the pitch and yaw

axes. The rate deadbands are 0.3°/sec on the roll axis and 0.2°/sec on the pitch and yaw axes.

The position and rate deadbands come into play in the position and rate feedback paths used by the attitude control loop. Negative rate and position feedback paths are employed to insure that the system errors are decreased when the vehicle axes error signals are processed by the vehicle attitude control law. In Figure II-2 the quantities A_0 and A_1 are shown multiplying the position and rate respectively before they are summed negatively to form the vehicle axes error signals. A_0 and A_1, given in Equations (II-3) and (II-4), represent a normalization procedure involving the position and rate deadbands.

$$A_0 = 1/\text{Position Deadband} \tag{II-3}$$

$$A_1 = 1/\text{Rate Deadband} \tag{II-4}$$

This normalization causes the relays to cut on when a value of unity is reached or exceeded. Inputs to a relay valued between 1.0 and 1.6 cause a minimum impulse firing (50 msec.) while all inputs greater than 1.6 cause a firing of a full second as shown by the relay characteristic in Figure II-4.

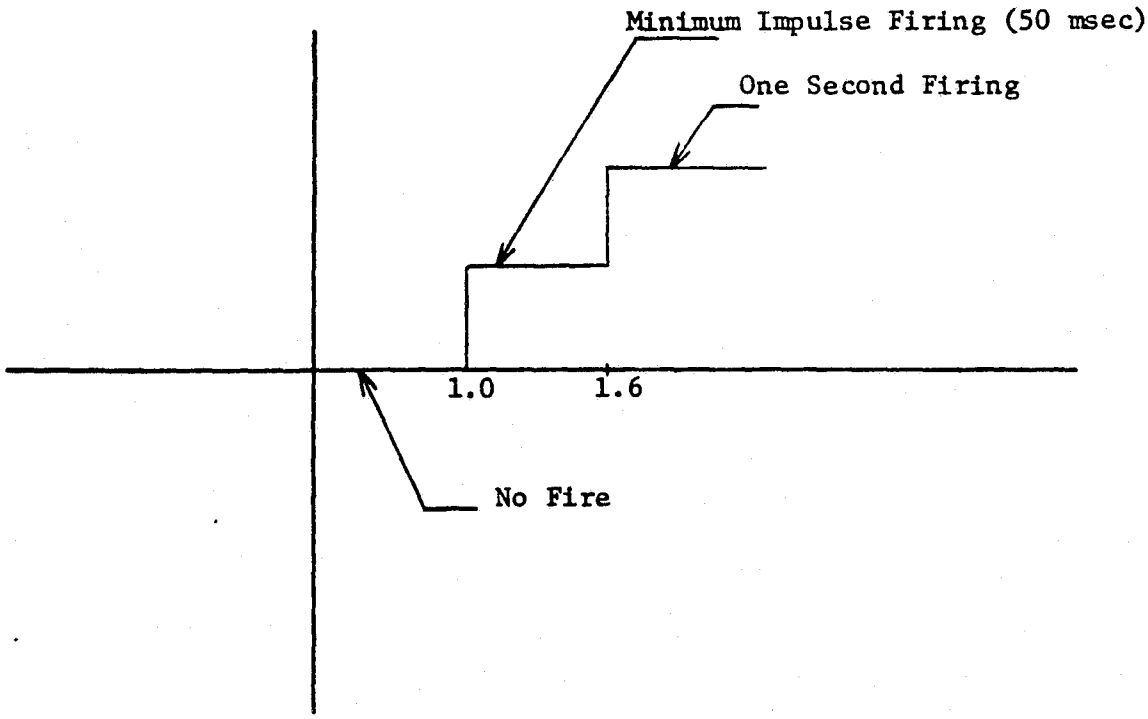

Figure II-4. Relay Characteristic for Normalized Input.

2. Rigid Body Dynamics

The dynamics of a spacecraft may be described by equations for both rigid body motion and bending deflections in the body of the vehicle. The vehicle bending dynamics are considered to be negligible, therefore the dynamics of the spacecraft in this study are described totally by rigid body equations of motion. A general set of rigid body dynamics equations are given in Equations (II-5), (II-6) and (II-7), where I_{ii} represents the principle moment of inertia of the ith axis, I_{ij} represents the cross product of inertia between axes i and j, and $\ddot{\phi}_i$, $\dot{\phi}_i$, and ϕ_i represent the acceleration, velocity and

position, respectively, in the ith axis of the vehicle coordinate system [3].

$$I_{xx}\ddot{\phi}_x = T_{xD} + T_{xR} - \dot{\phi}_y\dot{\phi}_z(I_{zz} - I_{yy}) - (I_{xz}\ddot{\phi}_z + I_{xy}\ddot{\phi}_y) + I_{yz}\dot{\phi}_z^{\,2} - \dot{\phi}_y^{\,2}I_{zy} - \dot{\phi}_y\dot{\phi}_x I_{zx} + \dot{\phi}_z\dot{\phi}_x I_{yx} \qquad \text{(II-5)}$$

$$I_{yy}\ddot{\phi}_y = T_{yD} + T_{yR} - \dot{\phi}_x\dot{\phi}_z(I_{xx} - I_{zz}) - (I_{yx}\ddot{\phi}_x + I_{yz}\ddot{\phi}_z) + I_{zx}\dot{\phi}_x^{\,2} - I_{xz}\dot{\phi}_z^{\,2} - \dot{\phi}_z\dot{\phi}_y I_{xy} + \dot{\phi}_x\dot{\phi}_y I_{zy} \qquad \text{(II-6)}$$

$$I_{zz}\ddot{\phi}_z = T_{zD} + T_{zR} - \dot{\phi}_x\dot{\phi}_y(I_{yy} - I_{xx}) - (I_{zx}\ddot{\phi}_x + I_{zy}\ddot{\phi}_y) + I_{xy}\dot{\phi}_y^{\,2} - I_{yx}\dot{\phi}_x^{\,2} - \dot{\phi}_x\dot{\phi}_z I_{yz} + \dot{\phi}_y\dot{\phi}_z I_{xz} \qquad \text{(II-7)}$$

If it is assumed that the vehicle coordinate system axes are taken along the principle axes of inertia all of the cross products of inertia are eliminated from Equations (II-5), (II-6) and (II-7) resulting in Equations (II-8), (II-9) and (II-10) [4].

$$I_{xx}\ddot{\phi}_x = T_{xD} + T_{xR} - \dot{\phi}_y\dot{\phi}_z(I_{zz} - I_{yy}) \qquad \text{(II-8)}$$

$$I_{yy}\ddot{\phi}_y = T_{yD} + T_{xR} - \dot{\phi}_x\dot{\phi}_z(I_{xx} - I_{zz}) \qquad \text{(II-9)}$$

$$I_{zz}\ddot{\phi}_z = T_{zD} + T_{zR} - \dot{\phi}_x\dot{\phi}_y(I_{yy} - I_{xx}) \qquad \text{(II-10)}$$

These simplified equations are used to describe the acceleration of the vehicle in the digital computer simulation.

The terms T_{iD} and T_{iR}, i = x,y,or z, represent the disturbance and restoring torques on the vehicle. Restoring torques are provided

by the cold gas thrusters described earlier while disturbance torques may come from several sources. These disturbance torques might be created by motions of men onboard the vehicle, by the elimination of wastes onboard the vehicle (venting), by aerodynamic forces on the exterior of the vehicle, or by forces from the Earth's gravitational field. The most prevalent of these disturbances is the cyclic torque caused by the Earth's gravity and is called gravity gradient. Gravity gradient torques are the only disturbances considered in this study and relationships describing these torques are derived in Appendix A and are given by Equations (II-11), (II-12), and (II-13) where GM is the universal gravitational constant multiplied by the mass of the Earth, R is the magnitude of the radius vector from the center of mass of the vehicle to the center of mass of the Earth, R_x, R_y, and R_z are the components of that radius vector along the vehicle coordinate axes, and I_{xx}, I_{yy}, and I_{zz} are the principle moments of inertia.

$$T_{ggx} = -\frac{3GM}{R^5} R_Y R_Z (I_{YY} - I_{ZZ}) \qquad \text{(II-11)}$$

$$T_{ggy} = -\frac{3GM}{R^5} R_X R_Z (I_{ZZ} - I_{XX}) \qquad \text{(II-12)}$$

$$T_{ggz} = -\frac{3GM}{R^5} R_X R_Y (I_{XX} - I_{YY}) \qquad \text{(II-13)}$$

3. Transformation Matrix

The function of the guidance and navigation system of a spacecraft is to generate a set of command signals which will steer the vehicle

toward some desired target. The information needed by the guidance and navigation system must be known relative to a space-fixed coordinate system. For this study that space-fixed reference frame has been termed the inertial coordinate system. The necessary inputs to an inertial navigation device are initial angular position and velocity as well as angular velocity and acceleration during flight, which are measured onboard the vehicle. Two common devices for acquiring these needed quantities are the stabilized platform and the analytic platform. The stabilized platform uses a gimballing system, torquers, servoloops and gyroscopes to keep the vehicle coordinate axes aligned with the inertial coordinate axes [1,5,6]. The analytic platform or "strapped-down system" uses sensors mounted directly to the vehicle and produces vehicle axis acceleration [1,5,6]. The dynamics of the digital computer program used to simulate the attitude control loop closely resembles the "strapped-down system" and it will be assumed that a "strapped-down system" is in use by the controller in this study.

Since the "strapped-down system" provides vehicle coordinate system angular rates and inertial coordinate system measurements are required for navigation and guidance, a transformation matrix is needed such as the one shown in Equation (II-14) [6].

$$\begin{bmatrix} \dot{\theta}_x \\ \dot{\theta}_y \\ \dot{\theta}_z \end{bmatrix} = \begin{bmatrix} A_{11} & A_{12} & A_{13} \\ A_{21} & A_{22} & A_{23} \\ A_{31} & A_{32} & A_{33} \end{bmatrix} \begin{bmatrix} \dot{\phi}_x \\ \dot{\phi}_y \\ \dot{\phi}_z \end{bmatrix} \qquad \text{(II-14)}$$

This transformation matrix is rotational in nature and therefore no translational transformation relating the origins of the two coordinate systems is necessary [6]. This transformation matrix is calculated by a digital computer throughout the flight when a "strapped-down system" is used. Several ways of calculating the matrix are presented in [6].

The results of each of these calculations are given in Equation (II-15).

$$\begin{bmatrix} \dot{\theta}_x \\ \dot{\theta}_y \\ \dot{\theta}_z \end{bmatrix} = \begin{bmatrix} 1 & -\tan\theta_z\cos\theta_x & \tan\theta_z\sin\theta_x \\ 0 & \cos\theta_x/\cos\theta_z & -\sin\theta_x/\cos\theta_z \\ 0 & \sin\theta_x & \cos\theta_x \end{bmatrix} \begin{bmatrix} \dot{\phi}_x \\ \dot{\phi}_y \\ \dot{\phi}_z \end{bmatrix} \qquad \text{(II-15)}$$

4. Inertial Error Measurement System

The vehicle navigation and guidance scheme produces what might be called a command matrix. This matrix represents the attitude which is desired and serves as a reference when a change in attitude is necessary. The command matrix is of the form of the transformation matrix between vehicle and inertial coordinate systems but employs desired or commanded inertial angles θ_{cx}, θ_{cy}, and θ_{cz} as shown in Equation (II-16). The commanded inertial angles describe the attitude that is desired by the navigation and guidance scheme.

The calculated inertial position vector elements are inserted into a test matrix called $[\theta_{VI}]$ identical to $[\theta_{CI}]$ as shown in Equation (II-17). $[\theta_{CI}]$ and $[\theta_{VI}]$ are compared to determine if the current attitude is in alignment with the attitude desired by the guidance and navigation

$$[\theta_{cI}] = \begin{bmatrix} \cos\theta_{cy}\cos\theta_{cz} & \sin\theta_{cz} & -\sin\theta_{cy}\cos\theta_{cz} \\ -\sin\theta_{cz}\cos\theta_{cy}\cos\theta_{cx} + \sin\theta_{cx}\sin\theta_{cy} & \cos\theta_{cz}\cos\theta_{cx} & \cos\theta_{cx}\sin\theta_{cz}\sin\theta_{cy} + \sin\theta_{cx}\cos\theta_{cy} \\ \sin\theta_{cx}\sin\theta_{cz}\cos\theta_{cy} + \cos\theta_{cx}\sin\theta_{cy} & -\sin\theta_{cx}\cos\theta_{cz} & -\sin\theta_{cx}\sin\theta_{cy}\sin\theta_{cz} + \cos\theta_{cx}\cos\theta_{cy} \end{bmatrix} \tag{II-16}$$

$$[\theta_{VI}] = \begin{bmatrix} \cos\theta_{y}\cos\theta_{z} & \sin\theta_{z} & -\sin\theta_{y}\cos\theta_{z} \\ -\sin\theta_{z}\cos\theta_{y}\cos\theta_{x} + \sin\theta_{x}\sin\theta_{y} & \cos\theta_{z}\cos\theta_{x} & \cos\theta_{x}\sin\theta_{z}\sin\theta_{y} + \sin\theta_{x}\cos\theta_{y} \\ \sin\theta_{x}\sin\theta_{z}\cos\theta_{y} + \cos\theta_{x}\sin\theta_{y} & -\sin\theta_{x}\cos\theta_{z} & -\sin\theta_{x}\sin\theta_{y}\sin\theta_{z} + \cos\theta_{x}\cos\theta_{y} \end{bmatrix} \tag{II-17}$$

scheme. The comparison is achieved by multiplying the inverse of $[\theta_{CI}]$ by $[\theta_{VI}]$ resulting in an error matrix, $[\theta_{VC}]$.

$$[\theta_{VC}] = [\theta_{CI}]^{-1}[\theta_{VI}] \tag{II-18}$$

The amount of position error is determined using the error matrix, $[\theta_{VC}]$. The off-diagonal terms of $[\theta_{VC}]$ are used to generate the current position error in vehicle coordinates as indicated in Equations (II-19), (II-20), and (II-21).

$$\phi_x = \tfrac{1}{2}(\theta_{VC_{23}} - \theta_{VC_{32}}) \tag{II-19}$$

$$\phi_y = \tfrac{1}{2}(\theta_{VC_{31}} - \theta_{VC_{13}}) \tag{II-20}$$

$$\phi_z = \tfrac{1}{2}(\theta_{VC_{12}} - \theta_{VC_{21}}) \tag{II-21}$$

These position errors are the terms which are multiplied by position feedback gain terms indicated as A_0 in the generalized block diagram shown in Figure II-2.

The current onboard procedure calls for rate and acceleration information to be supplied by the sensors only once every second. Consequently, the vehicle axes error signals are only calculated on those sample instants. This procedure is represented in the digital computer simulation by the block labelled "sampling operation" in Figure II-2.

The vehicle coordinate acceleration, $\overline{\ddot{\phi}}$, and the inertial coordinate velocity, $\overline{\dot{\theta}}$, were investigated and found to be slowly varying quantities. These quantities vary slowly enough that a simple

numerical integration process may be used to integrate them. Therefore the integrations, represented in Figure II-2 by the blocks with integral signs, are performed using the rectangular rule [7]. The integration interval used is 0.1 sec.

This completes the loop of the attitude controller which serves as the basic element of the digital computer simulation. A good indication of the effectiveness of the methods to be tried should be available from the simulation results despite the number of simplifications made. The remainder of the report is concerned with the configuration of the thrusters on the vehicle and with the method of deciding when to fire them. It is important to note here that the attitude control loop, as it has been constructed in this section, represents the current method of making the decision to fire a thruster. By the current method it is meant that the attitude errors are evaluated about the vehicle coordinate axes. Later, evaluation about a different set of axes will be investigated.

III. COMPARISONS OF NEW CONFIGURATIONS

A. Comparisons Via Simulation

No analytical method was deemed suitable for the task of comparing thruster configurations, so simulation was decided on as the comparison method. Several thruster configurations are described in this chapter and their performances are compared by relating the simulation results of each configuration. The attitude control loop explained in Chapter II was programmed for each different vehicle model using FORTRAN V language and processed on the IBM 360 model 50 computer. The attitude control efficiency of each model is measured using the digital computer simulations. A standard model is chosen and used as the basis for all comparisons.

B. Attitude Control Efficiency

The attitude control efficiency referred to above embraces two aspects which measure the effectiveness of the attitude control system: the amount of fuel consumed by the thrusters and the ability of the system to maintain a reference attitude when error is introduced externally. The digital computer simulations measure the amount of fuel consumed by recording the number of firings by each thruster and the length of each firing. Since the thrusters are assumed to create

a constant force, the amount of fuel expended during a one second firing and during a minimum impulse firing remains constant. Therefore, an indication of the amount of fuel consumed during an entire mission would be the total amount of time the thrusters are fired. This time will hereafter be referred to as thruster or engine on-time.

The ability to maintain a reference attitude is somewhat of an arbitrary property and could be measured in several different ways. In this study each simulation is initialized with the actual position of the vehicle in alignment with the reference position provided by the navigation and guidance scheme. For convenience and simplification, the reference position is assumed to be zero. External error is introduced into the system by putting an initial condition velocity on the vehicle. This causes the vehicle position to drift out of its deadband causing the thrusters to fire. In short, the attitude control capability of each configuration is determined by how well it can maintain a reference attitude when a disturbance is introduced in the form of a velocity.

The method of measuring the ability to maintain a reference attitude involves the norm of the vehicle position vector. Since the initial position is assumed in alignment with the reference position and the reference position is assumed to be zero, then the vehicle position vector describes the error present in the system. The norm

of the position error can be represented by Equation (III-1).

$$EN = \sqrt{(\phi_x)^2 + (\phi_y)^2 + (\phi_z)^2} \qquad \text{(III-1)}$$

If this position error norm is averaged over the length of the mission, it gives an indication of the effectiveness of the attitude control system at maintaining the vehicle at the reference attitude. ENAVG, as given by Equation (III-2), is calculated in the simulations every sampling instant, just as the position vector is.

$$ENAVG = \sum_{i=1}^{n} EN/n, \quad n = \text{number of sampling instants} \qquad \text{(III-2)}$$

C. The Standard 6 Engine Model

The thruster configuration to be used as the basis for all comparisons is a symmetrical placement of six engines and will be referred to hereafter as the standard 6 engine model. As shown in Figure III-1, this configuration utilizes two thrusters which provide pitch torques only while each of the remaining four thrusters provides both roll and yaw torques. The polarities of the torques produced by each thruster are enumerated in the torque diagram listed in Table III-1.

The vehicle attitude control law, as explained earlier, is determined by the torque polarities produced by each thruster. Noting the torque diagram in Table III-1, the vehicle attitude control law for the standard 6 engine model is realized using double-sided relays as shown in Figure III-2 where ε_x, ε_y, and ε_z represent the

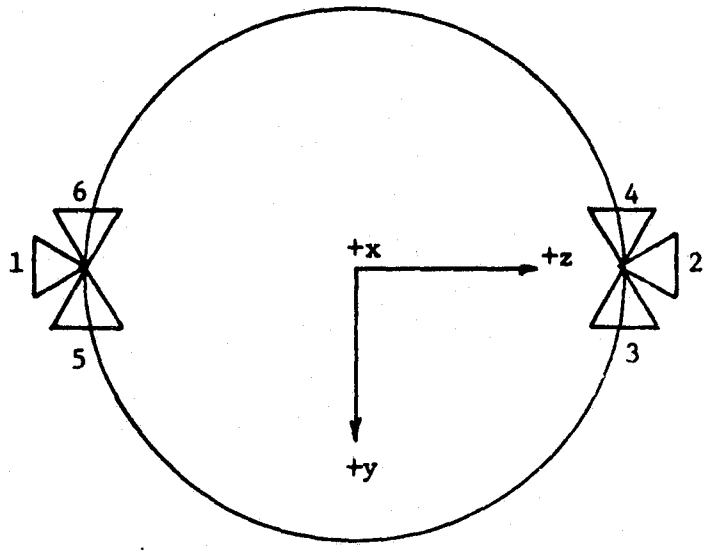

Figure III-1. Top View of the Standard 6 Engine Model.

Thruster	Torque Polarities X	Y	Z
1		-	
2		+	
3	+		-
4	-		+
5	-		-
6	+		+

Table III-1. Torque Diagram for the Standard 6 Engine Model.

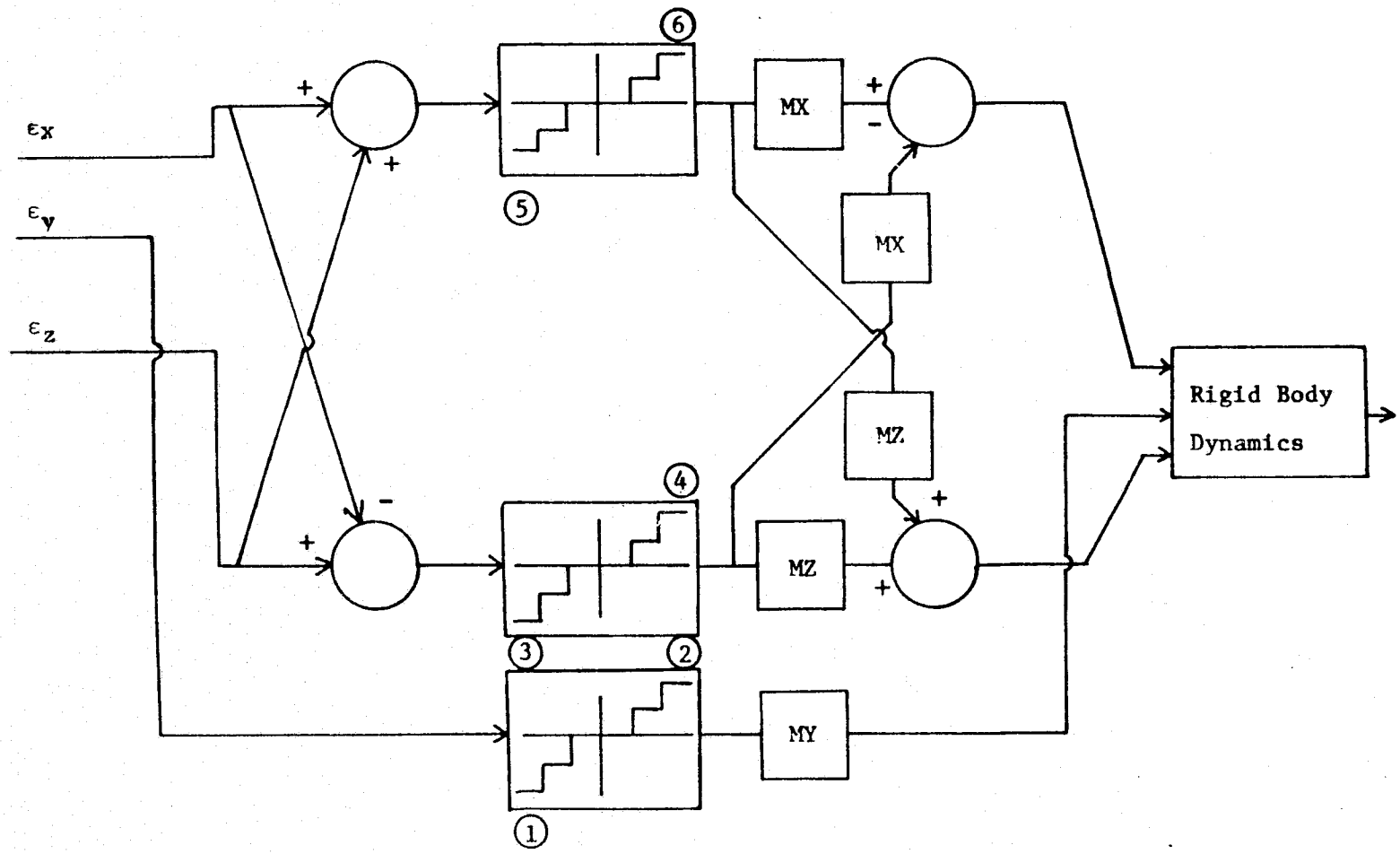

Figure III-2. Vehicle Attitude Control Law for the Standard 6 Engine Model.

vehicle axes error signals and MX, MY, and MZ represent the magnitude of the torques produced by any one thruster in the X, Y, or Z axis, respectively. The circled numbers in Figure III-2 indicate which thruster is firing when the relay is activated on the side with that number. This system, with a few modifications, is similar to one which has been employed in the space program previously. Double-sided relays are not used in subsequent model developments for reasons of simplification and clarification. The number of thrusters used to control the attitude of the vehicle is increased on most of the new models and, consequently, their vehicle attitude control laws become more complex. The implementation of the torque diagrams as vehicle attitude control laws for each of these new models is more easily understood when single-sided relays are used.

D. Descriptions of the New Configurations

The configurations introduced in this section might be thought of as challengers to the standard 6 engine model. The idea in mind as each is developed is to surpass the efficiency of the 6 engine model in terms of fuel consumption and error reducing capability. Two general methods are used in attempting to obtain better performance than that of the 6 engine model: skewing of the thrusters and the use of additional thrusters. When a thruster is skewed with respect to the three vehicle coordinate system axes, torques are produced in all three of those axes when that thruster is fired. This could possibly

increase the error correcting capability of the vehicle, especially with regard to errors occurring in all three axes at once. The use of additional thrusters allows more combinations of torques to be produced by firing individual thrusters. This could possibly eliminate some multiple engine firings and thereby reduce fuel consumption.

The combinations of torques mentioned with regard to the use of additional thrusters bear more explanation. Considering the number of different combinations of torques which may be produced about the three vehicle coordinate system axes, combinational logic reveals that 27 different torque polarities exist as shown in Table III-2. The self-imposed constraint requiring that thrusters only be placed on the upper periphery of the cylinder being used as the vehicle rules out polarity possibilities 22 and 23. These are the positive and negative roll torques and would require thrusters on the side of the vehicle which violates the constraint. Obviously, the zero torque possibility is also ruled out which leaves 24 possible torque polarity combinations.

No particular procedure or method is followed in the development of the new configurations. Instead, modifications and extensions are made on the 6 engine model and on the first new model developed, which employs skewed thrusters. Both orthogonal and skewed thrusters are added to these two basic models in an attempt to achieve better attitude control efficiency.

The first new configuration to be developed employs thruster skewing in an attempt to improve its performance with reference to the standard

	X-AXIS	Y-AXIS	Z-AXIS
1	0	0	0
2	+	+	+
3	+	+	-
4	+	-	-
5	+	-	+
6	-	+	+
7	-	+	-
8	-	-	+
9	-	-	-
10	+	+	
11	+	-	
12	-	+	
13	-	-	

14	+		+
15	+		-
16	-		+
17	-		-
18		+	+
19		+	-
20		-	+
21		-	-
22	+		
23	-		
24		+	
25		-	
26			+
27			-

Table III-2. Possible Torque Polarity Combinations.

6 engine model. The 4 engine model utilizes the fewest number of thrusters which are capable of achieving separate positive and negative motions about each of the three vehicle coordinate axes, i.e., positive and negative motions are available, independently, about the roll, pitch, and yaw axes when four skewed thrusters are used. Combinational logic indicates that there are eight combinations of the three polarity signals present when torques exist about all three coordinate axes. Each of the four thrusters provides torque in all three axes simultaneously and four of the eight possible combinations are available as shown in Table III-3.

Each of the thrusters is skewed 45° with respect to the pitch and yaw axes as indicated in Figure III-3. The skewing changes the torque characteristics somewhat from those of the standard 6 engine model. The moment arms are the same as those of the 6 engine model, but the magnitude of the force which produces torque about each coordinate axis is different. This is illustrated in Figure III-4 which shows the resolution of the force provided by thruster #3. The magnitudes of the torques produced by thruster #3 in the roll, pitch, and yaw axes are given by Equations (III-3), (III-4), and (III-5) where F is the force provided by the thruster, D is the diameter of the vehicle, and L is the length of the vehicle.

$$|T_{3x}| = F(\sin 45°)(D/2) \qquad \text{(III-3)}$$

$$|T_{3y}| = F(\cos 45°)(L/2) \qquad \text{(III-4)}$$

$$|T_{3z}| = F(\sin 45°)(L/2) \qquad \text{(III-5)}$$

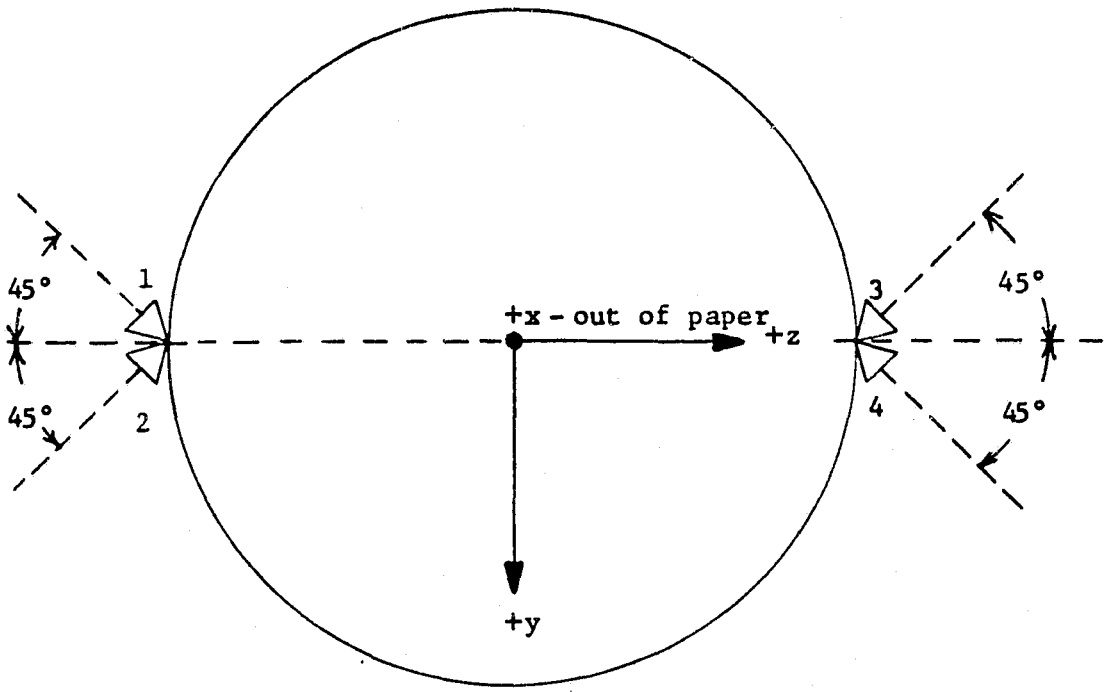

Figure III-3. Top View of the 4 Engine Model.

Thruster	Torque Polarities X	Y	Z
1	+	-	+
2	-	-	-
3	-	+	+
4	+	+	-

Table III-3. Torque Diagram for the 4 Engine Model.

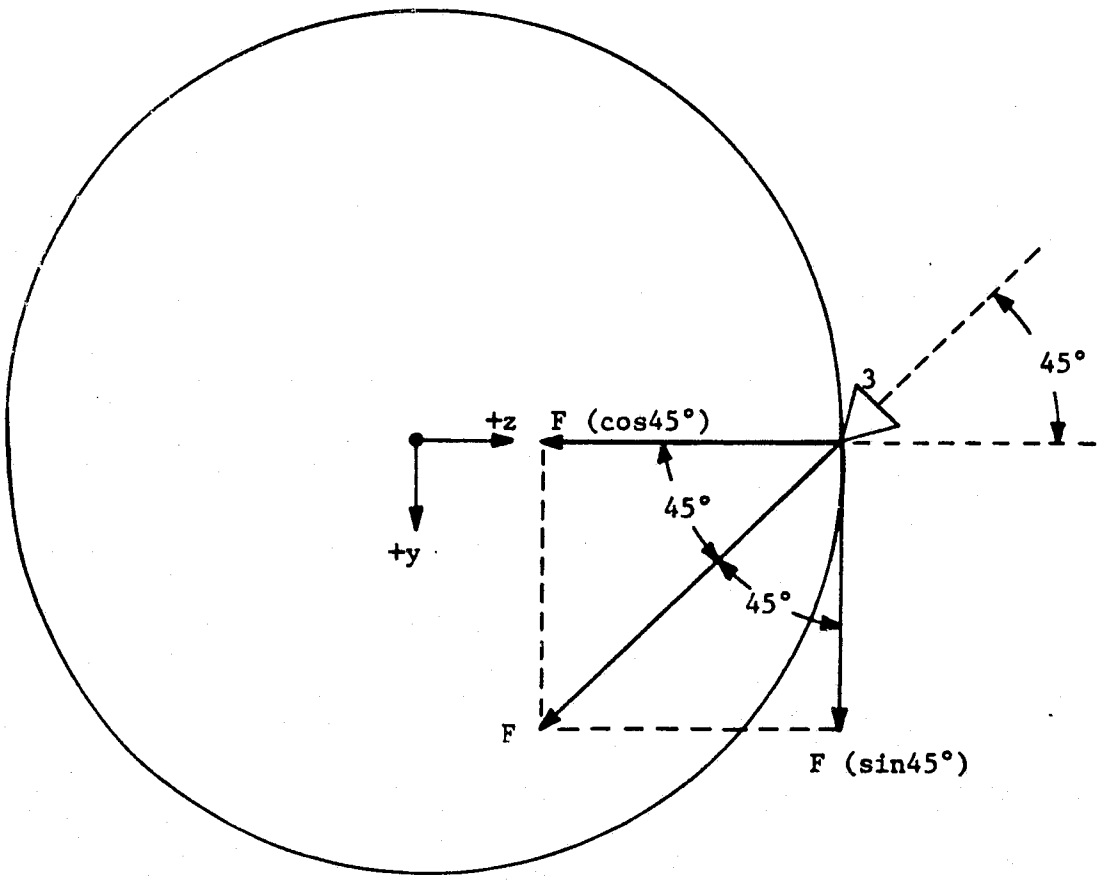

Figure III-4. Force Resolution for Thruster #3 of the 4 Engine Model.

The vehicle attitude control law for the 4 engine model is created by implementing the torque diagram in Table III-3 as shown in Figure III-5. The implementation of the torques for each thruster can be seen in the summing junctions positioned before and after each relay. Each single-sided relay controls the application of the torque provided by the thruster indicated above each relay.

The first 8 engine model, shown in Figure III-6, is merely an extension of the 4 engine model. Each of the eight thrusters is skewed 45° with respect to the vehicle coordinate system axes. All eight of the possible combinations of three torque polarities are implemented by the thrusters on this model as shown in Table III-4. The torque characteristics of this model vary from those of the 6 engine model in the same manner as did those of the 4 engine model.

The second 8 engine model, shown in Figure III-7, employs both skewing and additional orthogonal thrusters in an attempt to better the performance of the 6 engine model. The skewed thrusters used by this model provide torques in the pitch and yaw axes but not in the roll axis. The four unskewed thrusters, engines 1-4, are identical to the four engines employed by the 6 engine model to produce roll and yaw torques. The torques available from 8 engine model #2 are listed in Table III-5. The torque characteristics of this model are very similar to those of the 4 engine model despite the fact that the skewed thrusters of these two models are in different positions. Since the amount of engine skewing is the same, the effect on the forces which produce the torques in the y and z axes is the same.

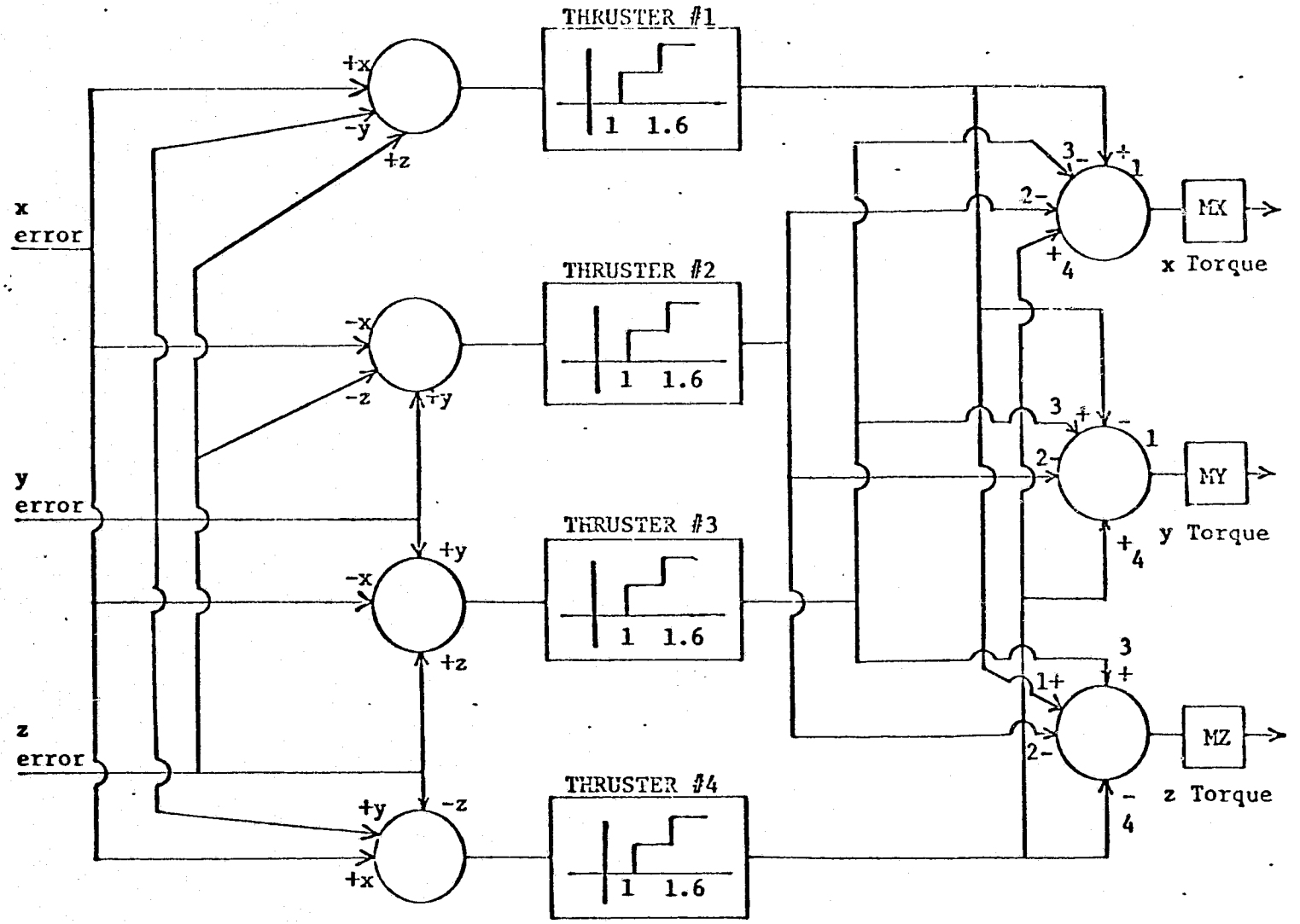

Figure III-5. Vehicle Attitude Control Law for the 4 Engine Model.

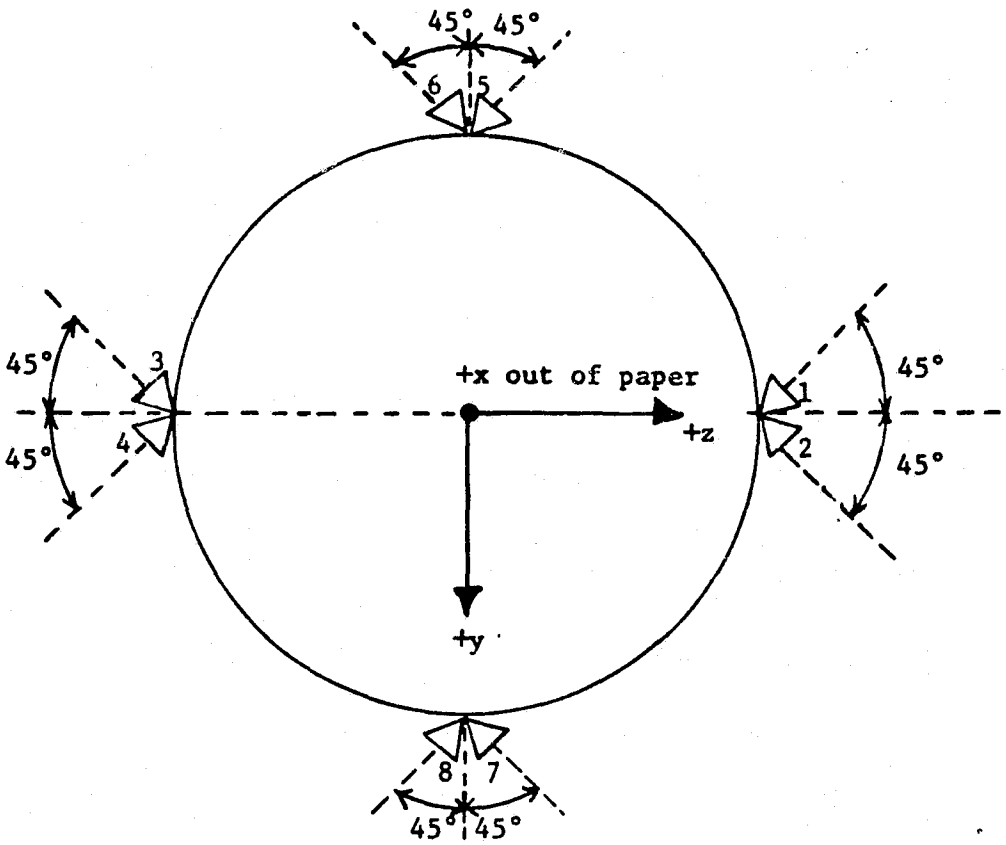

Figure III-6. Top View of 8 Engine Model #1.

Thruster	Torque Polarities X	Y	Z
1	-	+	+
2	+	+	-
3	+	-	+
4	-	-	-
5	+	+	+
6	-	-	+
7	-	+	-
8	+	-	-

Table III-4. Torque Diagram for 8 Engine Model #1.

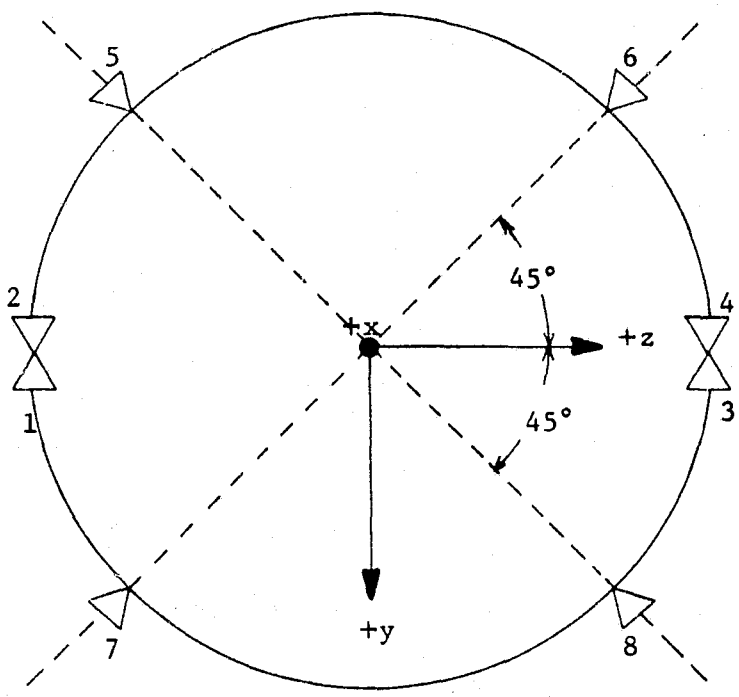

Figure III-7. Top View of 8 Engine Model #2.

Thruster	Torque Polarities X	Y	Z
1	-		-
2	+		+
3	+		-
4	-		+
5		-	+
6		+	+
7		-	-
8		+	-

Table III-5. Torque Diagram for 8 Engine Model #2.

This effect is shown in detail for one of the skewed thrusters in Figure III-8. The magnitudes of the torques produced by thruster #5 are given in Equations (III-6), (III-7), and (III-8) where again F is the force provided by the thruster and L is the length of the vehicle.

$$|T_{5x}| = [F(\cos 45°) - F(\sin 45°)](D/2) = 0 \qquad \text{(III-6)}$$

$$|T_{5y}| = F(\cos 45°)(L/2) \qquad \text{(III-7)}$$

$$|T_{5z}| = F(\sin 45°)(L/2) \qquad \text{(III-8)}$$

The first 12 engine model utilizes six additional thrusters to extend the design of the 6 engine model. Figure III-9 shows the configuration of the thrusters and Table III-6 lists the polarities of the torques produced by each of the thrusters. It might be noted that there are four groups of three orthogonal engines instead of two groups as used on the 6 engine model. This use of additional thrusters makes available a wider variety of torques from individual thrusters.

The next two models continue to extend the ideas tried by the models already developed. Twelve engine model #2, shown in Figure III-10, utilizes both skewing and additional thrusters in attempting to better the performance of the 6 engine model. Thrusters which provide pure pitch and yaw torques were added to 8 engine model #2 to form this configuration. The 16 engine model, shown in Figure III-11, is created by adding skewed thrusters to 12 engine model #1. The additional thrusters provide pitch and yaw torques simultaneously.

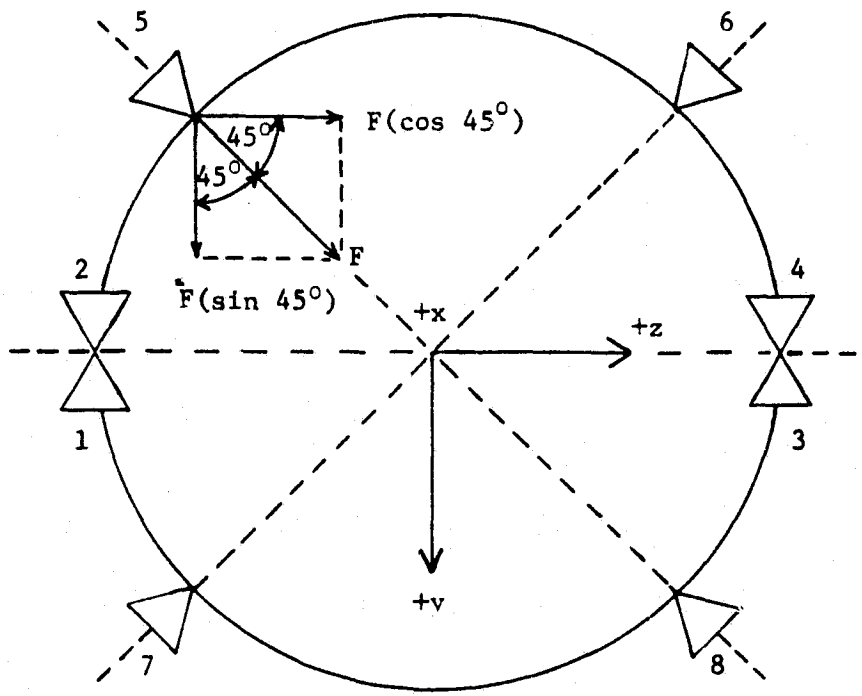

Figure III-8. Effect of Skew on the Force Produced By Thruster #5 of 8 Engine Model #2.

Thruster	Torque Polarities X	Y	Z
1			+
2			-
3	-	-	
4	+	+	
5	+	-	
6	-	+	
7		+	
8		-	
9	+		-
10	-		+
11	-		-
12	+		+

Table III-6. Torque Diagram for 12 Engine Model #1.

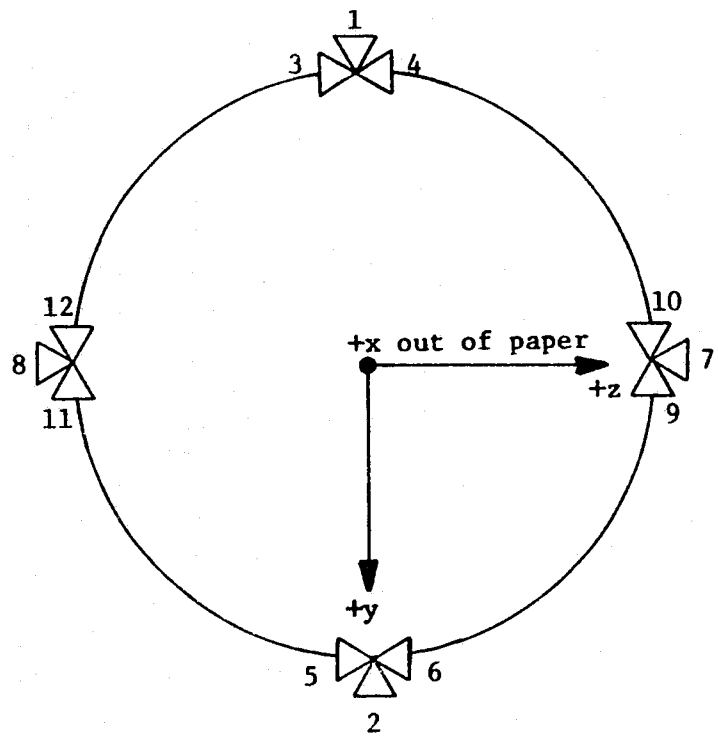

Figure III-9. Top View of 12 Engine Model #1.

Thruster	Torque Polarities X	Y	Z
1	-		-
2	+		+
3	+		-
4	-		+
5		+	
6		-	
7			+
8			-
9		-	+
10		+	+
11		-	-
12		+	-

Table III-7. Torque Diagram for 12 Engine Model #2.

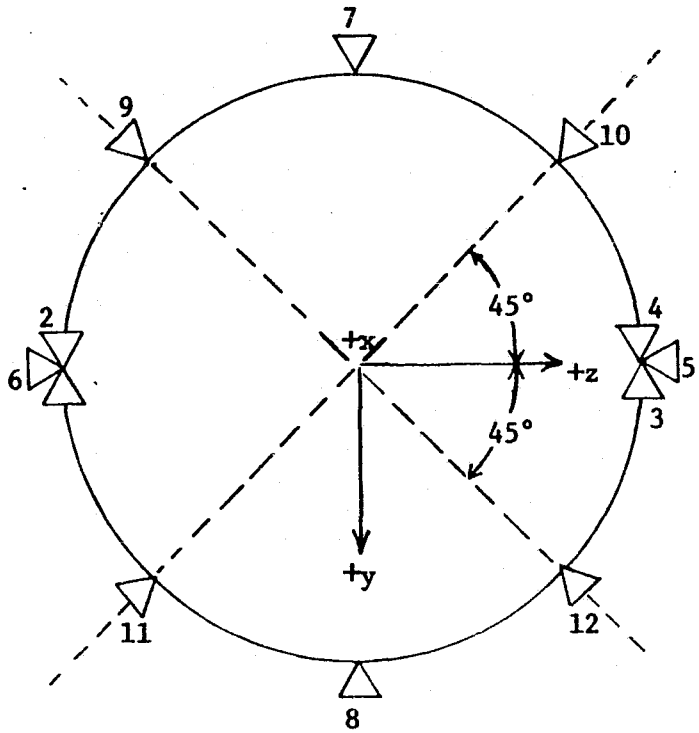

Figure III-10. Top View of 12 Engine Model #2.

Thruster	Torque Polarities X	Y	Z
1	-		-
2	+		+
3	+		-
4	-		+
5		+	
6		-	
7			+
8			-
9		-	+
10		+	+
11		-	-
12		+	-
13	-	-	
14	+	+	
15	+	-	
16	-	+	

Table III-8. Torque Diagram for the 16 Engine Model.

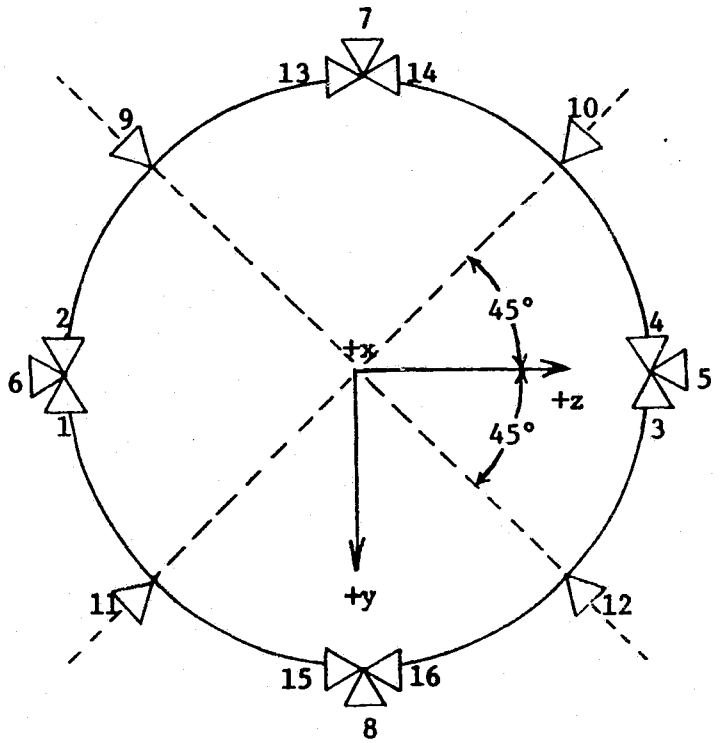

Figure III-11. Top View of the 16 Engine Model.

It was noted earlier that due to the constraints placed on the positioning of thrusters there were 24 different torque polarity combinations which could possibly be produced. The 24 engine model shown in Figure III-12, realizes each of those possible combinations. The torque diagram for the 24 engine model, given in Table III-9, may be compared with Table III-2 to verify this. This model is capable of providing corrective action for any of the twenty-four eligible errors with a single engine. This model represents a maximum effort with regard to variety in torque capabilities by single thrusters.

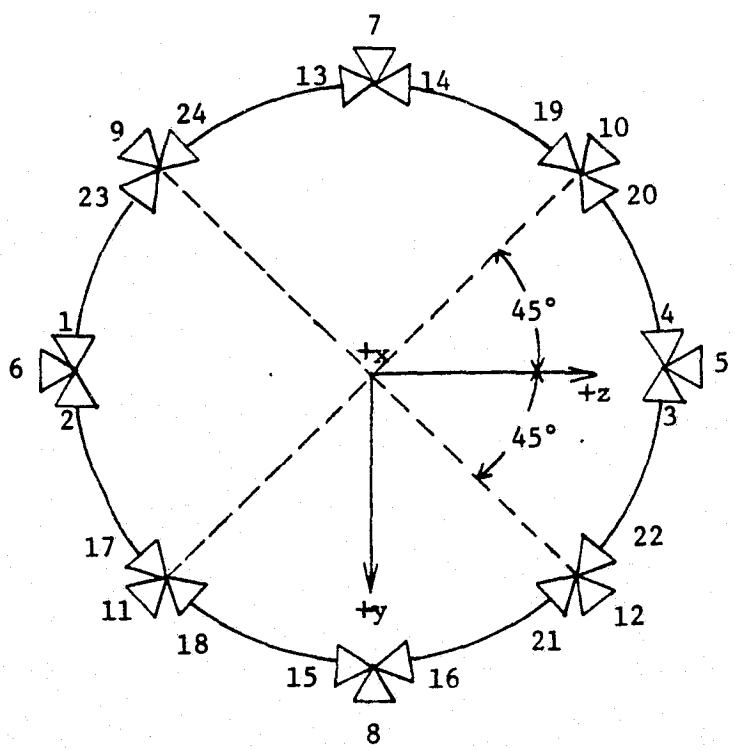

Figure III-12. Top View of the 24 Engine Model.

Thruster	Torque Polarities X	Y	Z		X	Y	Z
1	-		-	13	-	-	
2	+		+	14	+	+	
3	+		-	15	+	-	
4	-		+	16	-	+	
5		+		17	+	-	+
6		-		18	-	+	-
7			+	19	-	-	+
8			-	20	+	+	-
9		-	+	21	+	-	-
10		+	+	22	-	+	+
11		-	-	23	-	-	-
12		+	-	24	+	+	+

Table III-9. Torque Diagram for the 24 Engine Model.

E. Simulation Results

The torque diagrams for each of these configurations were implemented as vehicle attitude control laws and placed in attitude control loop simulations. As mentioned previously, error is introduced in the simulations by placing initial condition velocities in the system which cause the vehicle to drift out of the position and rate deadbands. It seems reasonable to assume that during actual missions errors will be present constantly on all three coordinate axes simultaneously. Therefore, in the simulations initial condition velocities will always be placed on the roll, pitch, and yaw axes simultaneously as each configuration is tested. The magnitude of the initial condition velocities will always be 0.1°/sec. This magnitude allows the vehicle to drift from its deadbands rather than being an impulse to the system and causes application of restoring torques in a relatively small amount of time. This rate input causes the vehicle to drift out of its largest position deadband (3°) in 30 seconds and when the rate deadband is considered, corrective action is actually required sooner. The simulations will be in operation 2000 seconds for each initial condition case. Two thousand seconds is enough time for the response of the attitude control system of each configuration to reach steady state conditions. The speed of response is considered as a by-product in this study since, in most cases, the amount of fuel consumed during steady state is less than that consumed during the transient period just after an error is introduced into the system.

All eight combinations of roll, pitch, and yaw initial condition velocities will be used as test cases. These combinations are listed only as polarities in Table III-10. Each of these combinations might be considered as covering a different section in an error coordinate frame. The vehicle coordinate system may be divided into eight equal parts by the x, y, and z axes, each part corresponding to one of the position errors created by the initial condition velocities.

Case	Initial Condition ϕ_{x0}	ϕ_{y0}	ϕ_{z0}
1	+	+	+
2	+	+	-
3	+	-	-
4	-	-	-
5	-	+	-
6	-	-	+
7	+	-	+
8	-	+	+

Table III-10. Initial Condition Velocity Combinations.

Each of the simulations of the individual configurations were initialized with the eight velocities just described. The attitude control efficiency, as explained earlier, was monitored by measuring the amount of engine on-time and the average of the position error was calculated. The results of these simulation runs are listed in Table III-11.

Initial Conditions	6 Engine Case	4 Engine Case	8 Engine Case #1	8 Engine Case #2	12 Engine Case #1	12 Engine Case #2	16 Engine Case	24 Engine Case
DPX = .1°/Sec DPY=DPZ = .1°/Sec	3.50 .0384	4.65 .0491	3.70 .0274	4.20 .0383	3.45 .0325	4.20 .0386	3.35 .0280	3.35 .0256
DPX=DPY = .1°/Sec DPZ = -.1°/Sec	3.80 .0395	6.40 .0417	3.50 .0265	4.15 .0384	3.55 .0317	4.05 .0381	3.40 .0258	3.25 .0244
DPX = .1°/Sec DPY=DPZ = -.1°/Sec	3.60 .0401	4.45 .0453	3.55 .0270	4.00 .0374	3.60 .0336	4.10 .0372	3.55 .0273	3.20 .0238
DPX = -.1°/Sec DPY=DPZ = -.1°/Sec	3.65 .0379	6.35 .0439	3.60 .0270	4.05 .0382	3.50 .0330	4.05 .0361	3.30 .0271	3.35 .0259
DPX=DPZ = -.1°/Sec DPY = .1°/Sec	3.50 .0384	4.65 .0491	3.70 .0273	4.20 .0383	3.45 .0325	4.20 .0386	3.35 .0280	3.35 .0256
DPX=DPY = -.1°/Sec DPZ = .1°/Sec	3.60 .0401	4.45 .0453	3.55 .0270	4.00 .0374	3.60 .0336	4.10 .0372	3.55 .0273	3.20 .0238
DPX=DPZ = .1°/Sec DPY = -.1°/Sec	3.65 .0379	6.35 .0439	3.60 .0270	4.05 .0382	3.50 .0330	4.05 .0361	3.30 .0271	3.35 .0259
DPX = -.1°/Sec DPY=DPZ = .1°/Sec	3.80 .0395	6.40 .0417	3.50 .0265	4.15 .0384	3.55 .0317	4.05 .0381	3.40 .0258	3.25 .0244
Average On-Time Average ENAVG	3.64 .0390	5.46 .0450	3.59 .0270	4.10 .0381	3.53 .0327	4.10 .0375	3.40 .0271	3.2875 .0249

Top number in each box = Engine On-time

Bottom number in each box = ENAVG, the average system error

Table III-11. Simulation Results for New Configurations.

These results are superficial in value when considered only as they appear in Table III-11. Since this study is concerned with improving the performance of the standard 6 engine model, the results of each of the other configurations should be compared in some manner with the reference model. This comparison can be made by normalizing the results of each configuration with respect to the results of the 6 engine model for each initial condition. The normalized results are listed in Table III-12.

The normalized results listed in Table III-12 become more meaningful when shown in graphical form. The graph shown in Figure III-13 represents the average results over all of the initial conditions considered. The normalized average error, $ENAVG_N$, is plotted versus the normalized engine on-time. The point plotted for each configuration should be viewed as the tip of a vector which represents its attitude control efficiency. Therefore, the shortest vector would represent the best system performance for the initial conditions considered. An evaluation of this type provides for equal weighting between engine on-time and error minimization. The closer the tip of the vector is to the horizontal axis, the more it favors error minimization. The closer the tip of the vector is to the vertical axis, the more it favors reduced engine on-time.

Examination of Figure III-13 reveals a trend of reduced average error by the new configurations. This trend is exhibited in the graph by the horizontal dashed line passing through the point plotted for the standard 6 engine model. Any points lying below this horizontal line

Initial Conditions	6 Engine Case	4 Engine Case	8 Engine Case #1	8 Engine Case #2	12 Engine Case #1	12 Engine Case #2	16 Engine Case	24 Engine Case
DPX = .1°/Sec DPY=DPZ = .1°/Sec	1.00 1.00	1.33 1.28	1.05 .714	1.20 .997	.986 .846	1.20 1.01	.957 .729	.957 .667
DPX=DPY = .1°/Sec DPZ = -.1°/Sec	1.00 1.00	1.68 1.06	.921 .671	1.09 .972	.934 .803	1.07 .965	.895 .653	.855 .618
DPX = .1°/Sec DPY=DPZ = -.1°/Sec	1.00 1.00	1.24 1.13	.986 .673	1.11 .933	1.00 .838	1.14 .928	.986 .681	.889 .594
DPX = -.1°/Sec DPY=DPZ = -.1°/Sec	1.00 1.00	1.74 1.16	.986 .712	1.11 1.01	.959 .871	1.11 .953	.904 .715	.918 .683
DPX=DPZ = -.1°/Sec DPY = .1°/Sec	1.00 1.00	1.33 1.28	1.05 .714	1.20 .997	.986 .846	1.20 1.01	.957 .729	.957 .667
DPX=DPY = -.1°/Sec DPZ = .1°/Sec	1.00 1.00	1.24 1.13	.986 .673	1.11 .933	1.00 .838	1.14 .928	.986 .681	.889 .594
DPX=DPZ = .1°/Sec DPY = -.1°/Sec	1.00 1.00	1.74 1.16	.986 .712	1.11 1.01	.959 .871	1.11 .953	.904 .715	.918 .683
DPX = -.1°/Sec DPY=DPZ = .1°/Sec	1.00 1.00	1.68 1.06	.921 .671	1.09 .972	.934 .803	1.07 .965	.895 .653	.855 .618
Average On-Time Average ENAVG	1.00 1.00	1.50 1.16	.986 .693	1.13 .978	.970 .840	1.13 .964	.936 .695	.905 .641

Top number in each box = Normalized Engine On-time

Bottom number in each box = Normalized ENAVG, the average system error

Table III-12. Normalized Simulation Results for New Configurations.

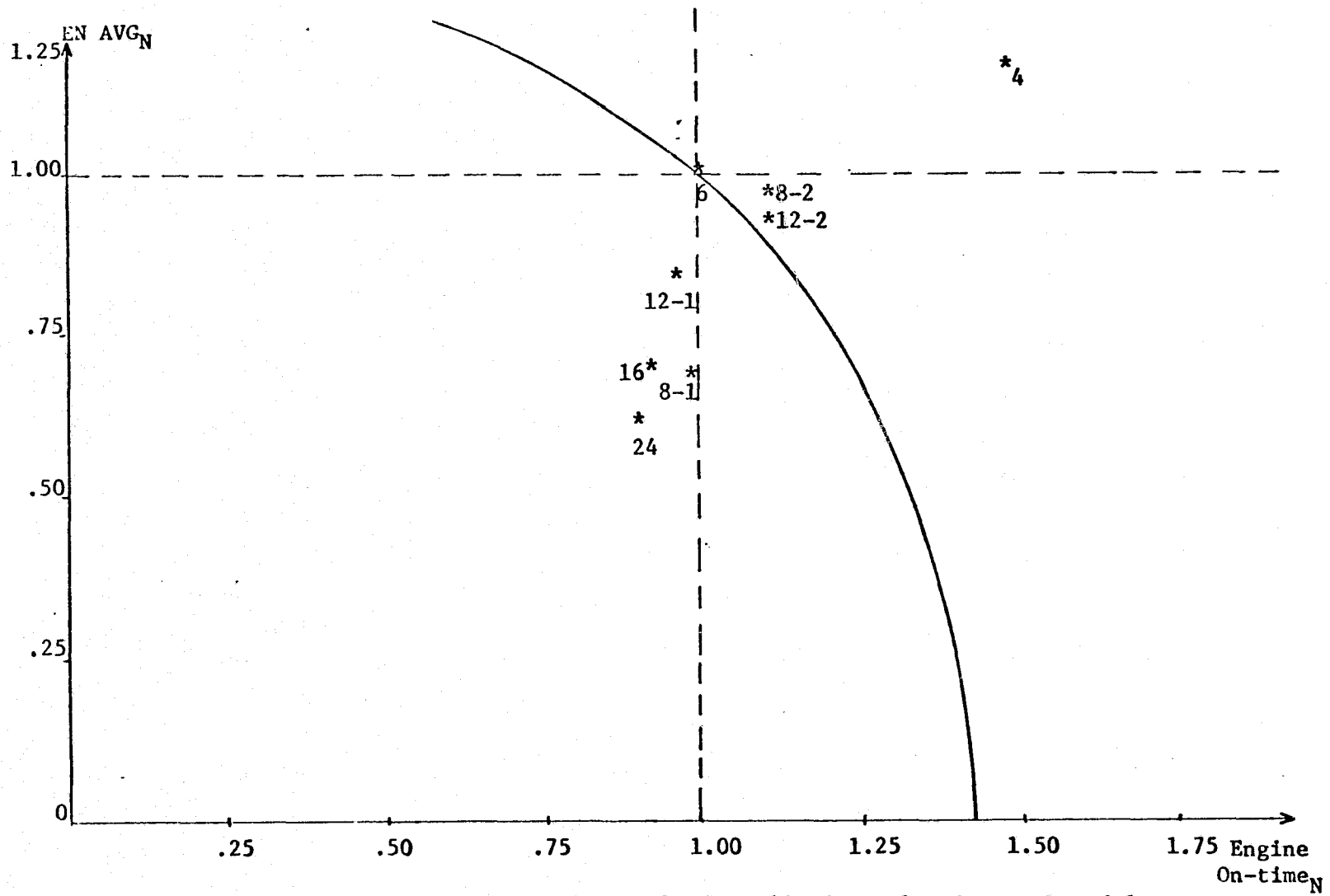

Figure III-13. ENAVG$_N$ vs. Engine On-time$_N$, the Normalized Results for Each Model.

represent an improved performance over the 6 engine model solely with respect to average error. The only model with a point plotted above the dashed horizontal line is the 4 engine model, which is the only configuration consisting of fewer thrusters than the 6 engine model. This indicates that an increased number of thrusters maintains the vehicle closer to the reference attitude when the external errors of this study are introduced. For models employing only orthogonal thrusters and for models employing both orthogonal and skewed thrusters, a definite trend is established. For these types of configurations, as the number of thrusters is increased, the average error in the system decreases. The models composed solely of skewed thrusters do not fit into this trend however. This is evidenced by the success with respect to error minimization of the first 8 engine model over both of the 12 engine models.

No consistent trend is established when engine on-time is considered. This is shown by the distribution of the points representing the configurations about the vertical dashed line. The amount of engine on-time is fairly constant among all models. The most improved performance over the 6 engine model with respect to engine on-time is only better by approximately 10% and the worst performance used only 10% more fuel. There is much more disparity in performances with respect to error minimization (40% between the performance of the 6 engine model and the 24 engine model). This lack of improvement with respect to engine on-time speaks well for the 6 engine model. If

the amount of error minimization provided by the 6 engine model is acceptable to a certain set of mission requirements, the additional cost of supplemental engines for, at most, a 10% reduction in engine on-time, may not be justified. This type of practicality comes plainly into view when the 24 engine model is considered. It keeps the vehicle closer to the reference attitude while using slightly less fuel, but the additional cost of four times as many thrusters as the 6 engine model may not be worth the increased efficiency.

Consider the circular arc in Figure III-13. Recalling that each point in this figure is to be viewed as the tip of a vector which represents the attitude control efficiency of the individual models, the arc represents the path of the vector for the 6 engine model if it were swept the entire 90° angle formed by the axes of the graph. Points which lie inside of this arc represent an improved overall performance over the 6 engine model. It is evident that four models lie inside of the arc and therefore have improved performances over the 6 engine model. These models are the first 8 engine model, the first 12 engine model, the 16 engine model and the 24 engine model. The configurations with improved performances had small (1% - 10%) decreases in engine on-time and significant (16% - 36%) decreases in average error. As the percentages just mentioned indicate, the four new models with better performances than the 6 engine model improved most with respect to error minimization. Since all models with more than six thrusters improved in reducing the average system error and

there was little improvement by any of the new configurations with respect to engine on-time, the reasons for better error correction are considered in the remainder of this section.

The improvement in error minimization is caused by the greater number of torque polarity combinations available from individual thrusters in configurations with more engines. This characteristic might be called variety of torques. Most of the models have the capability of providing each of the twenty-seven possible torque polarity combinations, but the factor that is important is how many thrusters a configuration must use in order to produce each of those combinations. The models with large numbers of engines can produce more of the 27 possible torque combinations with fewer thrusters than the models with small numbers of engines. The 24 engine model illustrates this characteristic. It has individual thrusters which can provide 24 of the 26 relevant torque combinations. The other two combinations are provided by firing two engines. For multiple axis errors the 24 engine model will, in most cases, fire a single engine for correction. If the magnitude of the error is large, more engines may eventually fire, but for errors of small or moderate magnitudes (such as gravity gradient torques and reasonable external disturbances) a single engine is capable of efficient correction. Not only does this normally reduce engine on-time, but the force provided by a single engine firing does not send the vehicle through its deadbands quickly causing reverse firings sooner than desired.

A single engine providing each of the torque polarity combinations has still other advantages. It equalizes the amount of torque applied to any single axis during a firing as much as possible. For example, consider an error which requires a positive pitch - yaw (y - z) torque combination for correction. The 6 engine model must fire three engines to achieve this combination and it developes twice as much torque about the yaw axis as it does about the pitch axis. This situation could cause a control problem. The large torque about the yaw axis causes the vehicle to pass through the yaw deadzone very quickly resulting in a reverse firing sooner than is desired. The 24 engine model fires a single engine to provide this torque combination and equal torques are produced about the pitch and yaw axes. By attacking the error uniformly, as the 24 engine model does, no new errors are produced which cause additional firings as is possible in the 6 engine model. This same situation occurs for other torque polarity combinations and the effect is felt on a long range basis. The example used shows the disparity between the 6 engine model and the most improved configuration, the 24 engine model. The improvements, in general, come in increasing amounts as more thrusters are added, except with the 8 engine model #1 where all thrusters are skewed.

Another advantage of having single engines provide each of the torque polarity combinations becomes evident when planning for the amount of force each engine will produce. If a model needs four engines to produce one torque polarity combination and only a single engine to produce another, determining how much force the individual engines

should produce can be difficult. When it is known that only a single engine (or any constant number of engines) will be fired initially for correction of most errors, the force provided by each of the engines could possibly be optimized for both less engine on-time and better error minimization. In many cases, the four engines which must fire simultaneously to produce a certain torque polarity combination have force cancellations which produce the required force in the necessary direction. Even if this situation occurs, it is obvious that it is very inefficient and should be avoided.

A specific look at some of the new configurations yields some interesting information. The successful performance of 8 engine model #1 could indicate that individual thrusters capable of producing torques about all three coordinate axes simultaneously are more important and useful than thrusters which provide torques about two axes or just a single axis. Its performance ranked very closely to the performances of configurations with many more engines (the 16 and 24 engine models). On the other hand, the success of this model may have been aided by the relationship between the initial conditions placed on the vehicle and the torque polarities available from the thrusters of this model. As explained earlier, the individual thrusters of this model correspond to one of the possible combinations of each of the torque polarities provided about three axes simultaneously. These same combinations of three axes errors are used as initial conditions on the vehicle. Since the error inputs on each of the axes were of equal magnitude, 8 engine model #1 fired single thrusters initially to correct for each of the error combinations introduced by this study.

This could be a decided advantage for the first 8 engine model since most of the other models require multiple thruster firings initially to produce the necessary torque polarity combinations for correction. Several additional simulation runs were made to determine if the success of the first 8 engine model was genuine. These runs used initial conditions on two axes simultaneously instead of three. These initial conditions were chosen because they forced the first 8 engine model to fire more than one engine initially for correction. This model performed favorably (13% decrease in engine on-time, 29% decrease in average error) with respect to the 6 engine model for several of the two axes errors. Therefore it is assumed that the success of the first 8 engine model is genuine. Genuine success by 8 engine model #1 is more important than the success of any of the other improved models from a practical standpoint. It performed nearly as well as the 16 and 24 engine models, yet has many fewer thrusters. The increased cost provided by eight thrusters as opposed to six is more easily justified than twenty-four thrusters opposed to six.

The other three successful models have the same basic configuration: that of the first 12 engine model shown in Figure III-9. This configuration features four pods consisting of three orthogonal thrusters each. Two factors contributed to the success of the three models with this basic configuration. The first of these factors is symmetry. The basic configuration of these three models is completely symmetrical, i.e. it has the same number of thrusters available to torque the vehicle about both of its transverse diameter axes (the

y and z axes). The longitudinal axis (the x axis) has an additional thruster available which aids in producing the same amount of torque about this axis as is developed about the y and z axes. The thrusters added to form the 16 and 24 engine models do not alter the symmetry about the transverse diameter axes.

The second factor which contributed to the success of the 16, 24, and the first 12 engine models has already been elaborated on. The individual thrusters of each of these models produce a wide variety of torque polarities. The importance of this characteristic has been mentioned previously as has the fact that the 24 engine model provides the ultimate in this type of variety.

The models which failed to improve on the performance of the 6 engine model reveal some interesting information. An unbalanced and unsymmetrical situation causes the 4 engine model to perform poorly. Recalling Table III-3, the torque polarities of the 4 engine model are identical with four of the eight possible combinations of three axes errors. Three of the four thrusters must be fired to synthesize each of the four torque polarity combinations not produced by the four thrusters composing the configuration. Another way of saying this is that when a single thruster in the 4 engine configuration fires, three thrusters are required for a reverse firing of exactly the opposite polarity. This lack of balance in the configuration caused a considerable number of firings and, obviously, more engine on-time than is desired.

The second 8 and 12 engine models are very similar. They both have more thrusters capable of producing yaw axis torques than pitch axis torques. Torques about each of these axes represent torques about the transverse diameter of the vehicle. The simulation results indicate that the importance of symmetry extends to having the same number of thrusters fire about each of the axes which represent the transverse diameter of the vehicle. Both of these models have variety of torques by individual thrusters which is comparable to that of the other models with similar numbers of thrusters. The unbalanced number of thrusters which torque about the two transverse diameter axes causes the problem and affects their performances adversely.

A brief discussion of the deficiencies of this study might help to bring the results into perspective. An investigation using simulation results has certain shortcomings which cause it to lose generality. It must be remembered that the results listed are for a large space vehicle. Vehicles of smaller dimensions and moments of inertia, or any number of different physical features may perform differently for the configurations developed. This simulation study was also limited by the number of simulation runs which could be carried out. Initial conditions were used which were believed to be representative of an actual mission. If many more initial conditions of a more varying variety had been used in additional runs, perhaps a better indication of the performance of each configuration would have resulted. On the other hand, more simulation runs may have merely been beating the subject to death rather than being thorough.

A quick recap of some of the results of this chapter might be useful in determining what beneficial information has been provided. The specific and general observations just completed can be correlated to yield some features characteristic of an efficient thruster configuration. Balance and symmetry are two key words which are indicative of the first important feature. Balance requires that a reverse firing produce a force exactly equal to the initial firing, but more importantly, that after an initial firing of some number of thrusters has caused the vehicle to cross through the deadzone, the reverse firing will involve the same number of thrusters. The 4 engine model is a graphic illustration of a lack of balance while the 24 engine model exhibits nearly flawless balance and symmetry.

Balance and symmetry are strongly linked with the second important characteristic of efficient configurations: variety of torques. There are two important parts to this characteristic. The first part maintains that an efficient configuration should be able to provide a wide variety of torque polarity combinations. It is almost imperative that each of the twenty-seven possible torque polarity combinations be available. The second part, which is altogether as important as the first, requires that each of the various torque polarity combinations be provided by the same number of thrusters. As mentioned earlier, this allows for torque equalization about the axes which represent the transverse diameter of the vehicle as well as about the longitudinal axis. In addition, an opportunity is afforded for optimizing the force of each individual thruster in a configuration. These

characteristics are important in the design of thruster configurations for attitude control systems of large space vehicles.

IV. ENGINE TORQUE AXES ERROR RESOLUTION

The attitude control loop feeds error signals which are in terms of vehicle coordinates to the relays which control the thruster firings. This chapter investigates the possibility of another error evaluation method existing which causes more efficient firings by the individual thrusters. The new error evaluation method developed is based on a single idea: error evaluation about axes more directly related to the thrusters in a configuration could produce better attitude control efficiency, i.e. fewer thruster firings and/or smaller system errors. The axes considered by this study to be more directly related to the thrusters of a configuration are called engine torque axes. The engine torque axes are those axes about which the thrusters torque the vehicle. The method of evaluating attitude errors about the engine torque axes is called engine torque axes error resolution.

A. Description of an Engine Torque Axis

A general description of an engine torque axis must be prefaced by the explanation of one definitive characteristic. The position of an engine torque axis is determined by the placement of a single thruster, not by the placements of any combination of several thrusters. This defining condition indicates that there is an engine torque axis corresponding to each thruster in a configuration. Therefore, if

there are six thrusters in a particular configuration, there are six engine torque axes, one corresponding to each thruster.

A quick review of statics indicates that a torque is a force applied over a distance sometimes termed a moment arm. It was explained in Chapter II that the thrusters torque the vehicle about its center of gravity when fired. Therefore an axis about which an engine torques the vehicle must pass through the center of gravity of the vehicle. The moment arm of the torque produced by a thruster exists between the line of action of the force provided by the thruster and the center of gravity of the vehicle. This moment arm is perpendicular to both the line of action of the force and the engine torque axis as shown in Figure IV-1. If the line of action of the force provided by the thruster and the line describing the position of the engine torque axis were translated so that they intersected, they would be perpendicular to each other.

Another property of engine torque axes defines them to have positive and negative polarities. The importance of this property will become apparent later in this chapter. The polarity of an engine torque axis is determined by the often used "right hand rule." The engine torque axes which correspond to any two thrusters from the same configuration may lie along the same line but will not have the same polarities. Therefore, under the constraints of this study, the polarity property makes it impossible for two engine torque axes corresponding to two thrusters from the same configuration to be exactly alike.

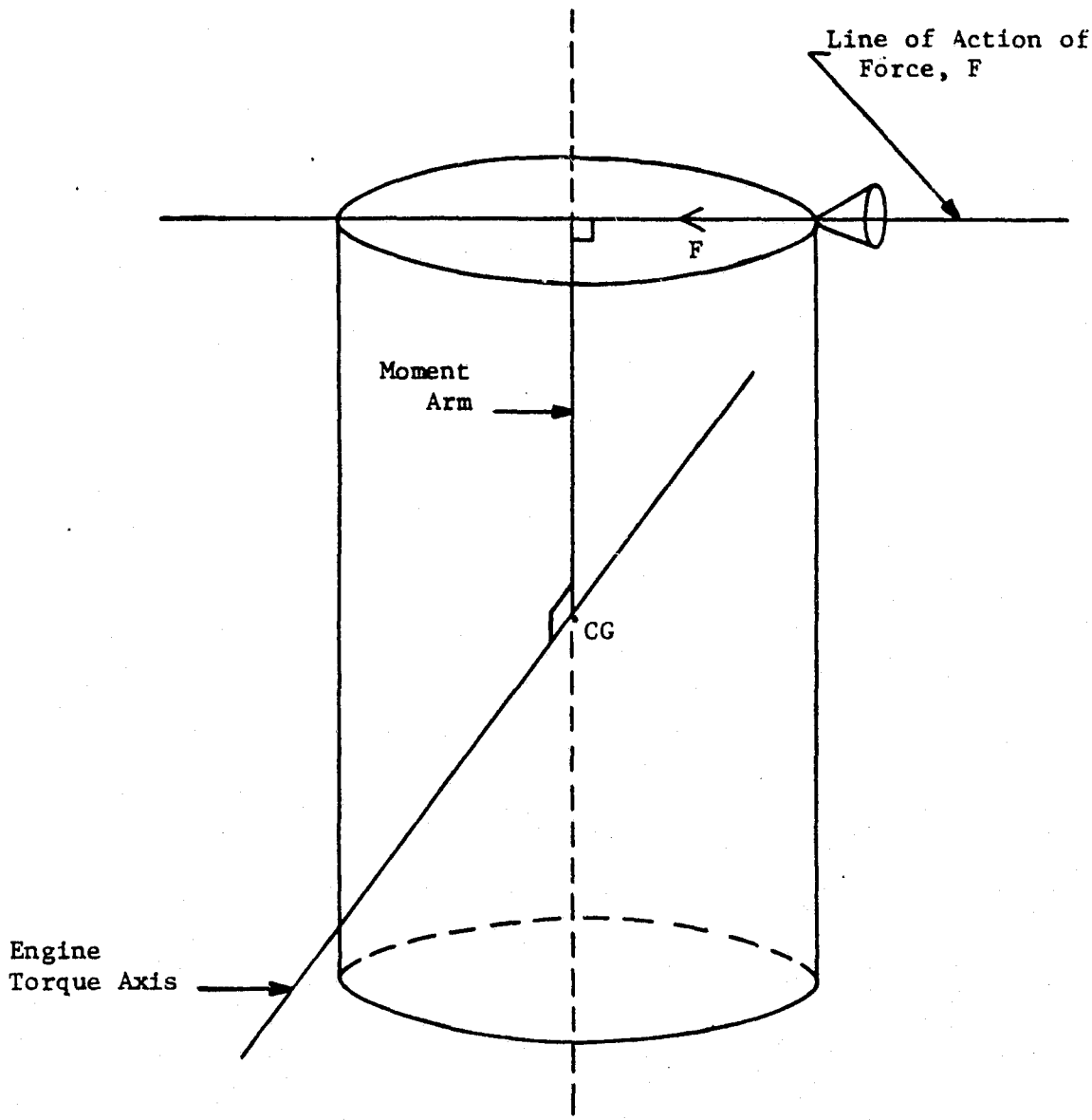

Figure IV-1. General Illustration of an Engine Torque Axis.

B. Engine Torque Axes For Several Types of Thruster Placements

As further illustration of the engine torque axis concept, the positions of several engine torque axes will be determined for several different thruster placements. The first of these placements calls for the thruster to produce a force which acts in a direction perpendicular to the upper periphery of the vehicle. This causes the line of action of the force produced by the thruster to intersect the longitudinal axis of the vehicle. Note that the longitudinal axis, shown as dashed lines in Figure IV-1, passes through the center of gravity of the vehicle. No matter where on the upper periphery of the cylindrical vehicle a thruster is positioned, if its force acts through the longitudinal axis the engine torque axis which corresponds to that thruster is always parallel to the surface formed by the upper periphery of the vehicle. The position of the engine torque axis for this engine placement is shown in Figure IV-2.

The second engine placement provides a force which acts along a line that is tangent to the upper periphery of the vehicle as shown in Figure IV-3(a.). This engine placement causes the vehicle to torque about both its longitudinal axis and its transverse diameter. Figure IV-3(b.) indicates the position of the engine torque axis for a thruster placement of this type. The engine torque axis is sloped since it must be perpendicular to the moment arm of the torque provided by the thruster. The amount of slope is determined solely by the length and diameter of the vehicle since the center of gravity is

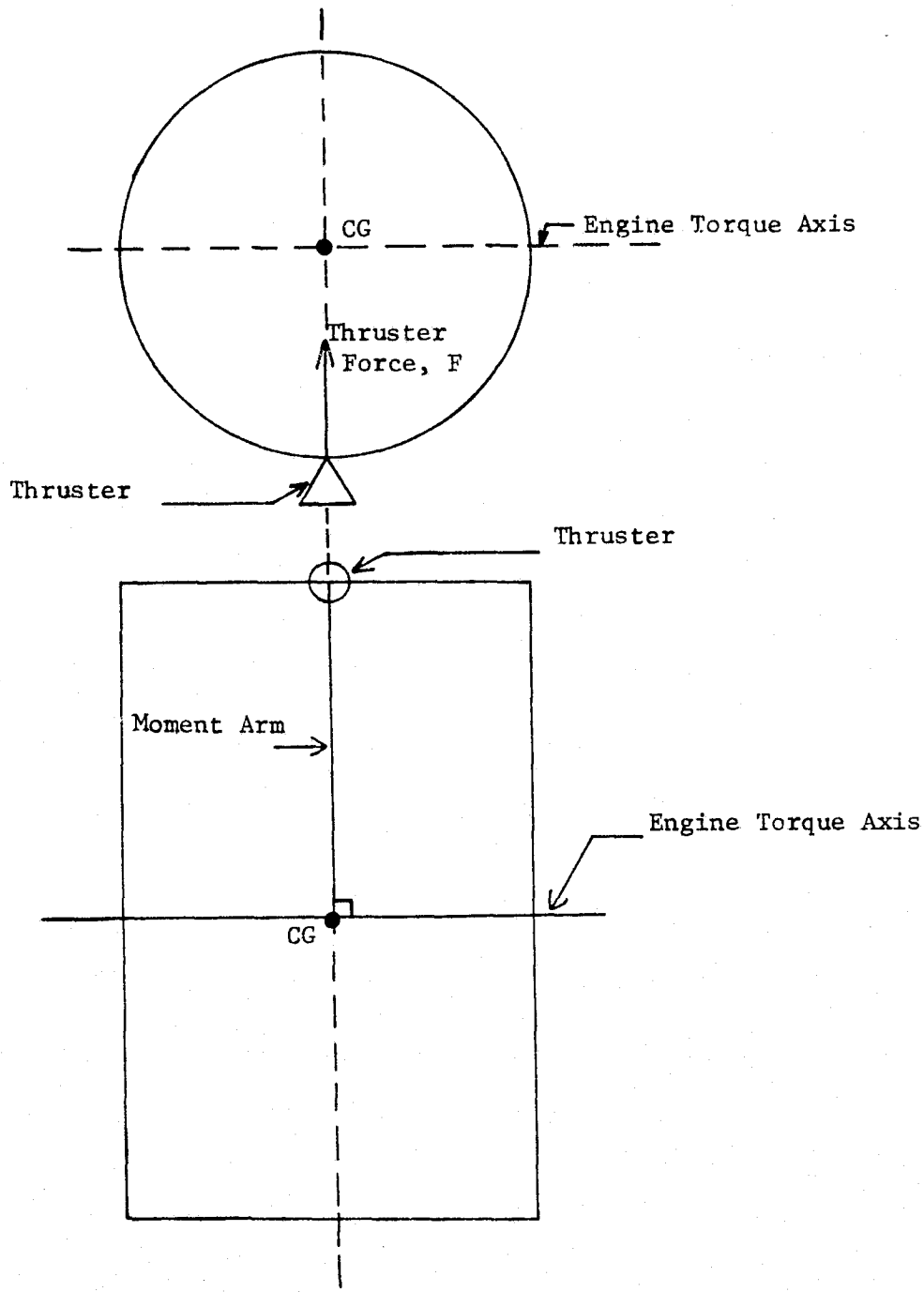

Figure IV-2. The First Engine Placement and its Corresponding Engine Torque Axis.

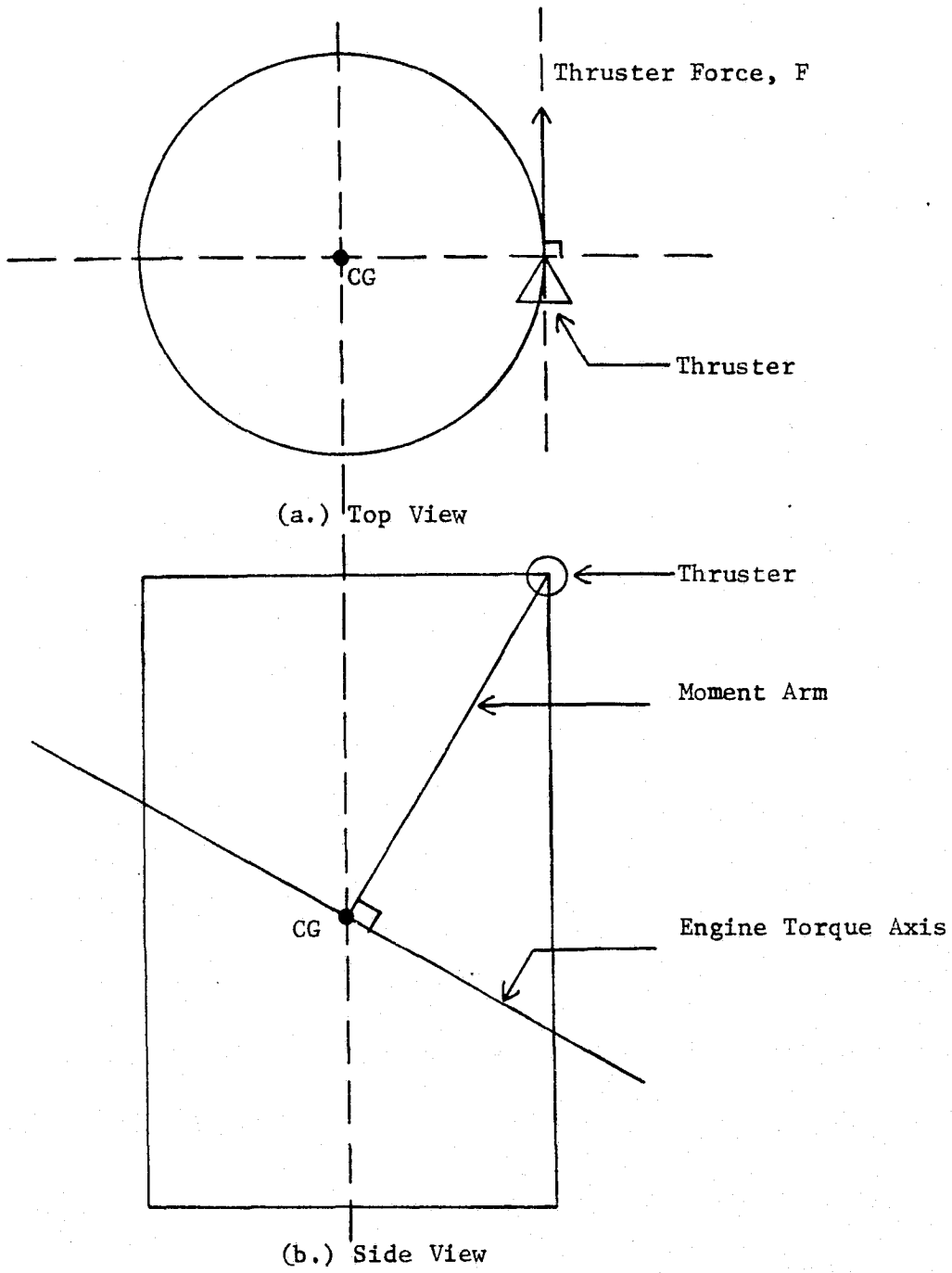

Figure IV-3. The Second Engine Placement and its Corresponding Engine Torque Axis.

assumed to be located at the geometrical center of the vehicle. In a more general sense the amount of slope is determined by the position of the center of gravity of the vehicle.

The third engine placement is the most general type of placement considered. This placement provides a force with a direction which may assume any angle between the force directions of the first and second engine placements. Configurations employing this type of engine placement will be called skewed configurations and the angles assumed by the thrusters will be called skewing angles. Skewing angles of 45° are the only ones considered in this study, but certain mission requirements might dictate the use of skewing angles different from this.

The first and second engine placements provide forces whose directions may be thought of as skewing angle limits. Figure IV-4 shows the directions of the forces provided by placements one, two and three. If the direction of F_1, the force from an engine in placement one, is considered as the reference, the direction of F_3, the force from an engine in placement three, may assume any angle not exceeding 90° on either side of F_1. Exactly 90° on either side of F_1 is the position of the second engine placement. An engine placement such as placement three causes the vehicle to torque about all three vehicle coordinate axes simultaneously. The engine torque axis for this placement is sloped in nearly the same manner as the one for the second placement. The difference comes in the amount of slope the

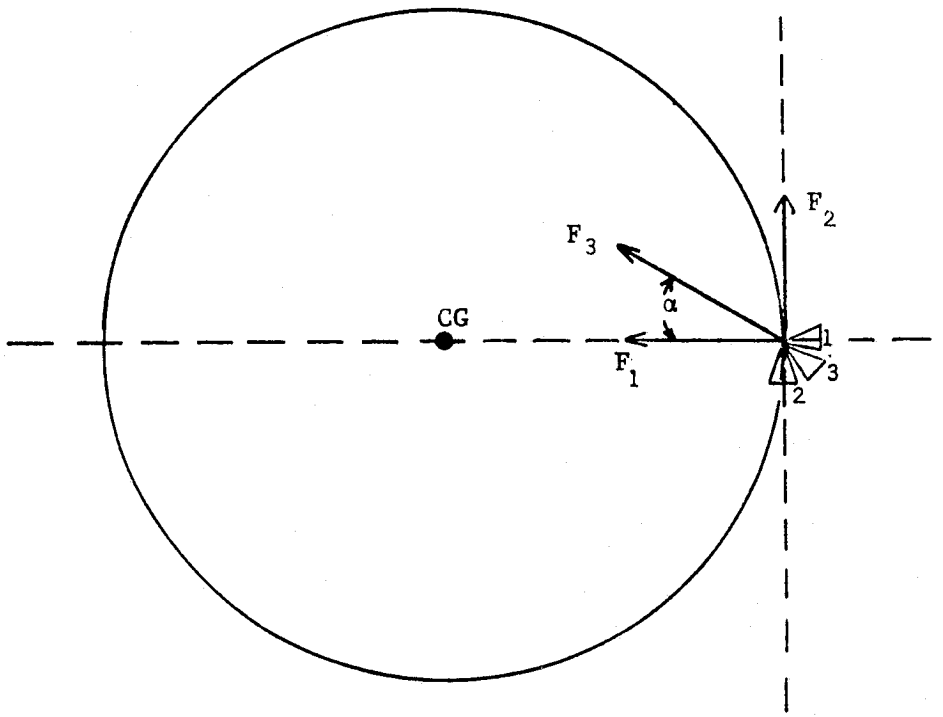

1st Engine Placement: $\alpha = 0°$
2nd Engine Placement: $\alpha = 90°$
3rd Engine Placement: $0° < \alpha < 90°$

Figure IV-4. Angular Relationships of Engine Placements One, Two, and Three.

axis assumes. The slope of the engine torque axis for the second placement was determined solely by the length and diameter of the vehicle. The engine torque axis slope for the third placement is dependent on the length and diameter of the vehicle but also on the amount the thruster is skewed. Figure IV-5 illustrates the position of an engine torque axis for a skewed thruster. A comparison of Figures IV-3 and IV-5 reveals that the moment arm of the third engine placement is shorter than that of the second engine placement. This causes the slope of the axis for the third placement to be less severe than that of the second placement.

The forces provided by the thrusters in the placements described in this section act in a plane formed by the upper periphery of the vehicle. These are the only types of placements that are considered in this study and are thought to encompass all relevant thruster positions. Thrusters skewed with respect to the plane mentioned would produce a force which would cause translation in space, which is not consistent with the purpose of attitude control systems.

C. Error Resolution Into the Engine Torque Axes

The engine torque axes which correspond to the thrusters of each of the configurations described in Chapter III are to be used to achieve better firing efficiency. This is attempted by resolving the errors in the vehicle coordinate system into each of the engine torque axes. A thruster is fired only when the error about its engine torque

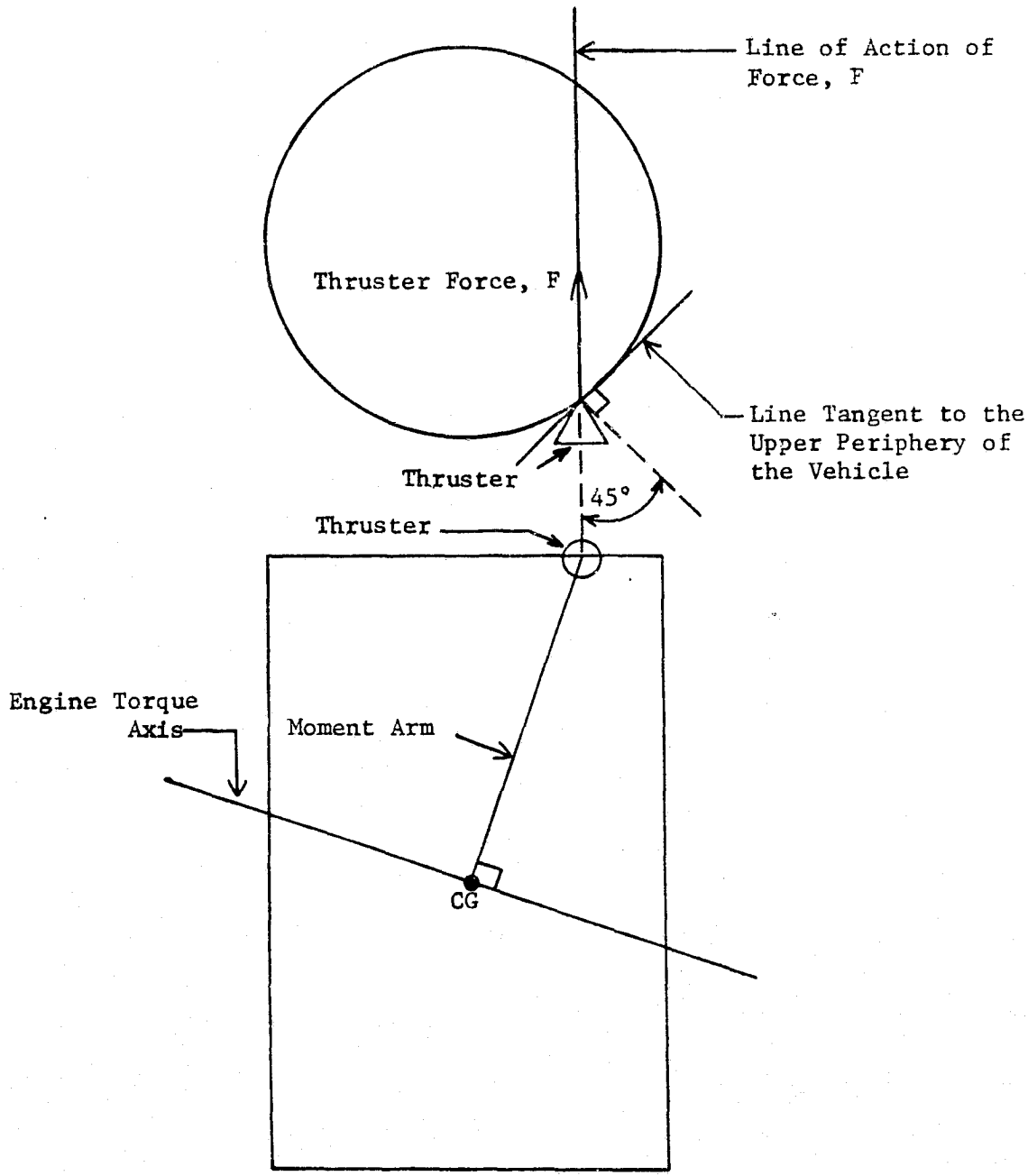

Figure IV-5. The Third Engine Placement and its Corresponding Engine Torque Axis.

axis exceeds the deadbands explained in Chapter II. This procedure is called engine torque axes error resolution. The same deadbands that are used in the original error evaluation system are used in the new system. The new system should bring about the elimination of some thruster firings which do not utilize the thrusters to their greatest effectiveness.

In the current system the vehicle attitude control law fires any and all thrusters which have the torque polarity capable of correcting the system error. As an example of this consider the 6 engine model and the 24 engine model. As shown in Table IV-1, the 6 engine model has two thrusters capable of producing positive roll torques. Table IV-2 reveals that the 24 engine model has eight

Engine	Torques Produced X	Y	Z
1		-	
2		+	
3	+		-
4	-		+
5	-		-
6	+		+

Table IV-1. Torque Polarities of the 6 Engine Model.

thrusters capable of producing positive roll torques. If a roll error exists of sufficient magnitude such that the vehicle is just outside of its roll deadband limit, the current method of error evaluation

Engine	Torques Produced X	Y	Z				
1	-		-	13	-	-	
2	+		+	14	+	+	
3	+		-	15	+	-	
4	-		+	16	-	+	
5		+		17	+	-	+
6		-		18	-	+	-
7			+	19	-	-	+
8			-	20	+	+	-
9		-	+	21	+	-	-
10		+	+	22	-	+	+
11		-	-	23	-	-	-
12		+	-	24	+	+	+

Table IV-2. Torque Polarities of the 24 Engine Model.

requires the 6 engine model to fire both of the positive roll thrusters. Similarly, if the current error evaluation method is used in the attitude control loop of the 24 engine model, it causes all eight of its positive roll thrusters to fire. It can be seen that the current error evaluation method fires any and all thrusters which produce torques that are of the polarity necessary to correct the system error. It is suspected that engine torque axes error resolution will cause greater discrimination in selecting which thrusters should fire. When the vehicle axes errors are resolved into the engine torque axes, a better judgement can be made as to whether or not the torque produced by a particular thruster will be effective in reducing the total system error.

The reason a better judgement could be possible is explained by an examination of the relationship between the errors and the torques produced for each error evaluation method. When a single thruster is fired the vehicle torques about the engine torque axis which corresponds to that particular thruster. Errors measured about that engine torque axis are a direct indication as to when the torque provided by that thruster can be used most effectively. Errors evaluated by using engine torque axes error resolution are on a one-to-one basis with the actual torque produced by each engine no matter what configuration is considered. This differs from the current system where errors measured about the vehicle axes are on a one-to-one basis with the torque polarities of all of the thrusters considered as a single unit, no matter how many are in a configuration.

As an example of the difference in the one-to-one relationships exhibited by the models with and without engine torque axes error resolution, consider a model with 3 thrusters as shown in Figure IV-6(A). If a pure z axis error were introduced to the attitude controller of this model and the current error evaluation method were in use, thrusters 1, 2 and 3 would fire to correct the error. If engine torque axes error resolution were in use, thruster 1 would fire first because axis 1, the engine torque axis for thruster 1, is coincident with the z axis and the resolved error would obviously be larger in this axis than in axes 2 and 3. If thruster 1 did not sufficiently correct the error, in a short time thrusters 2 and 3 would fire. The main idea to be illustrated by this example is that engine torque axes error resolution can reduce engine on-time. This is not intended to imply that engine torque axes error resolution saves on-time in every instance but, that in certain instances it will fire fewer thrusters than the conventional error evaluation method and still correct the error in the system.

The method used to resolve the errors in the vehicle coordinates into the individual engine torque axes bears close examination. A central idea to keep in mind during the course of the explanation is that, when summed vectorially, the error components expressed in the engine torque axes are to form the vehicle axes errors exactly. This idea necessitates that the errors in vehicle coordinates and those in the engine torque axes be thought of as vector quantities. The

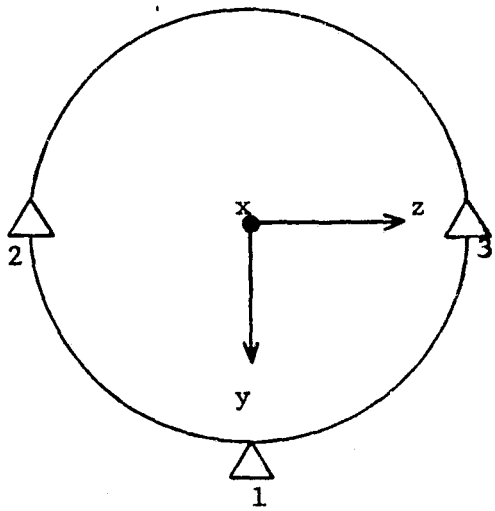

(a) Example Configuration

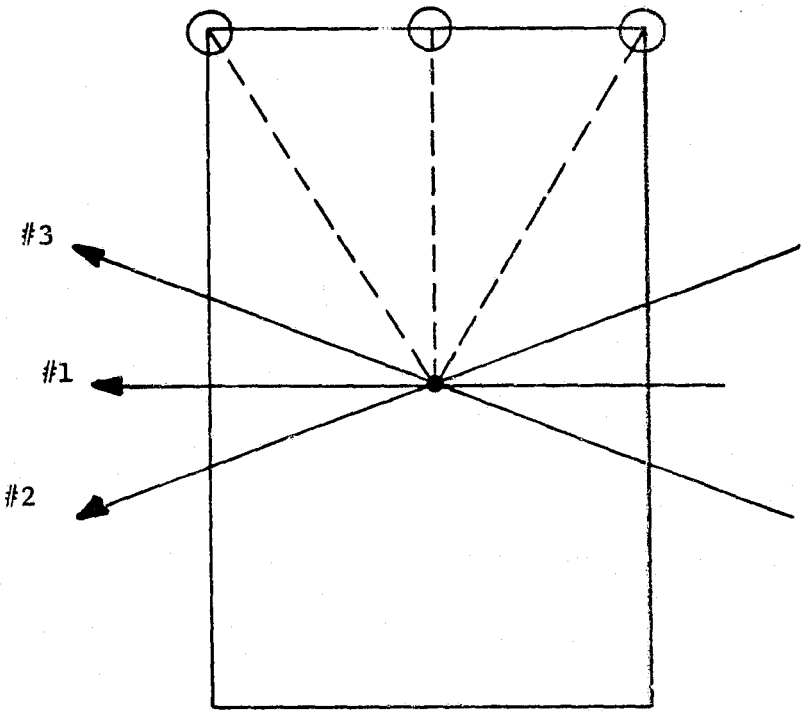

(b) Corresponding Engine Torque Axes

Figure IV-6. Example Model.

parallelogram law used in the addition of vectors is employed in the resolutions. This law, illustrated in Figure IV-7, requires that the two vectors summed to form a third vector must lie on the sides of a parallelogram that has opposite corners at the head and tail of the third vector. Note that in order to use this law $\overline{V}_1$, $\overline{V}_2$, and $\overline{V}_3$ must lie in the same plane.

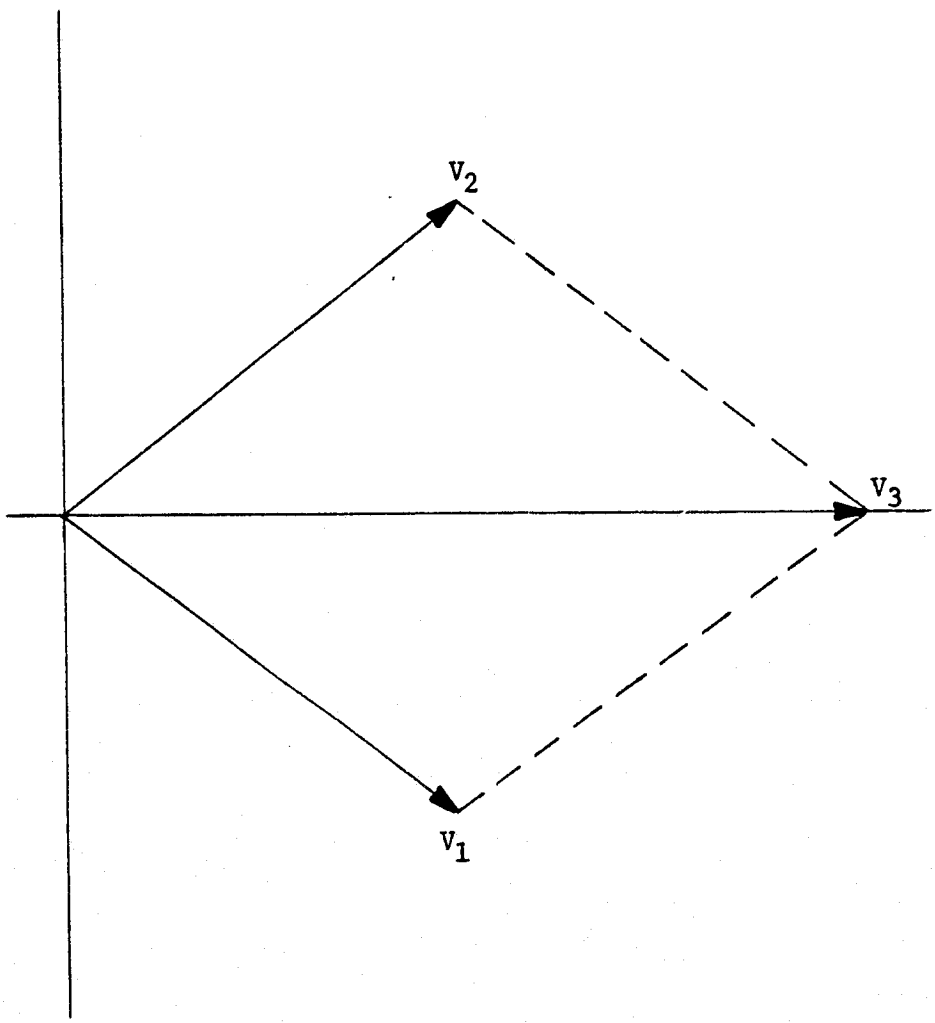

Figure IV-7. Parallelogram Law for Vector Addition.

At this point a generalized derivation is presented to illustrate the method employed to resolve the vehicle coordinate axes errors into the engine torque axes. Figure IV-8 shows the x and z axes of the vehicle coordinate system and two engine torque axes, all of which lie in the same plane. ε_z represents the error in the z axis while A and B represent the resolution of ε_z into the two engine torque axes respectively. The two engine torque axes are symmetrical with respect to the z axis as shown in Figure IV-8. Each of the configurations considered has symmetrical thruster placements which result in symmetrical pairs of engine torque axes. The resolution into each engine torque axis is achieved through the transformation derived below.

$$|\overline{OD}|\cos\alpha = |\overline{OB}| + |\overline{BC}| \tag{IV-1}$$

$$|\overline{BC}| = |\overline{BD}|\cos(2\alpha) \tag{IV-2}$$

Substituting from Equation (IV-2) into Equation (IV-1) gives

$$|\overline{OD}|\cos\alpha = |\overline{OB}| + |\overline{BD}|\cos(2\alpha) \tag{IV-3}$$

The angles, α, between each engine torque axis and the z axis are equal. Therefore:

$$|\overline{BD}| = |\overline{OA}| \tag{IV-4}$$

Substituting from Equation (IV-4) into Equation (IV-3) gives

$$|\overline{OD}|\cos\alpha = |\overline{OB}| + |\overline{OA}|\cos(2\alpha) \tag{IV-5}$$

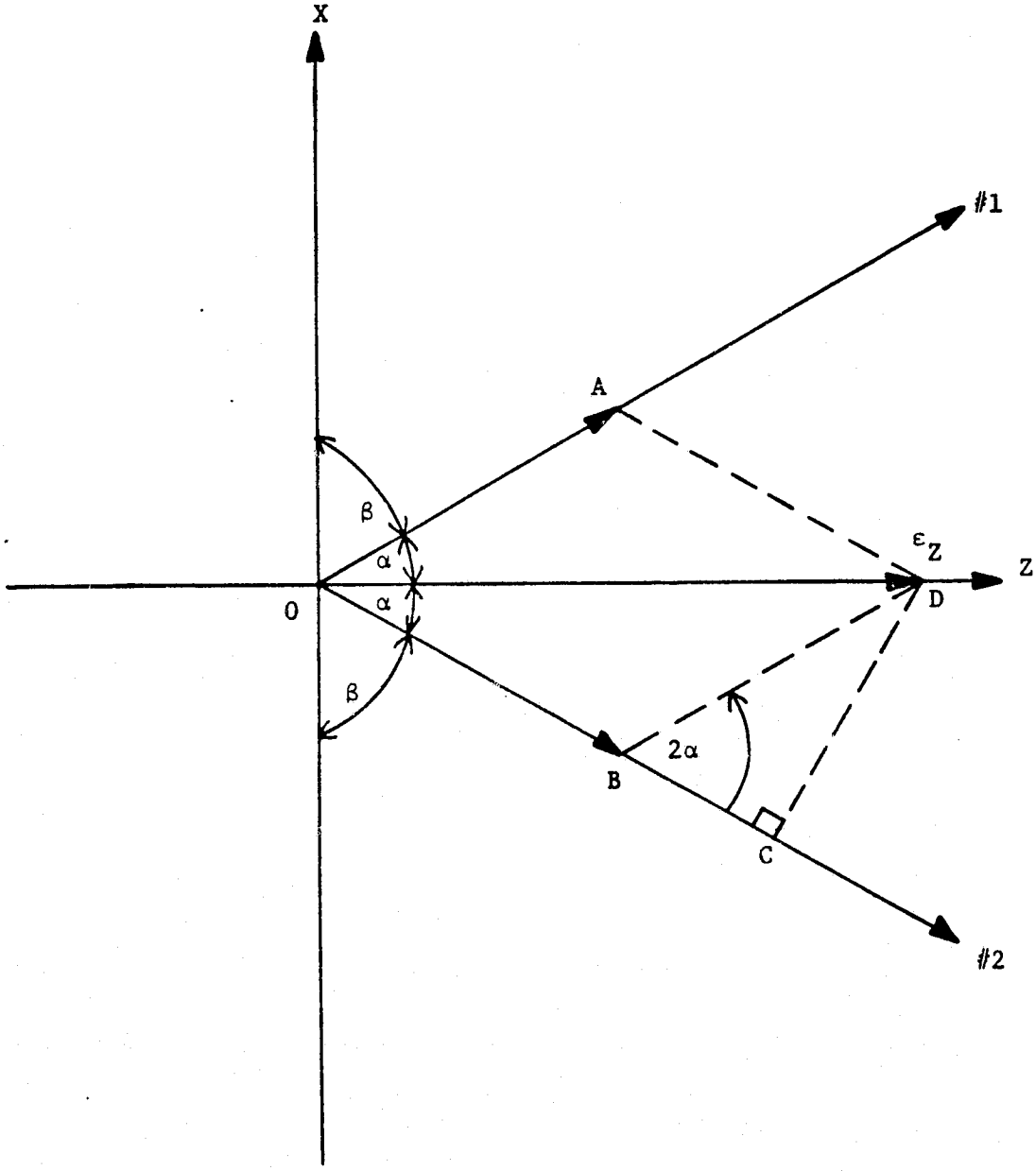

Figure IV-8. Resolution of Vehicle Errors Into Engine Torque Axes.

The parallelogram addition law for vectors indicates that

$$|\overline{OA}| = |\overline{OB}| \tag{IV-6}$$

substituting from Equation (IV-5)

$$|\overline{OD}| \cos\alpha = |\overline{OA}| (1 + \cos 2\alpha) \tag{IV-7}$$

$|\overline{OD}|$ represents the z axis error in vehicle coordinates, so

$$|\overline{OA}| = |\overline{OB}| = \left[\frac{\cos \alpha}{1 + \cos 2\alpha} \right] \varepsilon_z \tag{IV-8}$$

If thrusters #1 and #2 were the only thrusters which affect the z axis and there were an error only about the z vehicle coordinate axis, the decision to fire thrusters #1 and #2 would be made by determining if $|\overline{OA}|$ and $|\overline{OB}|$ exceed their deadband limits.

Transformations in the form of Equation (IV-8) are used in each of the simulations which describe the configurations from Chapter III. These transformations are placed in the simulation loops immediately following the sampling operation and before the vehicle attitude control law as shown in Figure IV-9. A more explicit example is illustrated in Figure IV-10 where the transformation blocks are shown multiplying the vehicle coordinate error signals just before they enter the vehicle attitude control law. XT_i, YT_i, and ZT_i (i = 1, 2, 3, 4) represent the individual transformations.

It is important to note that the engine torque axes always occur in pairs symmetrical with respect to the vehicle axes due to the corresponding symmetry of the thruster placements. This symmetry is

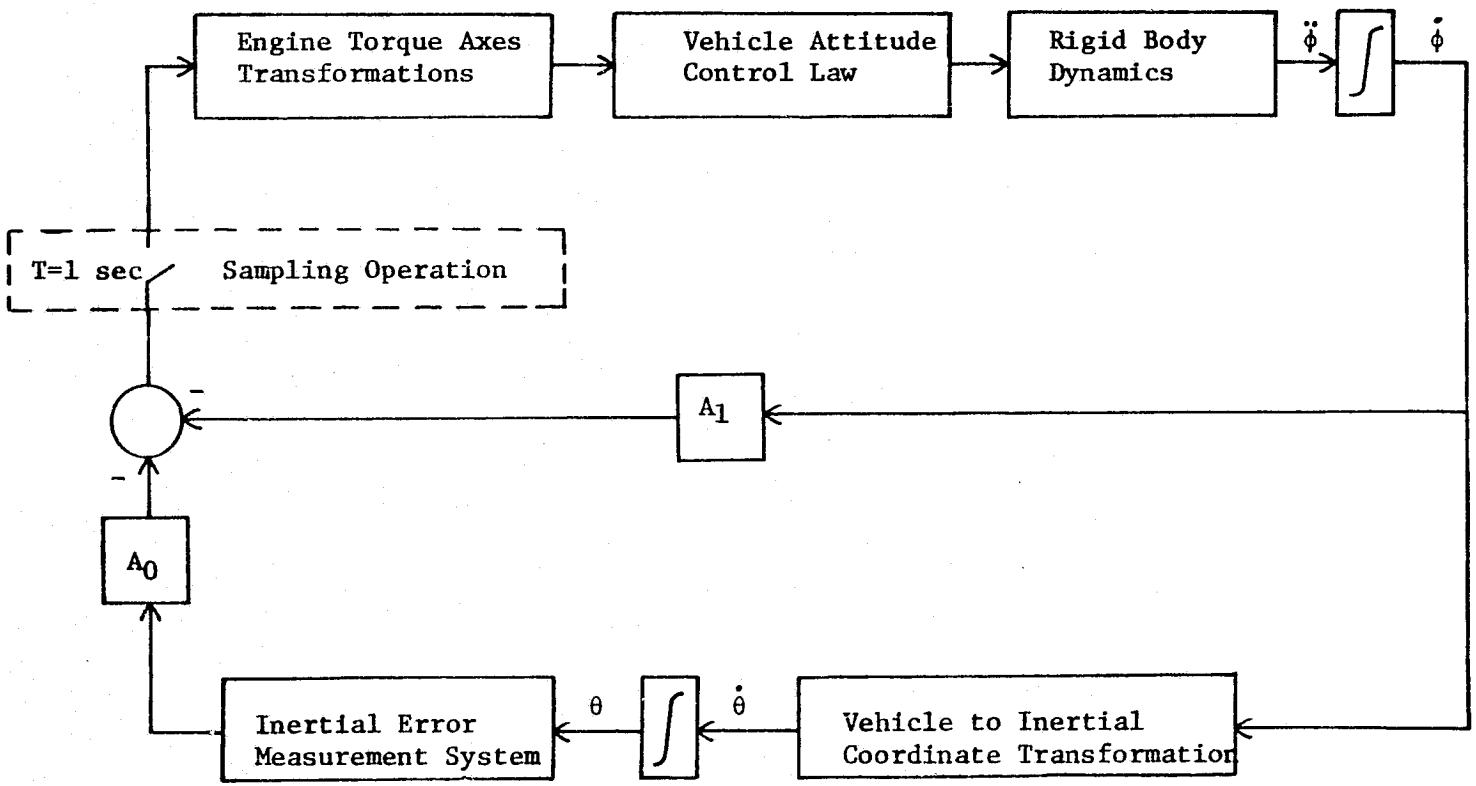

Figure IV-9. Generalized Block Diagram of the Simulation Attitude Control Loop with the Engine Torque Axes Transformations.

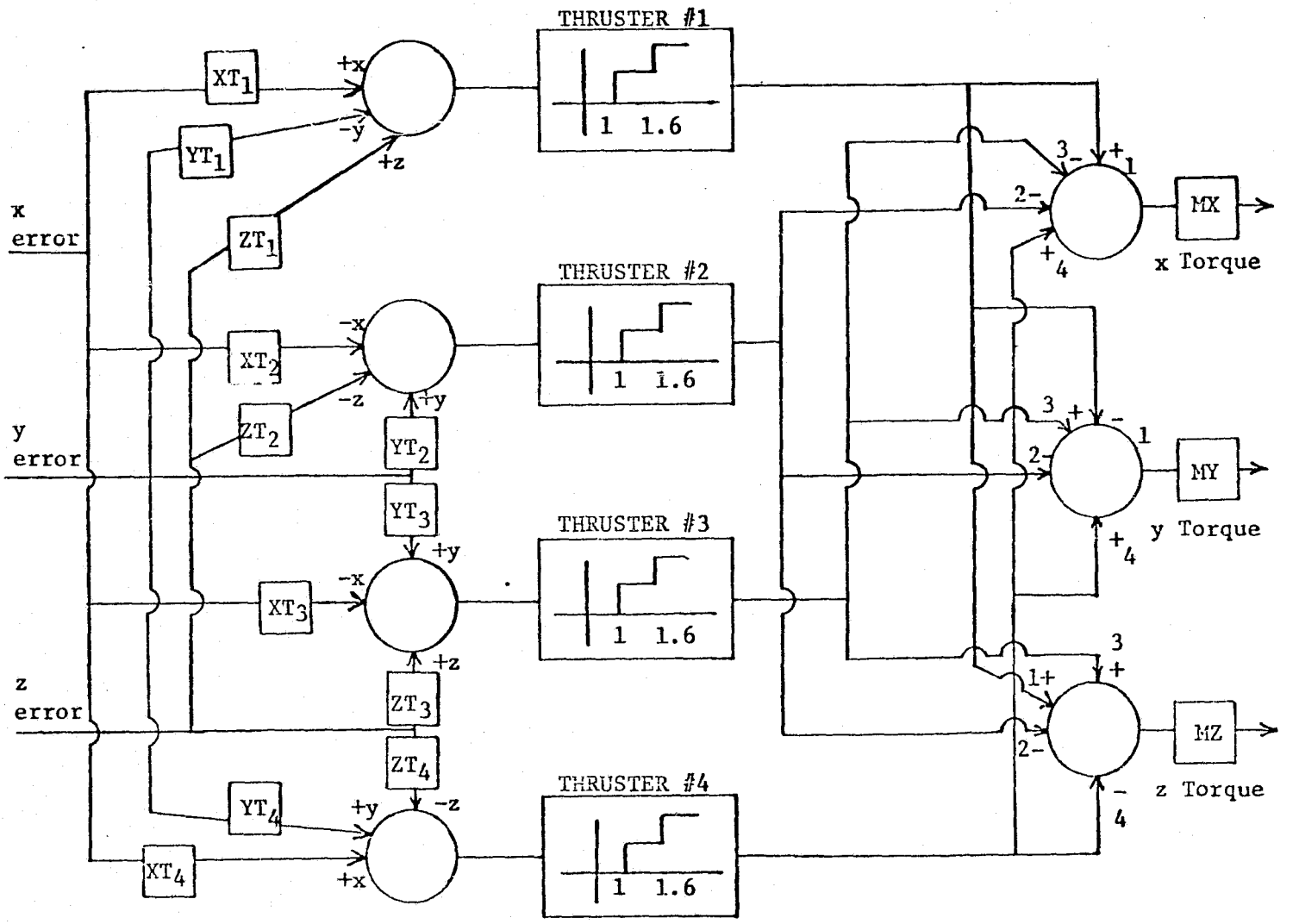

Figure IV-10. Transformation Blocks Included in the Attitude Control Law of the 4 Engine Model.

illustrated in Section D of this chapter, which describes the positions of the engine torque axes for each model. The pairs of engine torque axes which correspond to a configuration may assume a variety of positions, depending on the various placements of the thrusters. For configurations with large numbers of thrusters several different engine torque axes positions exist. Each different position requires a different transformation from each of the vehicle coordinate axes. The difference occurs in the angles which exist between each different engine torque axis and the vehicle axes.

The central idea used in the derivation of the transformations is that all error components expressed in the engine torque axes must sum vectorially to form the original vehicle axes errors. Equation (IV-8) describes the general, planar transformation into an engine torque axis. The parallelogram law this transformation is based on requires that all three vector quantities considered in the derivation lie in the same plane. This type of transformation limits to two the number of engine torque axes into which vehicle axes errors may be resolved. However, as shown by the models presented in Chapter III, there may be more than two torque axes into which an error in a given vehicle axis must be resolved. Since for many of the models there are more than one pair of axes to be resolved into from each vehicle axis, a problem occurs with the type of transformation used. This problem is circumvented by using a special technique.

This special technique is called the resolution plane test and it determines the proper number of engine torque axes into which the

errors from each vehicle axis should be resolved. Although the engine torque axes are actually infinite in length, consider for the moment that they begin at the origin of the vehicle coordinate system and proceed only in their defined positive direction. Suppose next that a plane intersects the origin and is perpendicular to one of the vehicle coordinate axes. The three dimensional space occupied by the vehicle coordinate system is then divided into two parts. Note that as the plane is placed perpendicular to each individual vehicle axis, several pairs of engine torque axes (positive parts only) can be seen extending into the portion of space denoted as positive or negative by the polarity of the vehicle coordinate axis. This is illustrated in Figure IV-11 for the z vehicle coordinate axis.

The rule used to determine the number of pairs of engine torque axes which are eligible for error resolution from a vehicle axis is as follows: errors in a particular vehicle axis will be resolved into those engine torque axes pairs which extend into the same portion of space as that vehicle axis. The three dimensional space is divided into portions by the resolution plane. Positive z axis errors are resolved into the torque axis pair formed by axes #1 and #2, while negative z axis errors are resolved into axes #3 and #4 in the example of Figure IV-11. Engine torque axes pairs are not considered for resolution if they lie in the resolution plane perpendicular to the vehicle axis from which errors are being resolved. Each perpendicular placement allows one to determine the number of engine torque axes pairs into which each particular vehicle axis error can be resolved.

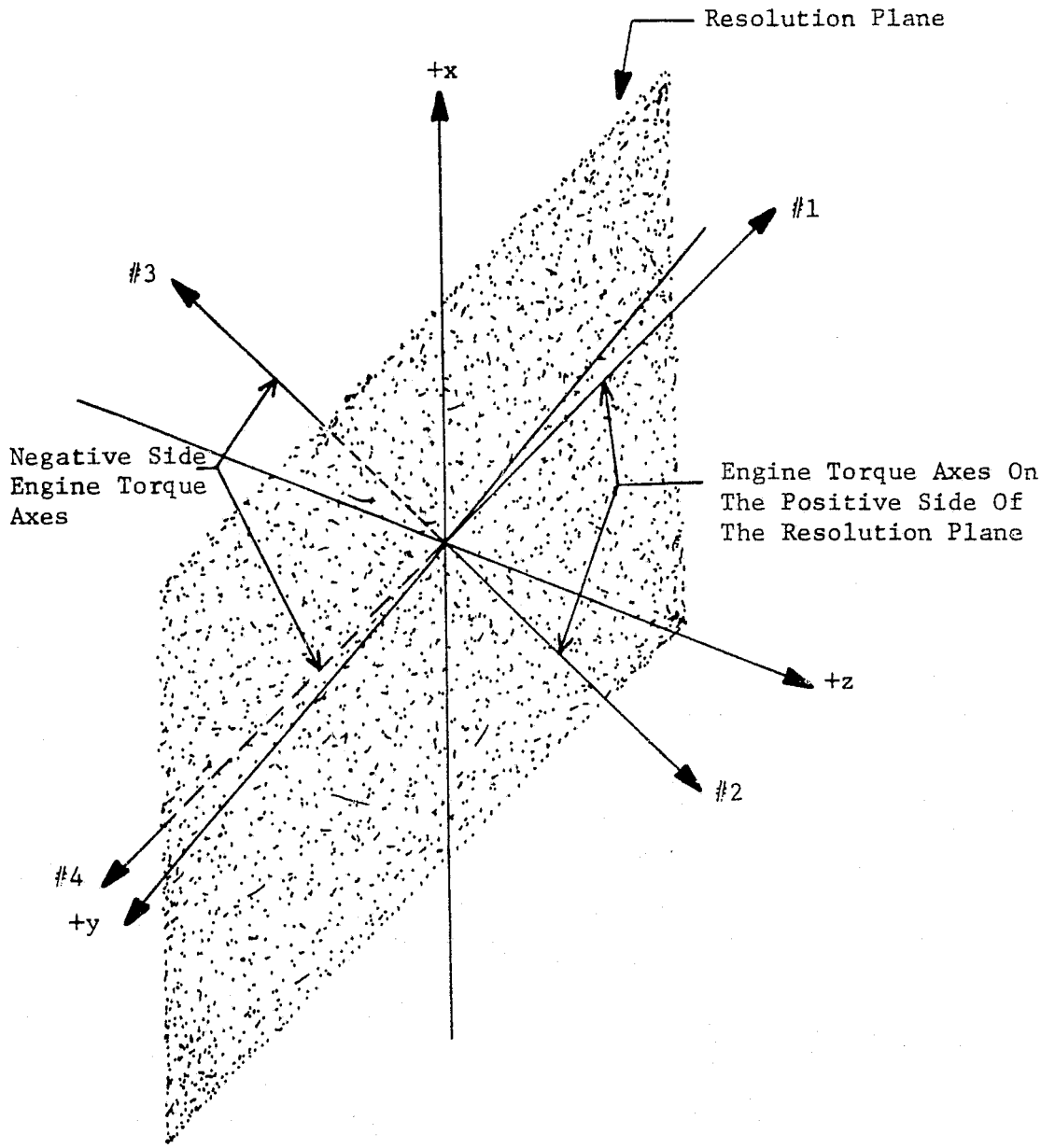

Figure IV-11. The Resolution Plane Perpendicular to the z Axis.

As mentioned earlier, these engine torque axes will, with one exception, always occur in symmetrical pairs. The exception occurs when both members of a pair of engine torque axes coincide with the vehicle axis from which errors are being resolved. This would occur in the example of Figure IV-11 if engine torque axis #1 were not in its present position but, instead, was coincident with the z axis.

In order to keep the vector sum of the errors in the engine torque axes equal to the error in the vehicle axis under consideration, the transformations are divided by the number of pairs of engine torque axes that are eligible for resolution from a particular vehicle axis. The section succeeding this one will explain the number of symmetrical engine torque axes eligible for resolution from the positive and negative portions of each of the vehicle axes. Section D will also offer a description of the positions of the engine torque axes and the transformations into each of those axes.

D. Angular Descriptions of the Positions of the Engine Torque Axes

To be completely specified, transformations from vehicle coordinate axes to engine torque axes derived in the preceding section require only the positions of the engine torque axes. This section endeavors to describe the positions of the engine torque axes for each of the configurations from Chapter III. The angles between the three vehicle coordinate axes and each engine torque axis are required for the transformations. These angles are illustrated in this section and derived where necessary. The method discussed in Section C of

this chapter which determines the number of engine torque axes to be resolved into from a particular vehicle coordinate axis will be referred to as the resolution plane test. The results of this test for each vehicle coordinate axis will be listed with the defining angular positions of the engine torque axes and several of the transformations into the engine torque axes. The angular positions of the engine torque axes for the 6 engine model and the 4 engine model are explained in more detail than the other configurations. This is due to the fact that the angular positions for the models with larger numbers of engines are, in most cases, similar or exactly like the positions of these models.

To illustrate the angular positions of the engine torque axes for the 6 engine model let us re-examine the thruster positions of this model. Figure IV-12 shows the thruster placements and the engine torque axes for thrusters 3, 4, 5, and 6. Thrusters 1 and 2 are of type 1 as defined in Section B of this chapter, while thrusters 3, 4, 5 and 6 are of type 2. Thrusters 1 and 2 have engine torque axes which are coincident with the y axis and the angular positions of these axes are obvious. The engine torque axes for thrusters 3-6 lie in the x-z plane and are not quite as obvious.

In all subsequent discussion, when reference is made to the angles which describe the position of an engine torque axis, the subscript 1 with an angle denotes the angle between the x vehicle axis and the engine torque axis in question. Likewise, a subscript 2 denotes the angle between the y vehicle axis and the engine torque axis,

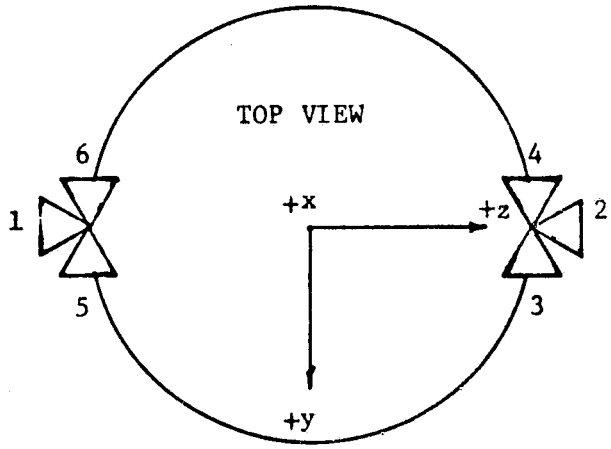

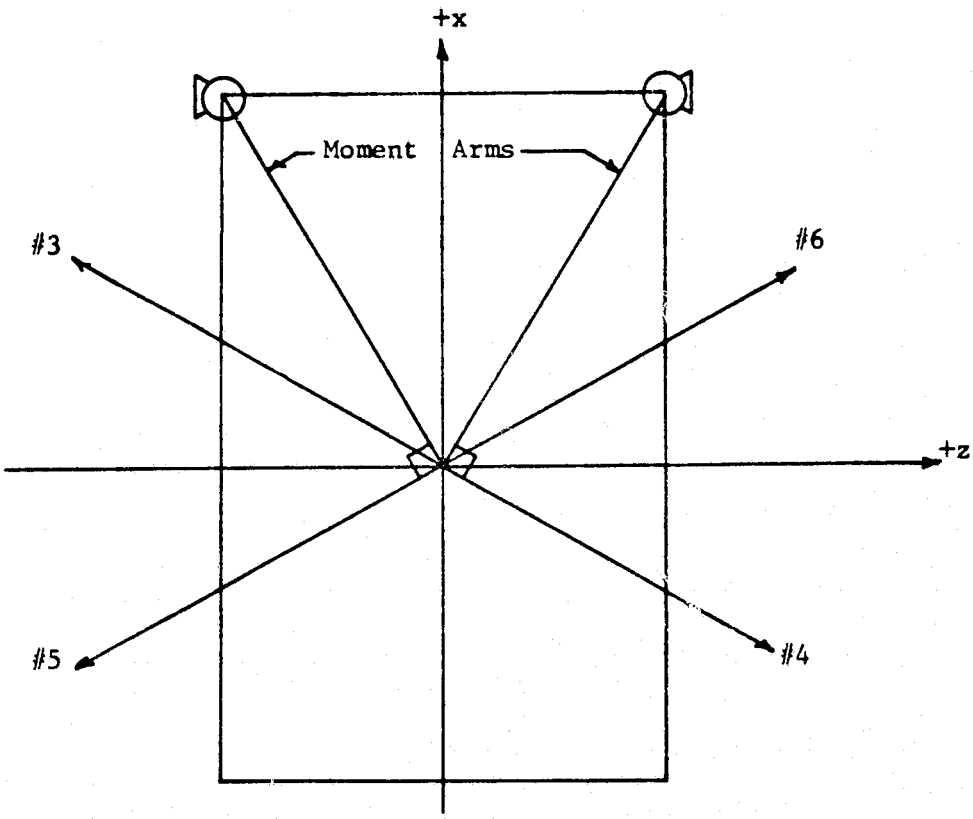

Figure IV-12. Thruster Placements and Engine Torque Axes for the 6 Engine Model.

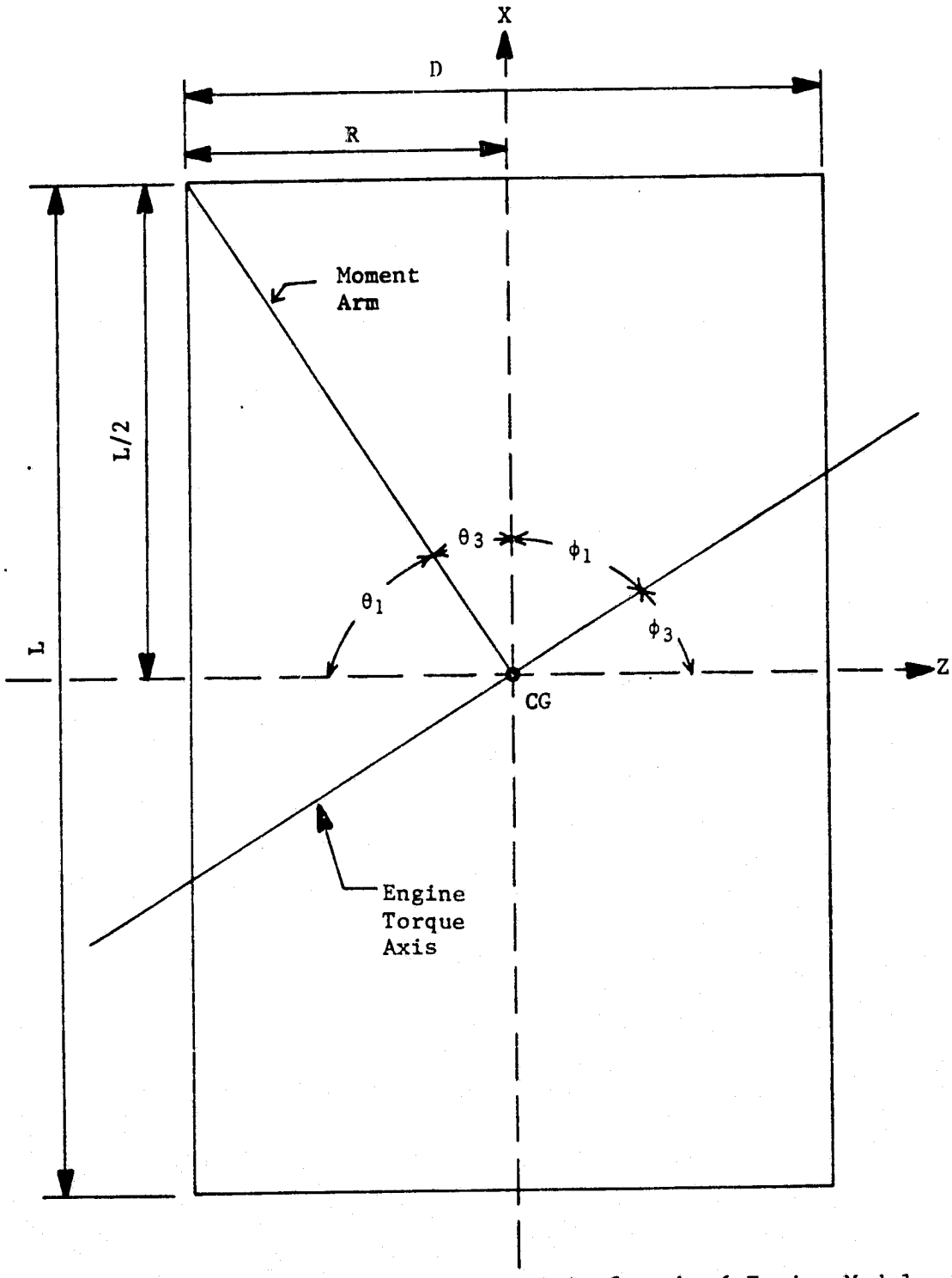

Figure IV-13. Detail of Engine Torque Axis for the 6 Engine Model.

and the subscript 3 indicates the angle measured from the z vehicle axis. Figure IV-13 shows the moment arm-engine torque axis-vehicle relationship in more detail for the 6 engine model. Consider angle ϕ_1 which describes the position of the engine torque axis with respect to the x vehicle axis. Angles ϕ_1 and θ_1 are equal, so if θ_1 is determined, then ϕ_1 is known. The laws of plane geometry determine θ_1 and the results are shown in Equation (IV-9), where L is the length of the vehicle and R is the radius of the vehicle.

$$\phi_1 = \theta_1 = \tan^{-1}\left[\frac{L/2.}{R}\right] \qquad \text{(IV-9)}$$

Since angles ϕ_1 and ϕ_3 form a right angle, Equation (IV-10) defines ϕ_3 and θ_3.

$$\phi_3 = \theta_3 = 90° - \phi_1 = 90° - \tan^{-1}\left[\frac{L/2.}{R}\right] \qquad \text{(IV-10)}$$

ϕ_3 describes the position of the engine torque axis shown in Figure IV-13 with respect to the z vehicle axis. The third angle necessary for a complete angular description of the engine torque axis is ϕ_2, the angle between the engine torque axis and the y vehicle axis. Since the engine torque axis lies in the x-z plane, the specification of ϕ_2 is simply a right angle. Figure IV-14 shows all six engine torque axes and lists the angular specifications for each one. Only the portions of the engine torque axes which exist about the positive parts of each vehicle axis are shown. The vehicle coordinate axes are shown as solid lines and the engine torque axes are shown as dashed lines with the

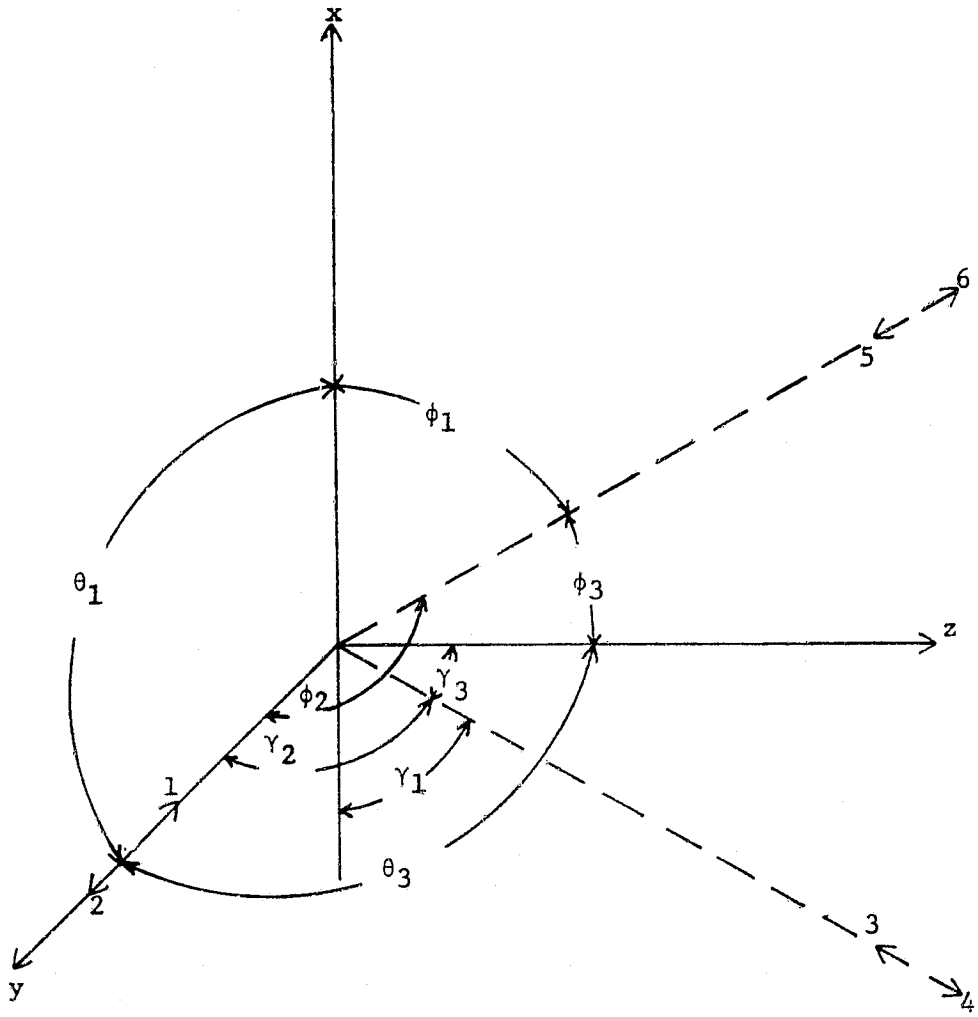

$\phi_1 = \gamma_1 = \tan^{-1} \frac{L/2}{R}$ $\qquad$ $\theta_1 = 90°$

$\phi_2 = \gamma_2 = 90°$ $\qquad$ $\theta_2 = 0°$

$\phi_3 = \gamma_3 = 90$ $\qquad$ $\theta_3 = 90°$

Figure IV-14. Engine Torque Axes for the 6 Engine Model.

exception of axes 1 and 2, which coincide with the y vehicle axis. The arrowheads with numbers by them on the engine torque axes indicate the positive direction of the axes as defined in Section A of this chapter. The dual arrowheads on each axis indicates that two engine torque axes are coincident. The part of each particular vehicle axis from which each angle is measured is intended to help show what part of three-dimensional space the engine torque axis lies in. In this case, angle γ_1 is measured from the negative x axis to show that engine torque axis 4 lies below the y-z plane.

Noting Figure IV-14, consider the resolution plane test (Section C, Chapter IV). For this consideration, the axes with arrows pointing to the origin must be considered to extend through and past the origin in the directions indicated by the arrows. If the resolution plane were placed perpendicular to the x axis first it is evident that two engine torque axes, 3 and 6, lie above it and are therefore eligible for resolution from the positive x axis. Likewise, engine torque axes 4 and 5 lie below the resolution plane and are, therefore, eligible for resolution from the negative x axis. Engine torque axes 1 and 2 are not eligible for resolution from any part of the x axis since they lie in the resolution plane. Next, the resolution plane is placed perpendicular to the y axis. In this case, torque axis 2 lies on the positive side of the resolution plane and torque axis 1 lies on the negative side. It is obvious which engine torque axis each side of the y axis resolves into. The other four engine torque axes lie in the resolution plane and are, therefore, not eligible for resolution from

C.2

the y axis. When the resolution plane is finally placed perpendicular to the z vehicle axis, it can be seen that engine torque axes 4 and 6 lie on the positive side and axes 3 and 5 lie on the negative side of the resolution plane. This indicates that the positive z axis resolves into engine torque axes 4 and 6 and the negative z axis resolves into axes 3 and 5.

As the resolution plane was placed perpendicular to each vehicle coordinate axis, only a single pair of symmetrical engine torque axes existed on each side of the plane. According to the rules set up for the resolution plane test, this indicates that the resolution transformations are to be divided by one. Recalling Equation (IV-8) as the basic vehicle axis-to-engine torque axis error transformation, the transformations for the 6 engine model are given by Equations (IV-11) - (IV-16). The subscripts indicate which axis the transformation applies to and ϕ_i, γ_i, and θ_i (i = 1, 2, or 3) are the angular descriptions of the individual engine torque axes.

$$XT_{1,2} = \left[\frac{\cos(\theta_1)}{1 + \cos(2\theta_1)}\right] = 0, \text{ since } \theta_1 = 90° \qquad \text{(IV-11)}$$

$$YT_{1,2} = \left[\frac{\cos(\theta_2)}{1 + \cos(2\theta_2)}\right] = 1, \text{ since } \theta_2 = 0° \qquad \text{(IV-12)}$$

$$ZT_{1,2} = \left[\frac{\cos(\theta_3)}{1 + \cos(2\theta_3)}\right] = 0, \text{ since } \theta_3 = 90° \qquad \text{(IV-13)}$$

$$XT_{3,4,5,6} = \left[\frac{\cos(\phi_1)}{1 + \cos(2\phi_1)}\right] \tag{IV-14}$$

$$YT_{3,4,5,6} = \left[\frac{\cos(\phi_2)}{1 + \cos(2\phi_2)}\right] \tag{IV-15}$$

$$ZT_{3,4,5,6} = \left[\frac{\cos(\phi_3)}{1 + \cos(2\phi_3)}\right] \tag{IV-16}$$

The engine torque axes of the 4 engine model are somewhat different from those of the 6 engine model. The engine placements for the 4 engine model are type 3 placements which cause torques about all three vehicle coordinate axes. The engine torque axes shown in Figure IV-15 appear to be exactly like those of the 6 engine model. But, note the different moment arm length, which affects the slope of the axes, and the different orientation of the engine torque axes with respect to the vehicle coordinate axes. There are actually four engine torque axes shown in Figure IV-15. The view shown causes two of the axes to overlap. Again, if θ_1 can be determined, ϕ_1 will be known. If θ_1 is to be determined by the same method used for the 6 engine model, R_1, the effective moment arm about the x axis, must be known. Figure IV-16 gives a more detailed view of R_1 from the top. R_1 can be determined by the method listed below.

$$|\overline{AB}| = |\overline{BC}| = |\overline{CD}| = |\overline{DA}| \tag{IV-17}$$

$$|\overline{BD}| = |\overline{AC}| = 2R = \text{Diameter of the Vehicle} \tag{IV-18}$$

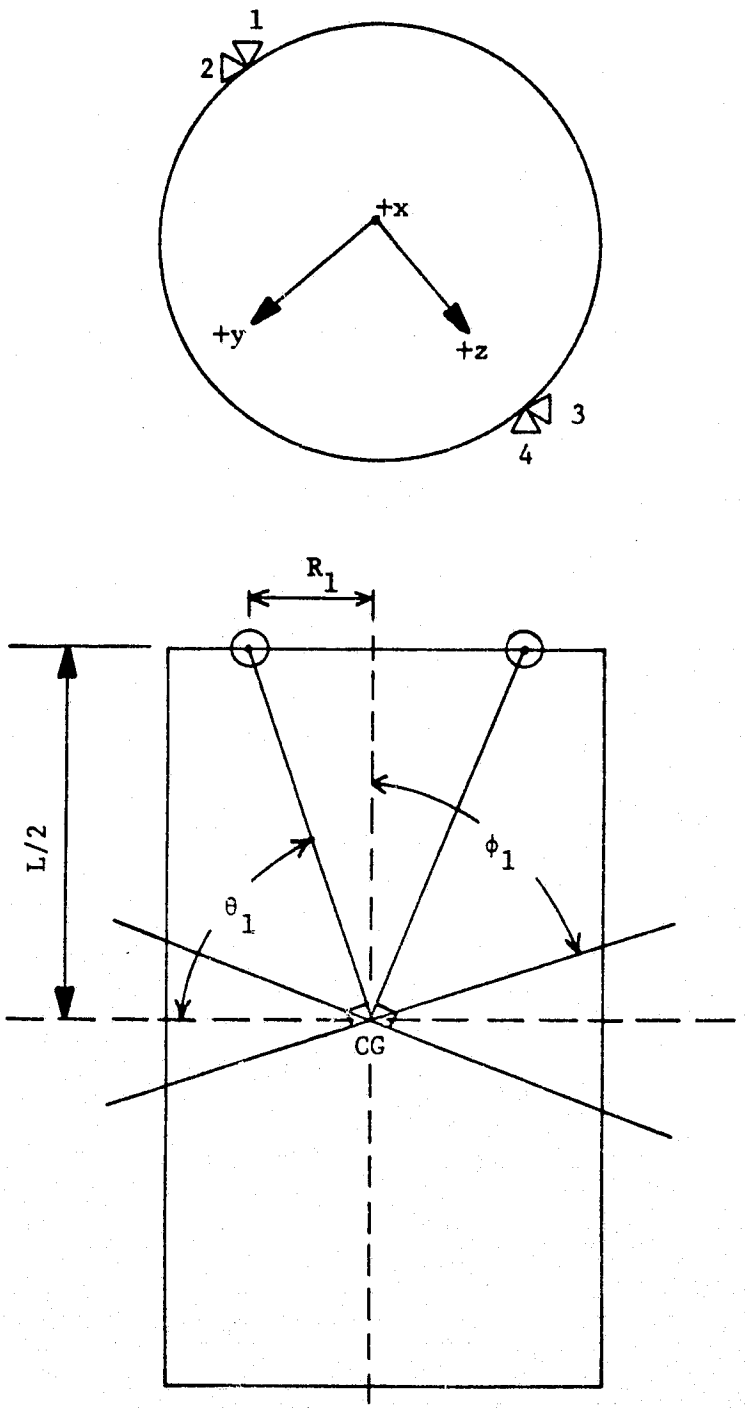

Figure IV-15. Oblique View of the Engine Torque Axes for the 4 Engine Model.

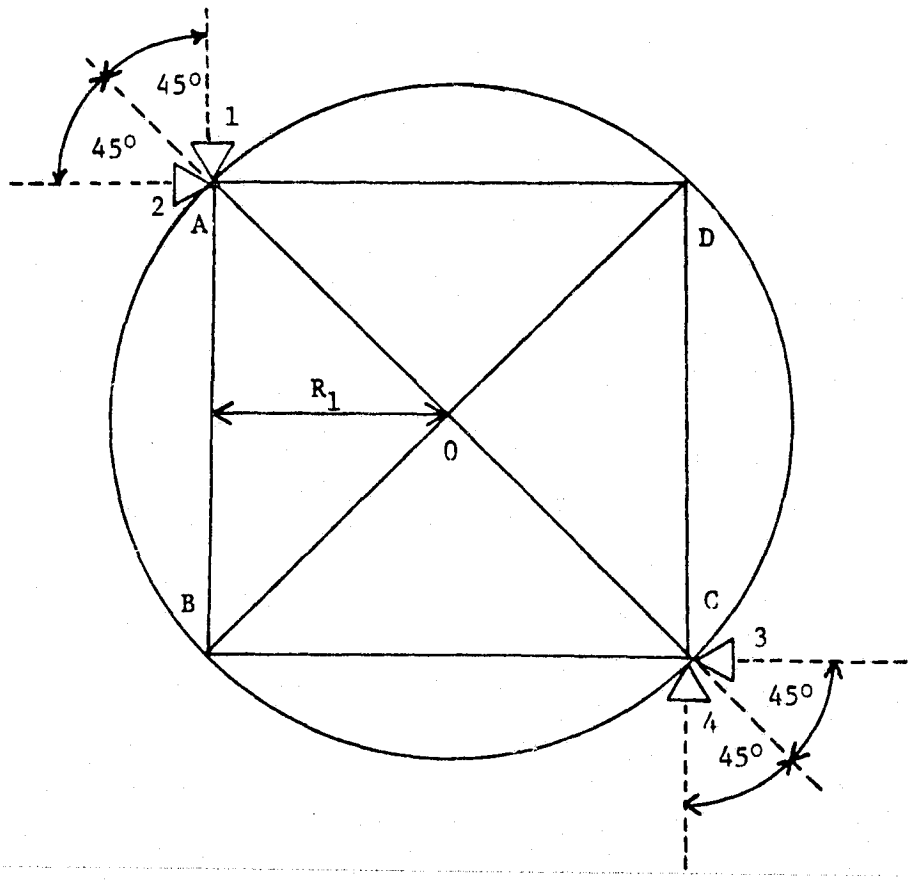

Figure IV-16. Effective Moment Arm About the x̄-Axis of the 4 Engine Model.

$$|\overline{OA}| = |\overline{OB}| = |\overline{OC}| = |\overline{OD}| = R = \text{Radius of the Vehicle} \quad \text{(IV-19)}$$

$$|\overline{AB}| = \sqrt{(|\overline{AO}|)^2 + (|\overline{OB}|)^2} = \sqrt{R^2 + R^2} = \sqrt{2R^2} = \sqrt{2}\,R \quad \text{(IV-20)}$$

Since R_1 bisects the line segment $\overline{AB}$

$$R_1 = 1/2\ |AB| = \frac{\sqrt{2}R}{2} = \frac{R}{\sqrt{2}} \quad \text{(IV-21)}$$

Now that R_1 is known, ϕ_1, the angle between each of the engine torque axes and the x-axis, can be calculated.

$$\phi_1 = \theta_1 = \tan^{-1}\left[\frac{(L/2)}{R_1}\right] \quad \text{(IV-22)}$$

Substituting for R_1 from Equation (IV-21),

$$\phi_1 = \tan^{-1}\left[\frac{L/2}{R/\sqrt{2}}\right] = \tan^{-1}\left[\frac{L}{\sqrt{2}R}\right] \quad \text{(IV-23)}$$

All of the engine torque axes lie the same angular distance from the x-axis because some of the angles are measured from the positive x-axis and some from the negative x-axis, depending on the positive direction of the particular engine torque axis. This will be illustrated in a subsequent figure, but first the other defining angles will be derived.

Figure IV-17 shows the relationships of the four engine torque axes from a view looking down the x axis. In this view the angle between each engine torque axis and the two vehicle axes on either side of it is 45°. But Figure IV-18 shows that each engine torque axis is either lowered or elevated from the y-z plane. This means that the

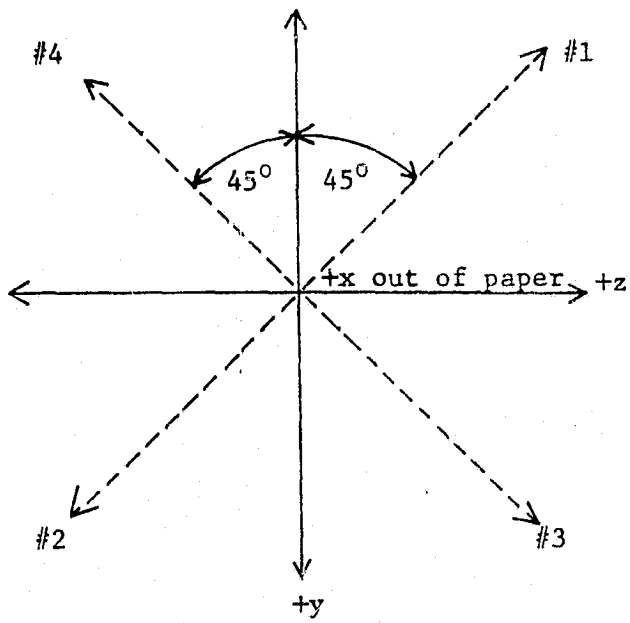

Figure IV-17. Relationship of the Engine Torque Axes for the 4 Engine Model With the y and z Vehicle Axes.

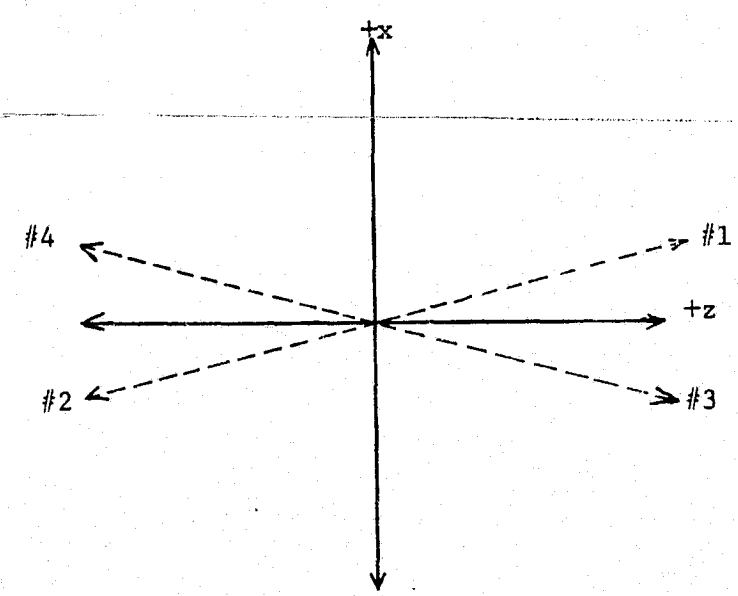

Figure IV-18. Relationship of the Engine Torque Axes for the 4 Engine Model With the y-z Plane.

actual angle between any engine torque axis and either the y or z axis is not exactly 45°. These actual angles are the angles which define the position of the engine torque axes and they are also the angles used in the transformations. The angles between any engine torque axis and the y axis is equal to the angle between that same engine torque axis and the z axis. This is shown in Figure IV-19 where ϕ_2 and ϕ_3 are equal, as well as, γ_2 and γ_3, Ψ_2 and Ψ_3, and θ_2 and θ_3. In addition, all of the angles listed above are equal due to the symmetry of the engine placements.

The derivation of the angles between each engine torque axis and the y and z axes respectively begins with Figure IV-20 where ε_Z is the vehicle axis error to be resolved into the engine torque axis shown. This figure gives an exaggerated view of one of the engine torque axes. Several items in this figure are known quantities. ϕ_1 has already been derived and Figure IV-17 showed that when an engine torque axis is projected onto the y-z plane, it lies 45° from both the y and z axes. Therefore, line segment $|\overline{OD}|$ lies 45° from the y and z axes. First, consider triangle OAD shown in Figure IV-21. Let

$$|\overline{OA}| = |\overline{AD}| = a \tag{IV-24}$$

Therefore,

$$|\overline{OD}| = \sqrt{a^2 + a^2} = \sqrt{2a^2} = \sqrt{2}\, a \tag{IV-25}$$

Now consider triangle OCD shown in Figure IV-22.

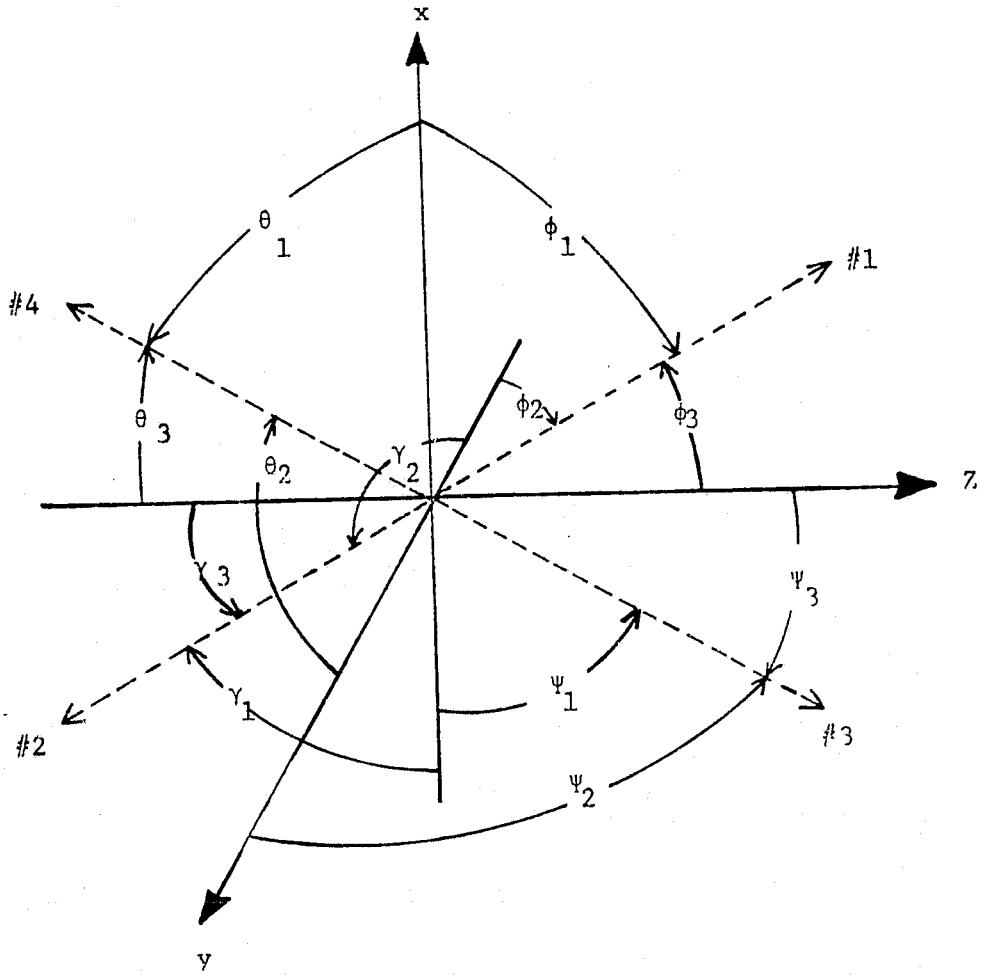

Figure IV-19. Engine Torque Axes for the 4 Engine Model.

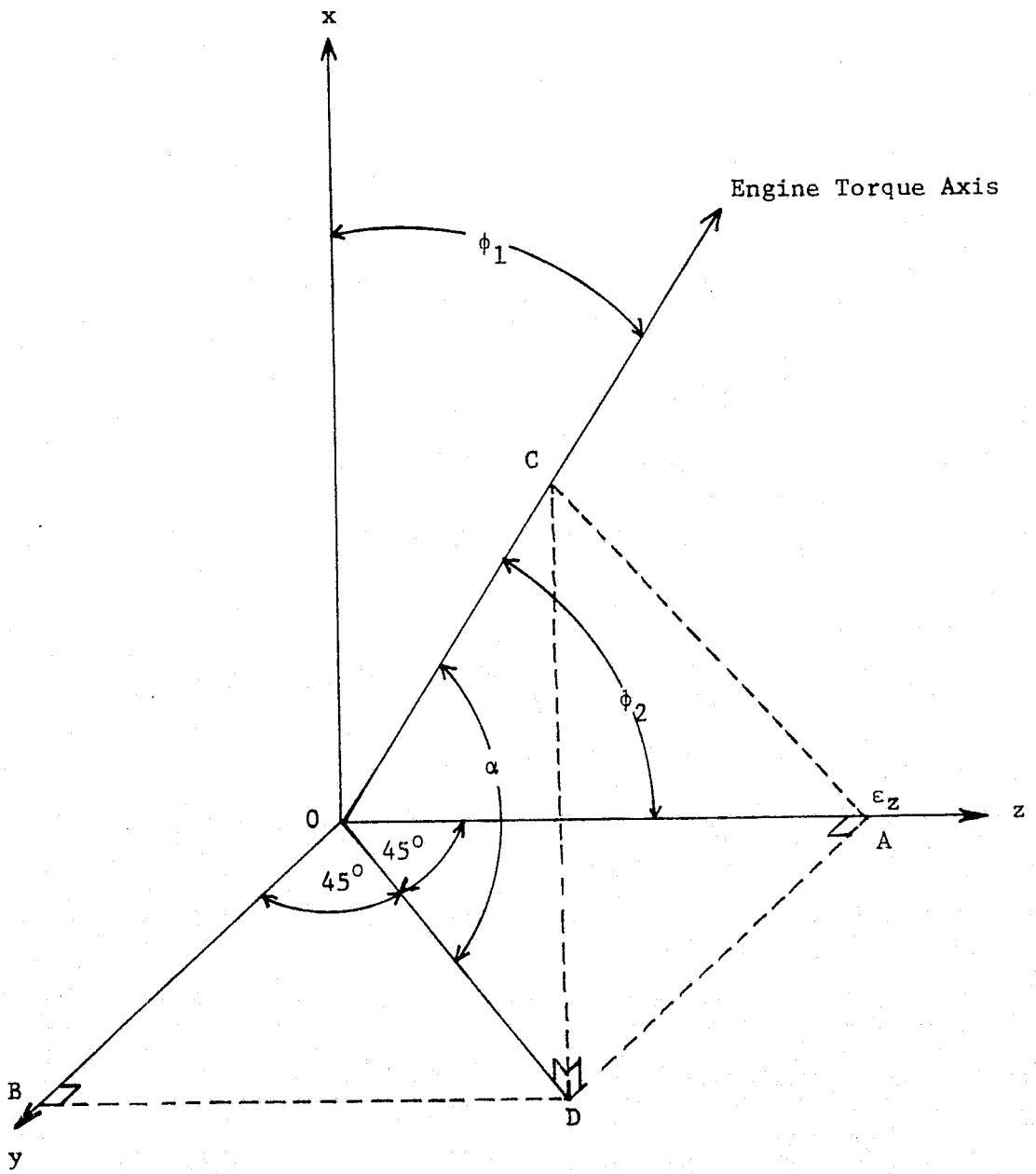

Figure IV-20. Detail View of an Engine Torque Axis.

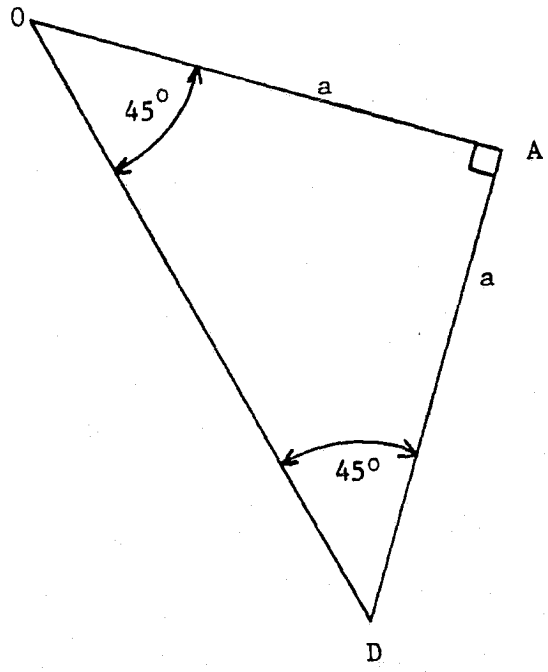

Figure IV-21. Triangle OAD.

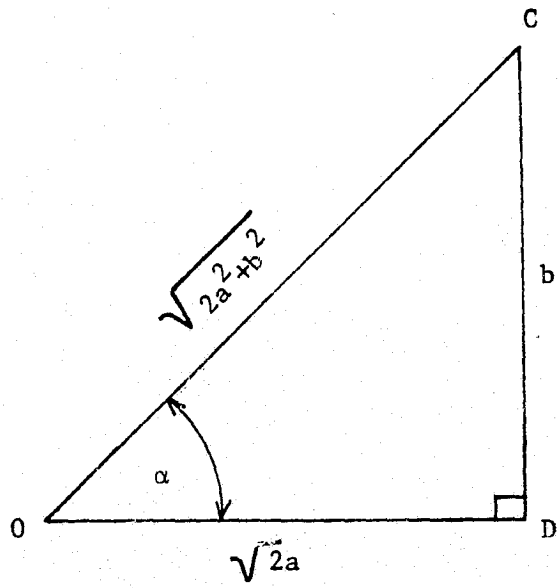

Figure IV-22. Triangle OCD.

$$\tan(\alpha) = \frac{|\overline{CD}|}{|\overline{OD}|} \tag{IV-26}$$

Substituting for $|\overline{OD}|$ from Equation (IV-25),

$$\tan(\alpha) = \frac{|\overline{CD}|}{\sqrt{2}\ a} \tag{IV-27}$$

Therefore,

$$|\overline{CD}| = \sqrt{2}\ a \tan(\alpha) \tag{IV-28}$$

Let

$$\sqrt{2}\ a \tan(\alpha) = b \tag{IV-29}$$

Now,

$$|\overline{OC}| = \sqrt{\left(\sqrt{2}\ a\right)^2 + \left(b\right)^2} = \sqrt{2a^2 + b^2} \tag{IV-30}$$

Next, consider triangle OCA shown in Figure IV-23. Line segment $|\overline{CE}|$ is the perpendicular bisector of line $|\overline{OA}|$. Therefore, from Equation (IV-24),

$$|\overline{OE}| = |\overline{EA}| = \frac{a}{2} \tag{IV-31}$$

Using the result of Equations (IV-30) and (IV-31) and the Pythagorean Theorem, $|\overline{CE}|$ can be determined.

$$|\overline{OC}| = \sqrt{\left(|\overline{OE}|\right)^2 + \left(|CE|\right)^2} \tag{IV-32}$$

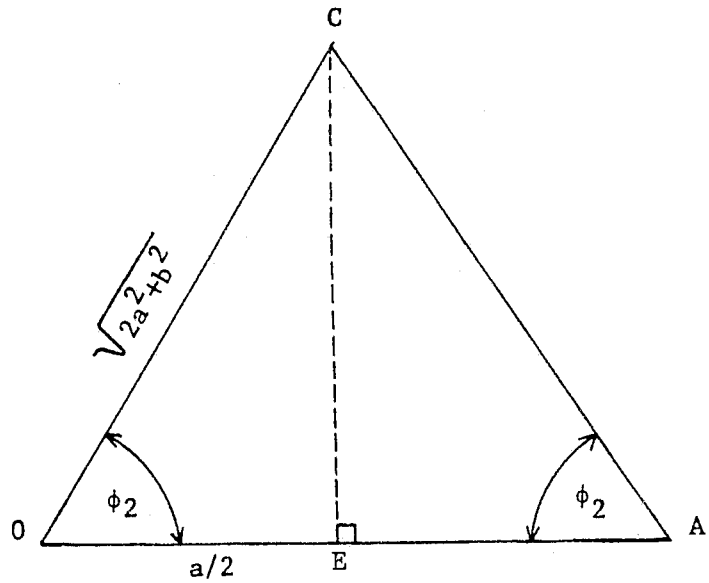

Figure IV-23. Triangle OCA.

$$\left(|\overline{CE}|\right)^2 = \left(|\overline{OC}|\right)^2 - \left(|\overline{OE}|\right)^2 \tag{IV-33}$$

$$|\overline{CE}| = \sqrt{\left(\sqrt{2a^2 + b^2}\right)^2 - \left(\frac{a}{2}\right)^2} \tag{IV-34}$$

$$|\overline{CE}| = \sqrt{2a^2 + b^2 - \frac{a^2}{4}} \tag{IV-35}$$

Substituting for b from Equation (IV-29),

$$|\overline{CE}| = \sqrt{2a^2 + \left[\sqrt{2}\ a\ \tan(\alpha)\right]^2 - \frac{a^2}{4}} \tag{IV-36}$$

$$|\overline{CE}| = \frac{a}{2}\sqrt{7 + 8\ \tan^2(\alpha)} \tag{IV-37}$$

Now, ϕ_2 may be determined,

$$\tan(\phi_2) = \frac{|\overline{CE}|}{|\overline{OE}|} \tag{IV-38}$$

Substituting for $|\overline{CE}|$ and $|\overline{OE}|$ from Equations (IV-37) and (IV-31),

$$\tan(\phi_2) = \frac{\frac{a}{2}\sqrt{7 + 8\tan^2(\alpha)}}{\frac{a}{2}} \tag{IV-39}$$

Therefore,

$$\phi_2 = \tan^{-1}\left[\sqrt{7 + 8\tan^2(\alpha)}\right] \tag{IV-40}$$

Also, it is known that,

$$\alpha = 90° - \phi_1 \tag{IV-41}$$

Therefore,

$$\phi_2 = \tan^{-1}\left[\sqrt{7 + 8\tan^2(90° - \phi_1)}\right] \tag{IV-42}$$

Since ϕ_2 and ϕ_3 are equal, all of the angular measurements for the 4 engine model have been defined.

$$\phi_1 = \gamma_1 = \Psi_1 = \theta_1 = \tan^{-1}\left[\frac{L}{\sqrt{2}\,R}\right] \tag{IV-43}$$

$$\phi_2 = \gamma_2 = \Psi_2 = \theta_2 = \tan^{-1}\left[\sqrt{7 + 8\tan^2(90° - \phi_1)}\right] \tag{IV-44}$$

$$\phi_3 = \gamma_3 = \Psi_3 = \theta_3 = \tan^{-1}\left[\sqrt{7 + 8\tan^2(90° - \phi_1)}\right] \tag{IV-45}$$

The resolution plane test must be applied to this model before the transformations can be finalized. The results of this test indic

that all three vehicle coordinate axes have only one pair of symmetrical engine torque axes into which their errors may be resolved. According to the rules of the resolution plane test, this means that the transformations from each of the vehicle axes to each of the engine torque axes should be divided by unity. These transformations are listed in Equations (IV-46) - (IV-48).

$$XT_{1,2,3,4} = \left[\frac{\cos(\phi_1)}{1 + \cos(2\phi_1)}\right] \tag{IV-46}$$

$$YT_{1,2,3,4} = \left[\frac{\cos(\phi_2)}{1 + \cos(2\phi_2)}\right] \tag{IV-47}$$

$$ZT_{1,2,3,4} = \left[\frac{\cos(\phi_3)}{1 + \cos(2\phi_3)}\right] \tag{IV-48}$$

The transformation equations for the remaining models are of the same form as the ones for the 6 and 4 engine models. The only difference in these transformations and transformations of subsequent models is the division by the proper number of symmetrical pairs of engine torque axes as determined by the resolution plane test. Since the transformations are similar in form, they will not be listed in equation form hereafter. Instead, only the results of the resolution plane test will be listed. This will reveal the number each transformation should be divided by.

The engine torque axes of 8 engine model #1 are very similar to those of the 4 engine model. Since there are eight engines in this

configuration, as shown in Figure III-6, there are eight separate engine torque axes. All eight axes lie along the 4 lines which define the positions of the engine torque axes for the 4 engine model. The difference is that there are two engine torque axes lying along each line with positive polarities in opposite directions. This is shown in Figure IV-24 where the numbers by the arrowheads indicate the positive polarities of the individual engine torque axes.

Only part of each engine torque axis is shown in Figure IV-24. The arrowheads pointing toward the origin indicate engine torque axes with positive polarities in that direction which extend through the origin. This is mentioned for the sake of the application of the resolution plane test. As the resolution plane is placed perpendicular to each vehicle axis, in each case two symmetrical pairs of engine torque axes are lying on each side of it. The rules of this test indicate that each of the transformations from vehicle axes to engine torque axes should be divided by two. The transformation equations are like those of the 4 engine model given by Equations (IV-46) - (IV-48) except they are all divided by two.

Eight engine model #2 utilizes thrusters of type 1 and 2 as shown in Figure III-7. Thrusters 1-4 of this model are identical to thrusters 3-6 of the 6 engine model and, therefore, have identical engine torque axes. Thrusters 4-8 of 8 engine model #2 are of type 1 and, therefore, have engine torque axes which lie in the y-z plane as described earlier in this chapter. The orientation of the engine torque axes for thrusters 4-8 with respect to the y-z plane is shown

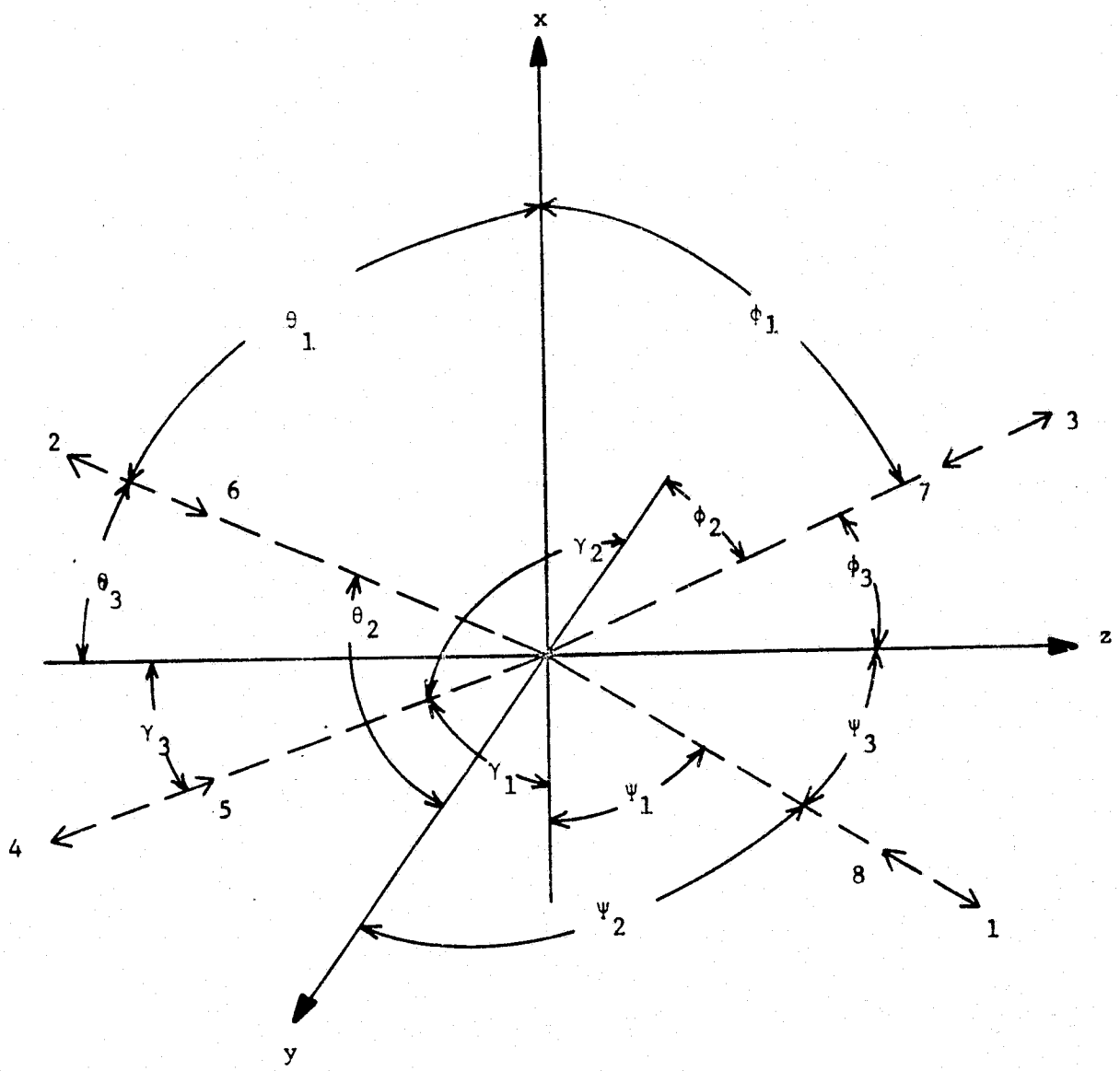

Figure IV-24. Engine Torque Axes for 8 Engine Model #1.

in Figure IV-25. All of the engine torque axes are shown in Figure IV-26.

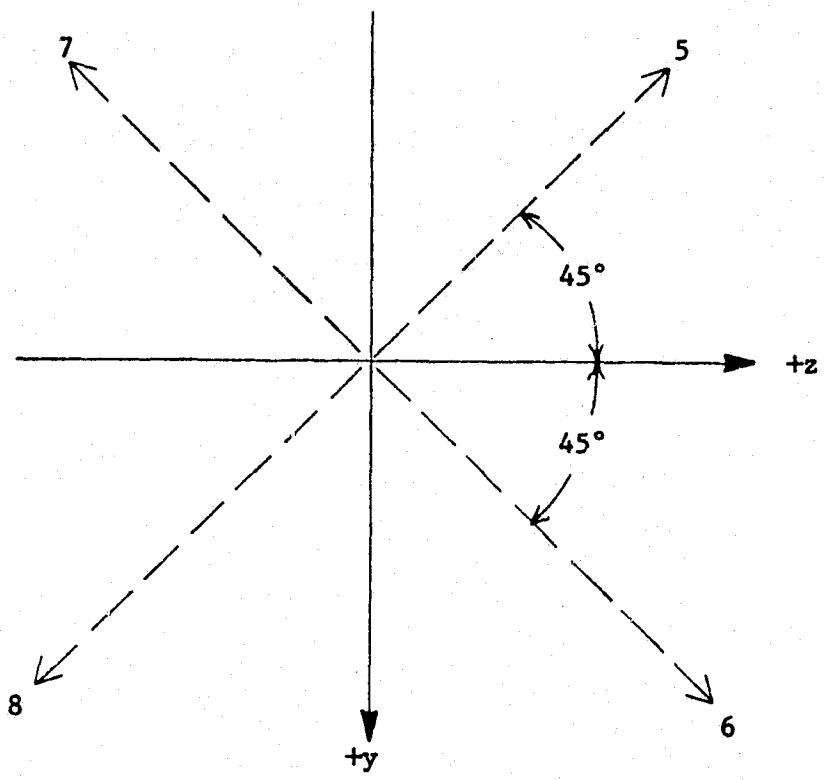

Figure IV-25. Engine Torque Axes for Thrusters 4-8 of 8 Engine Model #2.

Again, Figure IV-26 does not show each engine torque axis in its entirety. Instead, just enough is shown so that the angular positions may be defined. The angles shown in Figure IV-26 are defined in Equations (IV-49) - (IV-54).

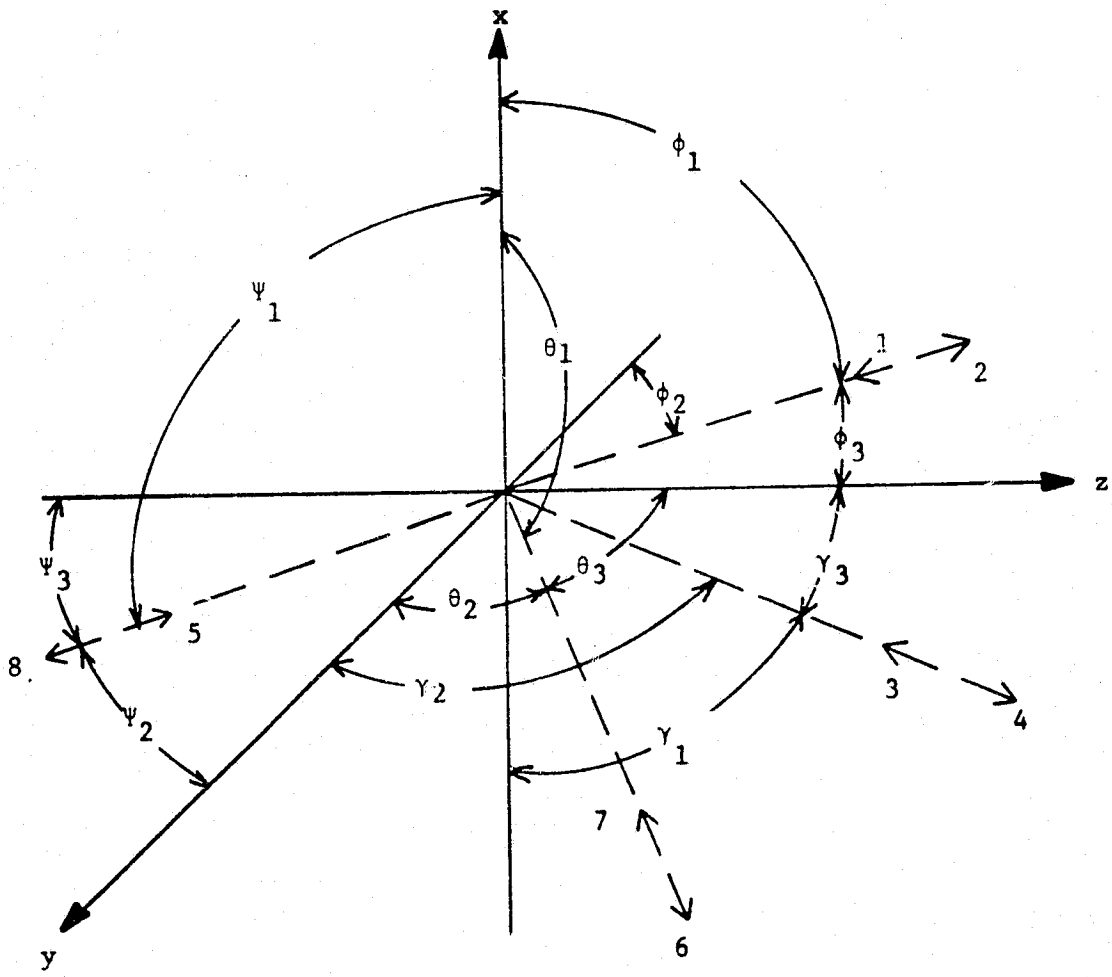

Figure IV-26. Engine Torque Axes for 8 Engine Model #2.

$$\phi_1 = \gamma_1 = \tan^{-1}\left[\frac{L}{2R}\right] \tag{IV-49}$$

$$\phi_2 = \gamma_2 = 90° \tag{IV-50}$$

$$\phi_3 = \gamma_3 = 90° \tag{IV-51}$$

$$\theta_1 = \Psi_1 = 90° \tag{IV-52}$$

$$\theta_2 = \Psi_2 = 45° \tag{IV-53}$$

$$\theta_3 = \Psi_3 = 45° \tag{IV-54}$$

The resolution plane test reveals that there is only one symmetrical pair of axes to be resolved into from both the x and y vehicle axes. There are two symmetrical pairs of engine torque axes to be resolved into from the z axis, therefore, the z axis transformation must be divided by two.

Twelve engine model #1, shown in Figure III-9, has engine torque axes which are composed of two sets of axes like those for the 6 engine model. Figures IV-27 and IV-28 show these axes. They are shown in two separate figures to eliminate confusion over the angular measurements shown. The angular measurements are defined in Equations (IV-55) - (IV-66).

$$\alpha_1 = 90° \tag{IV-55}$$

$$\alpha_2 = 0° \tag{IV-56}$$

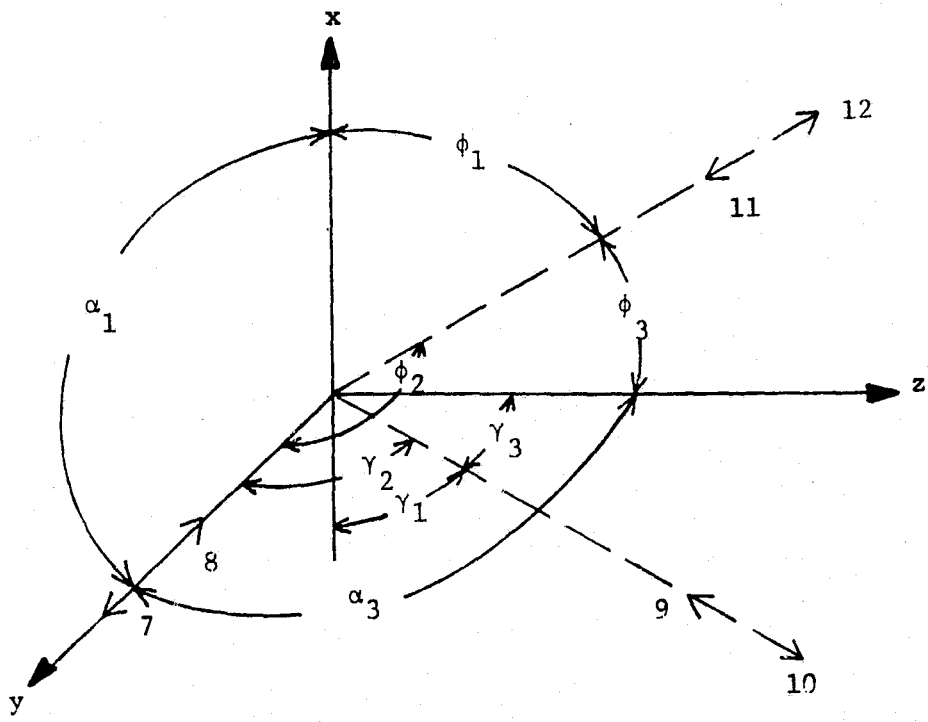

Figure IV-27. Engine Torque Axes for Thrusters 7-12 of 12 Engine Model #1.

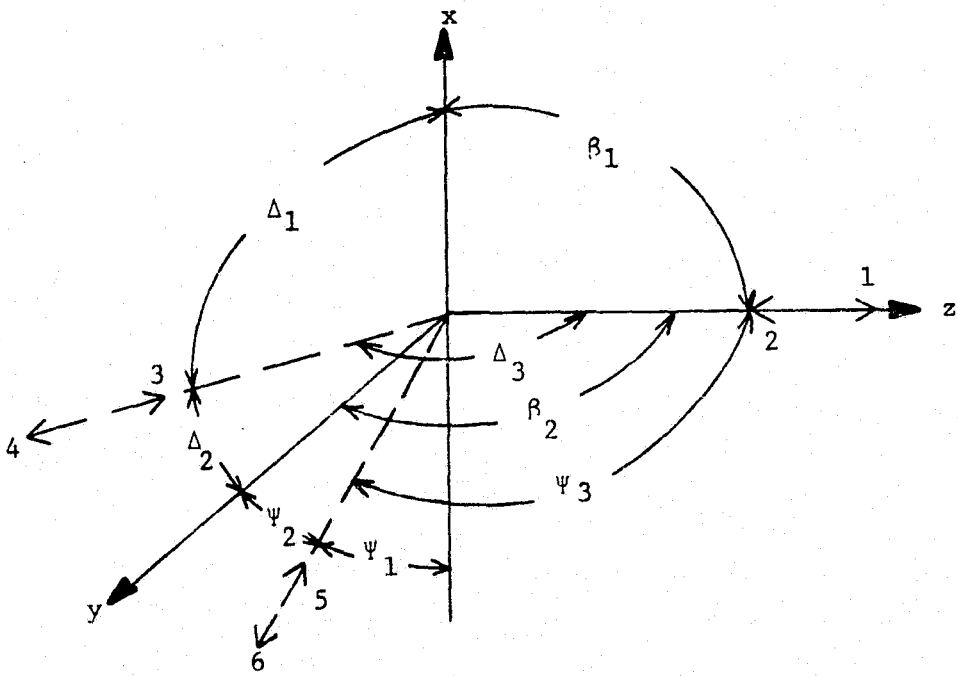

Figure IV-28. Engine Torque Axes for Thrusters 1-6 of 12 Engine Model #1.

$$\alpha_3 = 90° \tag{IV-57}$$

$$\beta_1 = 90° \tag{IV-58}$$

$$\beta_2 = 90° \tag{IV-59}$$

$$\beta_3 = 0° \tag{IV-60}$$

$$\phi_1 = \gamma_1 = \tan^{-1}\left[\frac{L}{2R}\right] \tag{IV-61}$$

$$\phi_2 = \gamma_2 = 90° \tag{IV-62}$$

$$\phi_3 = \gamma_3 = 90° - \phi_1 \tag{IV-63}$$

$$\Delta_1 = \Psi_1 = \tan^{-1}\left[\frac{L}{2R}\right] \tag{IV-64}$$

$$\Delta_2 = \Psi_2 = 90° - \Delta_1 \tag{IV-65}$$

$$\Delta_3 = \Psi_3 = 90° \tag{IV-66}$$

The resolution plane test reveals that there are two symmetrical pairs of engine torque axes eligible for resolution from each of the vehicle coordinate axes. Note that there are four engine torque axes coincident with vehicle axes, two each on the y and z axes. According to the conditions of the resolution plane test, an engine torque axis which lies on a vehicle axis counts as one symmetrical pair. For example, if the resolution plane is placed perpendicular to the z axis,

engine torque axes 1, 10, and 12 lie in the space occupied by the positive z axis. Engine torque axes 10 and 12 form one symmetrical pair and axis 1 counts as a second symmetrical pair, therefore, the z axis transformation must be divided by two. This same situation exists for the y axis resolution test. The x axis test has four engine torque axes which form the two symmetrical pairs. Since there are two pairs of axes eligible for resolution from each vehicle axis, each of the transformations must be divided by two.

The engine torque axes for 12 engine model #2 are shown in Figures IV-29 and IV-30. A single figure view of the engine torque axes would be confusing, so they are shown in two figures. The angular measurements for 12 engine model #2 are given by Equations (IV-67) - (IV-71).

$$\phi_1 = \gamma_1 = \tan^{-1}\left[\frac{L}{2R}\right] \tag{IV-67}$$

$$\phi_3 = \gamma_3 = 90° - \phi_1 \tag{IV-68}$$

$$\phi_2 = \gamma_2 = \alpha_1 = \theta_1 = \theta_3 = \beta_1 = \Psi_1 = \Psi_2 = 90° \tag{IV-69}$$

$$\alpha_2 = \alpha_3 = \beta_2 = \beta_3 = 45° \tag{IV-70}$$

$$\theta_2 = \Psi_3 = 0° \tag{IV-71}$$

The resolution plane test indicates that the x axis has only a single pair of symmetrical engine torque axes eligible for resolution. The y axis has two symmetrical pairs and the z axis has three symmetrical

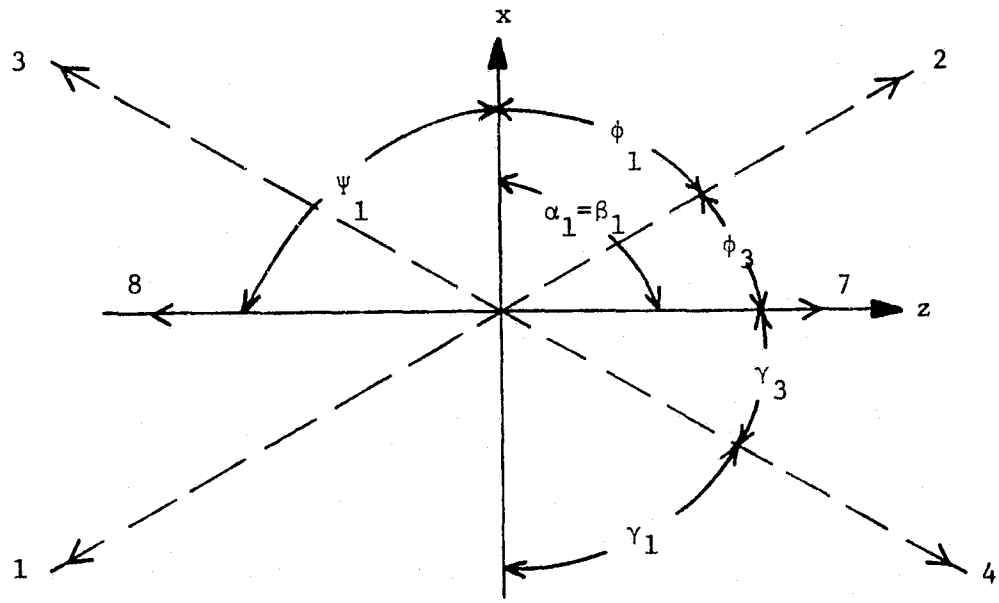

Figure IV-29. Engine Torque Axes for 12 Engine Model #2 Which Lie in the x-z Plane.

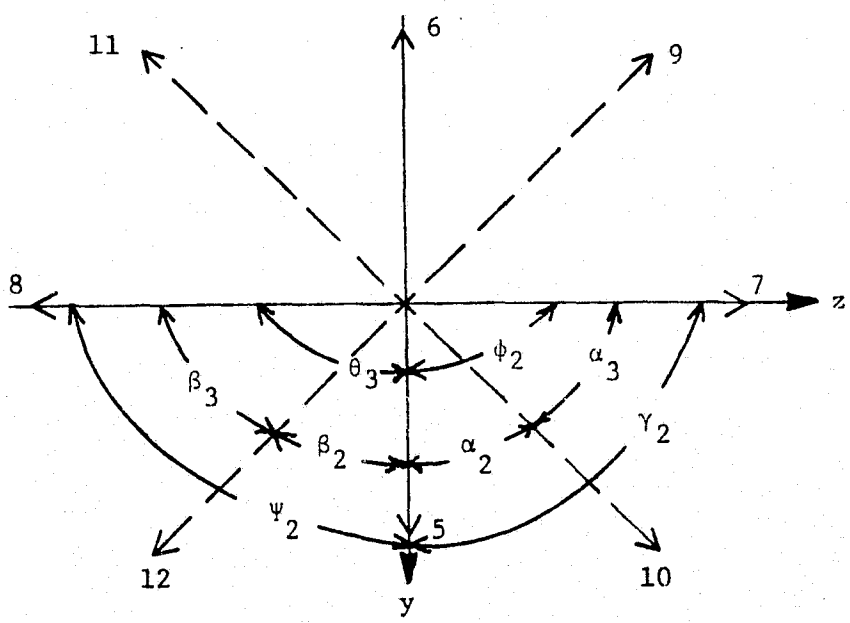

Figure IV-30. Engine Torque Axes for 12 Engine Model #2 Which Lie in the y-z Plane.

pairs. Therefore, the x axis transformation is divided by unity, the y axis transformation by two, and the z axis transformation by three.

The engine torque axes of the 16 engine model are composed of the 12 engine model #1 axes plus four additional ones. Figures IV-27 and IV-28 show the axes from 12 engine model #1 while the four additional axes are shown in Figure IV-31.

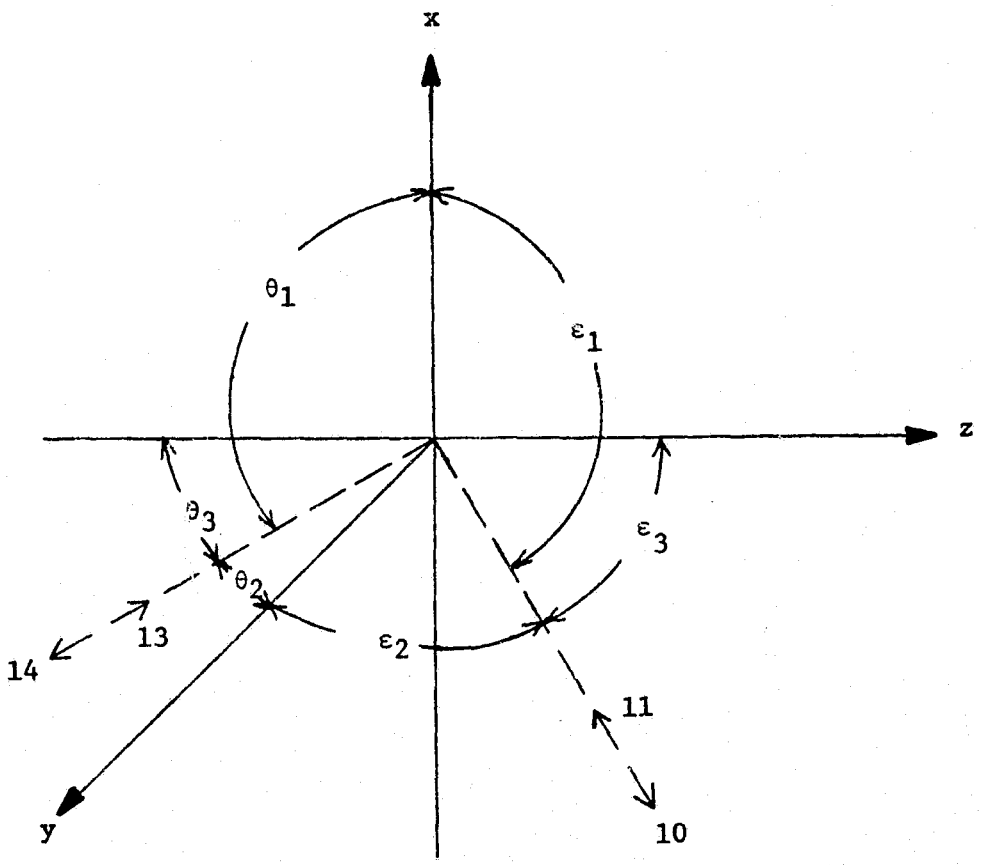

Figure IV-31. Engine Torque Axes 10, 11, 13 and 14 of the 16 Engine Model.

The defining angles for the four additional axes are given by Equations (IV-72) and (IV-73).

$$\theta_1 = \varepsilon_1 = 90° \tag{IV-72}$$

$$\theta_2 = \theta_3 = \varepsilon_2 = \varepsilon_3 = 45° \tag{IV-73}$$

The resolution plane test results for the 16 engine model are different from those of 12 engine model #1. The x axis has two symmetrical pairs eligible for resolution while the y and z axes have three symmetrical pairs eligible. This means that the x axis transformation is divided by two and the y and z axes transformations are divided by three.

The engine torque axes of the 24 engine model are identical to those of the 16 engine model plus eight additional axes. These eight additional axes look like those of the first 8 engine model shown in Figure IV-25. The defining angles of the eight additional axes are given by Equations (IV-74) and (IV-75).

$$\delta_1 = \tan^{-1}\left[\frac{L}{2R}\right] \tag{IV-74}$$

$$\delta_2 = \delta_3 = \tan^{-1}\left[\sqrt{7 + 8\tan^2(\alpha)}\right] \tag{IV-75}$$

The resolution plane test results indicate that there are four symmetrical pairs to resolve into from the x axis while the y and z axes have five symmetrical pairs eligible for resolution. This once

again indicates the numbers which divide the transformations: the x axis transformation by four and the y and z axes transformations by five.

E. Results of Simulations With Engine Torque Axes Error Resolution

The transformation equations spoken of in Section D were implemented in the digital computer simulations for each model. The simulations were run under the same constraints and for the same initial conditions used when the models were tested without engine torque axes error resolution. Again, the attitude control efficiency was monitored by measuring the amount of engine on-time and the average system error for each initial condition case. The results of the simulation runs are listed in Table IV-3. Just as was done in Chapter III, the results are brought into perspective by normalization with respect to the 6 engine model without engine torque axes error resolution. These normalized results are listed in Table IV-4. To make the normalized average results listed in Table IV-4 more meaningful, they are shown in graphical form by Figure IV-32. The points plotted in Figure IV-32 represent the attitude control efficiency of the model whose number is printed beside each point. It is important to note that one of the points plotted represents the performance of the 6 engine model without engine torque axes error resolution. This point is shown for comparison purposes.

The horizontal and vertical dashed lines shown in Figure IV-32 help in understanding the general trends established. Consider first

Initial Conditions	6 Engine Case	4 Engine Case	8 Engine Case #1	8 Engine Case #2	12 Engine Case #1	12 Engine Case #2	16 Engine Case	24 Engine Case
DPX = .1°/Sec DPY=DPZ = .1°/Sec	3.80 .0414	4.50 .0219	3.45 .0304	4.70 .0504	3.70 .0685	3.30 .0666	3.45 .0814	3.70 .0808
DPX=DPY = .1°/Sec DPZ = -.1°/Sec	3.75 .0357	9.50 .0206	3.40 .0326	4.55 .0494	3.55 .0690	3.25 .0585	3.55 .0923	3.40 .0834
DPX = .1°/Sec DPY=DPZ = -.1°/Sec	3.80 .0437	4.60 .0200	3.20 .0308	4.60 .0489	3.55 .0771	3.40 .0738	3.25 .0901	3.30 .0879
DPX = -.1°/Sec DPY=DPZ = -.1°/Sec	3.55 .0345	9.20 .0175	3.25 .0328	4.90 .0499	3.40 .0762	3.20 .0665	3.30 .0833	3.45 .0879
DPX=DPZ = -.1°/Sec DPY = .1°/Sec	3.80 .0414	4.50 .0219	3.45 .0304	4.70 .0504	3.70 .0685	3.30 .0666	3.45 .0814	3.70 .0808
DPX=DPY = -.1°/Sec DPZ = .1°/Sec	3.80 .0437	4.60 .0200	3.20 .0308	4.60 .0489	3.55 .0771	3.40 .0738	3.25 .0901	3.30 .0879
DPX=DPZ = .1°/Sec DPY = -.1°/Sec	3.55 .0345	9.20 .0175	3.25 .0328	4.90 .0499	3.40 .0762	3.20 .0665	3.30 .0833	3.45 .0879
DPX = -.1°/Sec DPY=DPZ = .1°/Sec	3.75 .0357	9.50 .0206	3.40 .0326	4.55 .0494	3.55 .0690	3.25 .0585	3.55 .0923	3.40 .0834
Average On-Time Average ENAVG	3.73 .0388	6.95 .0200	3.33 .0317	4.69 .0497	3.55 .0727	3.29 .0664	3.39 .0868	3.46 .0850

Top number in each box = Engine On-time

Bottom number in each box = ENAVG, the average system error

Table IV-3. Simulation Results for New Configurations With Engine Torque Axes Error Resolution.

Initial Conditions	6 Engine Case	4 Engine Case	8 Engine Case #1	8 Engine Case #2	12 Engine Case #1	12 Engine Case #2	16 Engine Case	24 Engine Case
DPX = .1°/Sec DPY=DPZ = .1°/Sec	1.09 1.08	1.29 .57	.986 .792	1.34 1.31	1.06 1.78	.943 1.73	.986 2.12	1.06 2.1
DPX=DPY = .1°/Sec DPZ = -.1°/Sec	.987 .903	2.5 .518	.895 .825	1.20 1.25	.934 1.75	.855 1.48	.934 2.34	.895 2.11
DPX = .1°/Sec DPY=DPZ = -.1°/Sec	1.06 1.09	1.28 .499	.889 .768	1.28 1.22	.986 1.92	.944 1.84	.903 2.25	.917 2.19
DPX = -.1°/Sec DPY=DPZ = -.1°/Sec	.973 .911	2.52 .462	.89 .865	1.34 1.31	.932 2.01	.877 1.75	.904 2.25	.945 2.32
DPX=DPZ = -.1°/Sec DPY = .1°/Sec	1.09 1.08	1.29 .57	.986 .792	1.34 1.31	1.06 1.78	.943 1.73	.986 2.12	1.06 2.10
DPX=DPY = -.1°/Sec DPZ = .1°/Sec	1.06 1.09	1.28 .499	.889 .768	1.28 1.22	.986 1.92	.944 1.84	.903 2.25	.917 2.19
DPX=DPZ = .1°/Sec DPY = -.1°/Sec	.972 .910	2.52 .462	.89 .865	1.34 1.32	.932 2.01	.877 1.75	.904 2.20	.945 2.32
DPX = -.1°/Sec DPY=DPZ = .1°/Sec	.987 .904	2.5 .518	.895 .825	1.20 1.25	.934 1.75	.855 1.48	.934 2.34	.895 2.11
Average On-Time Average ENAVG	1.02 .995	1.91 .513	.915 .813	1.29 1.27	.975 1.86	.904 1.70	.931 2.23	.951 2.18

Top number in each box = Normalized Engine On-time

Bottom number in each box = Normalized ENAVG, the average system error

Table IV-4. Normalized Simulation Results for New Configurations With Engine Torque Axes Error Resolution.

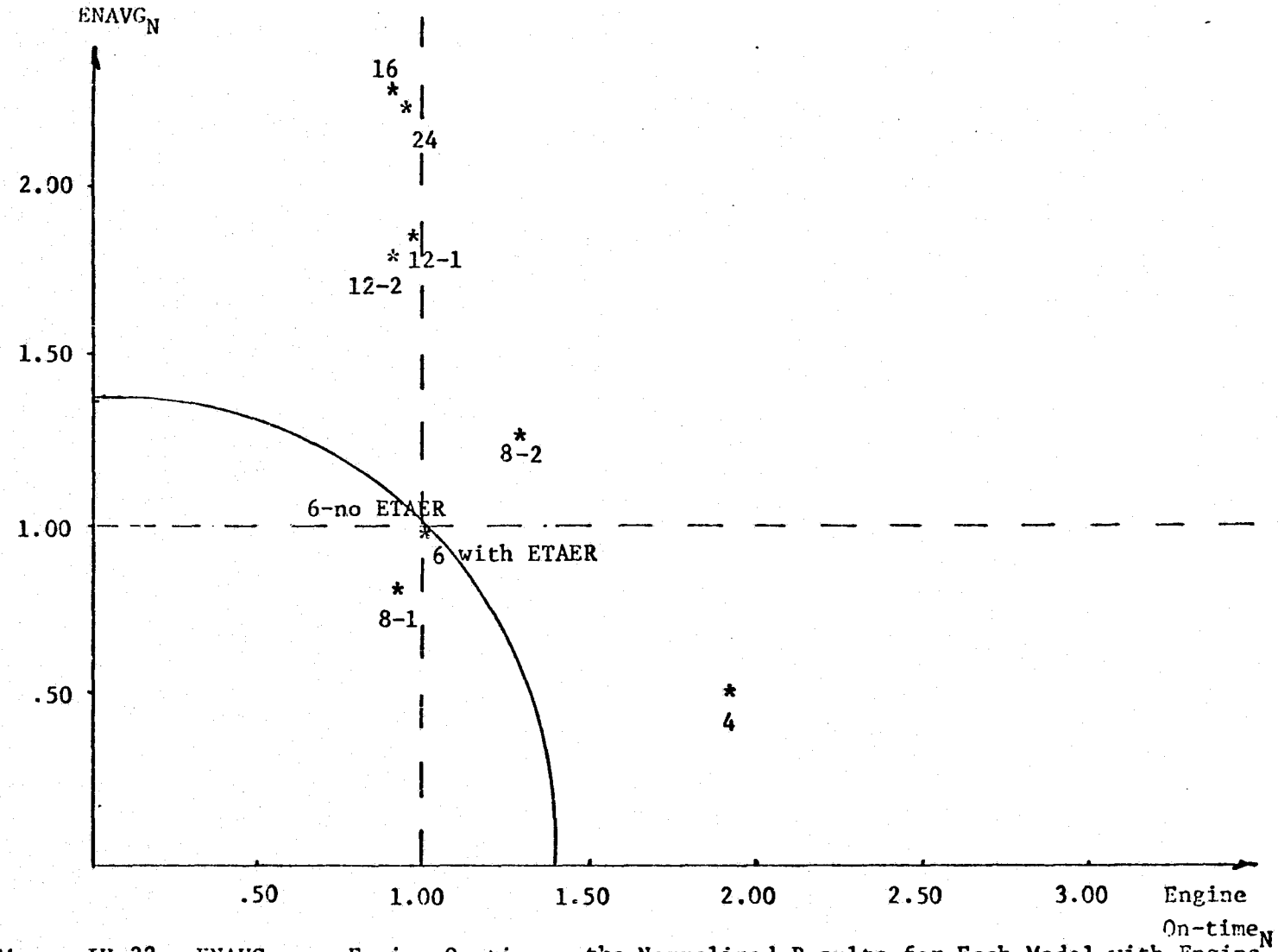

Figure IV-32. ENAVG$_N$ vs. Engine On-time$_N$, the Normalized Results for Each Model with Engine Torque Axes Error Resolution.

the vertical line. Any points which lie to the right of this line indicate models whose engine on-time is greater than that of the 6 engine model when it did not use engine torque axes error resolution. Points which lie to the left of this line indicate models which have better performances with respect to engine on-time. It is evident that only two models, the second 8 engine model and the 4 engine model, have performances with respect to engine on-time which are significantly different from that of the 6 engine model without engine torque axes error resolution. This is much like the results for the models without engine torque axes error resolution where most of the performances with respect to engine on-time were similar to that of the 6 engine model. The 4 engine model has nearly twice as much engine on-time as the reference model, while 8 engine model #2 has only approximately 30% more on-time. The increased on-time for the 4 engine model was explained in Chapter III where it was described how this model's lack of balance causes many problems. The second 8 engine model had a mediocre performance without engine torque axes error resolution and its general inefficiency can be attributed as the reason for its additional on-time in this case.

Now consider the horizontal dashed line in Figure IV-32. Any points which lie above this line represent models with less ability to minimize the average system error than the 6 engine model without engine torque axes error resolution. Any points which lie below the dashed horizontal line represent models with better error minimization performances than that of the 6 engine model. Both of the

configurations which employ skewed thrusters exclusively, the 4 engine model and the first 8 engine model, have average errors less than that of the 6 engine model without engine torque axes error resolution. All but one of the models which employ either orthogonal thrusters, or a combination of skewed and orthogonal thrusters have average errors greater than the 6 engine model. That single improved model, the 6 engine model with engine torque axes error resolution, has a slightly better (1%) error minimization performance than the 6 engine model without engine torque axes error resolution. All of these models with increased average error follow a trend related to the number of thrusters in the configuration. As the number of thrusters in the configuration increased, the average system error also increased. This trend is exactly the opposite of the trend established by the same models without engine torque axes error resolution.

The trend of increasing average error for configurations with more thrusters is caused by the error resolution technique used. Since the vector sum of the errors, when resolved are the same as the vector sum before resolution, the resolved errors in the engine torque axes become smaller as the number of thrusters is increased. If the engine firing deadbands in the torque axes are chosen to be the same as the deadbands in the vehicle axes, then increasingly larger errors in the vehicle axes are required to cause firings of the thrusters as the number of thrusters in increased. This causes the increase in average errors as the number of thrusters is increased.

In order to reduce the average system errors which result from the current resolution method, the basic characteristics of the vehicle axes errors must be altered. The transformation divisions have been shown to reduce the vehicle axes errors as they are resolved into the engine torque axes so that the errors in the vehicle axes must become large before the initial thruster firings. If this transformation division technique were abandoned, the average system errors should be reduced. However, the vector sum of the errors expressed in the engine torque axes would no longer equal the original vehicle axes errors, but rather some multiple of those errors.

After the divisions of the transformations are deleted from the simulations, each model performed as listed in Table IV-5. After normalization with respect to the 6 engine model, these results appear as in Table IV-6. The normalized results are shown in graphical form as Figure IV-33. This figure shows nearly a complete reversal from the cases illustrated in Figure IV-32 with respect to minimization of average error. Now the models with larger numbers of engines have increasingly smaller average errors rather than increasingly larger ones.

The performance of the first 8 engine model (not shown due to the scale of the graph) is somewhat surprising. A rapid limit cycling action developes in this model. As each initial condition is introduced, several engines fire full force (1 second firings), shooting the vehicle quickly across its deadzones resulting in a reverse firing of equal force by an equal number of engines. This limit

Initial Conditions	6 Engine Case	4 Engine Case	8 Engine Case #1	8 Engine Case #2	12 Engine Case #1	12 Engine Case #2	16 Engine Case	24 Engine Case
DPX = .1°/Sec DPY=DPZ = .1°/Sec	3.80 .0414	4.50 .0219	385.6 .0257	4.40 .0411	3.25 .0357	3.75 .0342	3.30 .0316	2.95 .0295
DPX=DPY = .1°/Sec DPZ = -.1°/Sec	3.75 .03568	9.50 .0205	868.5 .0272	4.15 .0414	3.30 .0361	3.70 .0334	3.30 .0328	2.85 .0296
DPX = .1°/Sec DPY=DPZ = -.1°/Sec	3.80 .04366	4.60 .0200	843.5 .0285	4.40 .0406	3.30 .0361	3.40 .033	3.50 .0316	3.10 .0319
DPX = -.1°/Sec DPY=DPZ = -.1°/Sec	3.55 .03453	9.20 .0175	387.2 .0236	4.55 .0418	3.30 .0374	3.45 .0339	3.35 .0315	3.10 .0311
DPX=DPZ = -.1°/Sec DPY = .1°/Sec	3.80 .04140	4.50 .0219	385.6 .0257	4.40 .0411	3.25 .0357	3.75 .0342	3.30 .0316	2.95 .0295
DPX=DPY = -.1°/Sec DPZ = .1°/Sec	3.80 .0437	4.60 .0200	843.5 .0285	4.30 .046	3.30 .0361	3.40 .033	3.50 .0316	3.10 .0319
DPX=DPZ = .1°/Sec DPY = -.1°/Sec	3.55 .0345	9.20 .0175	387.18 .0236	4.55 .0418	3.30 .0374	3.45 .0399	3.35 .0315	3.10 .0311
DPX = -.1°/Sec DPY=DPZ = .1°/Sec	3.75 .0357	9.50 .0206	868.53 .0272	4.15 .0414	3.30 .0361	3.70 .0399	3.30 .0328	2.85 .0296
Average On-Time Average ENAVG	3.73 .0388	6.95 .0200	621.2 .0262	4.35 .0419	3.29 .0363	3.58 .0336	3.36 .0319	3.00 0.030

Top number in each box = Engine On-time

Bottom number in each box = ENAVG, the average system error

Table IV-5. Simulation Results for Each Model Without Transformation Divisions.

Initial Conditions	6 Engine Case	4 Engine Case	8 Engine Case #1	8 Engine Case #2	12 Engine Case #1	12 Engine Case #2	16 Engine Case	24 Engine Case
DPX = .1°/Sec DPY=DPZ = .1°/Sec	1.09 1.08	1.29 .57	110.2 .669	1.26 1.07	.929 .930	1.07 .891	.943 .823	0.843 0.786
DPX=DPY = .1°/Sec DPZ = -.1°/Sec	1.07 .903	2.5 .518	248.1 .689	1.19 1.05	.943 .914	1.06 .846	.943 .830	0.750 0.749
DPX = .1°/Sec DPY=DPZ = -.1°/Sec	1.06 1.09	1.28 .499	234.3 .711	1.19 1.01	.917 .900	.944 .823	.972 .788	0.861 0.796
DPX = -.1°/Sec DPY=DPZ = -.1°/Sec	.973 .911	2.52 .462	106.1 .623	1.25 1.10	.904 .987	.945 .894	.918 .831	0.849 0.821
DPX=DPZ = -.1°/Sec DPY = .1°/Sec	1.09 1.08	1.29 .57	110.2 .669	1.25 1.07	.929 .930	1.07 .891	.943 .823	0.843 0.786
DPX=DPY = -.1°/Sec DPZ = .1°/Sec	1.05 1.09	1.28 .499	243.3 .711	1.19 1.15	.917 .900	.944 .823	.972 .788	0.861 0.796
DPX=DPZ = .1°/Sec DPY = -.1°/Sec	.972 .910	2.52 .462	106.1 .623	1.25 1.10	.904 .987	.945 .894	.918 .831	0.849 0.821
DPX = -.1°/Sec DPY=DPZ = .1°/Sec	.987 .904	2.5 .518	228.6 .689	1.09 1.05	.868 .914	.974 .846	.868 .830	0.750 0.749
Average On-Time Average ENAVG	1.02 .995	1.91 .513	170.7 .672	1.20 1.07	.904 .931	.984 .862	.923 .818	0.824 0.782

Top number in each box = Normalized Engine On-time

Bottom number in each box = Normalized ENAVG, the average system error

Table IV-6. Normalized Simulation Results for Each Model Without Transformation Divisions.

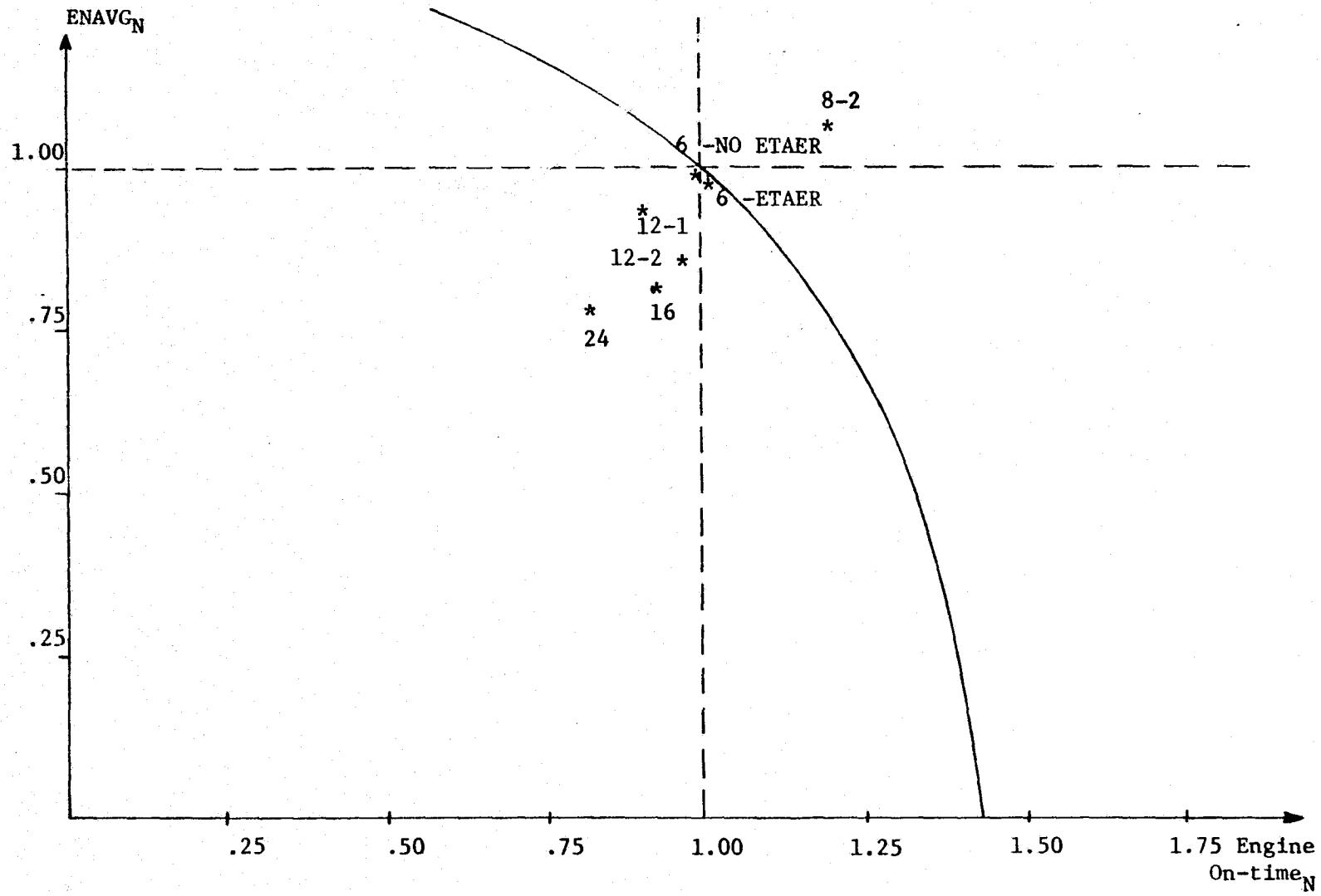

Figure IV-33. ENAVG$_N$ vs. Engine On-time$_N$, the Normalized Results for Each Model With No Transformation Divisions.

cycling action occurred because the numerical values of each of the transformations (with division) for this model are all greater than one. Most of the transformations employed by the other models have values less than one. The resolved errors in these models normally cause minimum impulse firings initially, rather than full force firings. The effect of the transformations of the first 8 engine model were reduced to less than one by the divisions determined by the resolution plane test. This is the reason for its good performance during the tests of the first resolution method.

Unfortunately, the improvements over the 6 engine model by most of the models is not significant enough to warrant implementation of an error evaluation method of this sort. The largest improvement over the 6 engine model with respect to engine on-time is only an 18% decrease while the largest decrease in average error is only 22%. Both of these decreases are achieved by the 24 engine model, which makes practicality an important factor again. The improvements listed are probably not worth the added expense of sixteen additional thrusters. As the number of thrusters decreases, the amount of improvement decreases. The returns on investment are not justifiable for any of the configurations utilizing this type of error evaluation. It simply does not produce performances which improve enough over the 6 engine model to justify further investigation.

REFERENCES

[1] J. L. Lowry, et al, "An Introduction To Analytic Platforms For Inertial Guidance", Technical Report, Contract NAS8-20004, Auburn University, April, 1966.

[2] Carleton G. Fanger, Engineering Mechanics: Statics and Dynamics, Charles E. Merrill Publishing Company, Columbus, Ohio, 1970.

[3] Simulation Data Base For Flight Software Verification, NASA-Marshall Space Flight Center Report 50M37944, July 1, 1971, Revision #1.

[4] D. A. Wells, Theory and Problems of Lagrangian Dynamics, Schaum Outline Series, McGraw-Hill Book Company, 1967.

[5] J. Stanley Ausman, Thomas J. Burns, David P. Chandler, Robert L. Doty, Alvin N. Drucker, George A. Harter, Jacques Heilfron, John J. Jarosh, George A. Kachickas, Robert F. Nease, George R. Pitman, Jr., William T. Russell, Charles W. Sarture, John M. Slater. Edited by George R. Pitman, Jr., Inertial Guidance, John Wiley and Sons, Inc., New York. London, 1962.

[6] D. H. Burdeshaw, "Methods of Computing the Transformation Matrix Associated with Gimballess Inertial Measurement Units", NASA Technical Memorandum, NASA TM X-53294, Marshall Space Flight Center, July 13, 1965.

[7] Curtis F. Gerald, Applied Numerical Analysis, Addison-Wesley Publishing Company, Reading, Massachusetts, 1970.

Appendix A

Derivation of Gravity Gradient Torque Equations

Appendix A

Derivation of Gravity Gradient Torque Equations

The basic principle of orientation by gravity gradient is that a body in a gravitational field which has one moment of inertia less than the other two will experience a torque tending to align the axis of least inertia with the field direction. This action may be determined as follows. In Figure A-1 let $\hat{i}$, $\hat{j}$, and $\hat{k}$ be unit vectors along the principal axes of inertia of the vehicle (X, Y, Z coordinates) with origin at the center of gravity of the vehicle. Now let dm be an element of mass located by $\vec{\rho}$ and let $\vec{R}$ be the vector from the center of gravity of the vehicle to the earth's center. The torque acting on the vehicle is then given as

$$\vec{T}_{gg} = \int_{\text{volume}} (\vec{\rho} \times \nabla\vec{B})\, dm \qquad \text{(A-1)}$$

where $B = -\frac{GM}{\vec{A}}$, and GM is the universal gravitational constant times the mass of the earth. Then,

$$\nabla\vec{B} = -GM \frac{\partial}{\partial|\vec{A}|}\left[\frac{1}{|\vec{A}|}\right]\frac{\vec{A}}{|\vec{A}|} = \frac{GM}{|\vec{A}|^3}\ \vec{A} \qquad \text{(A-2)}$$

Also,

$$\vec{\rho} = X\hat{i} + Y\hat{j} + Z\hat{k} \qquad \text{(A-3)}$$

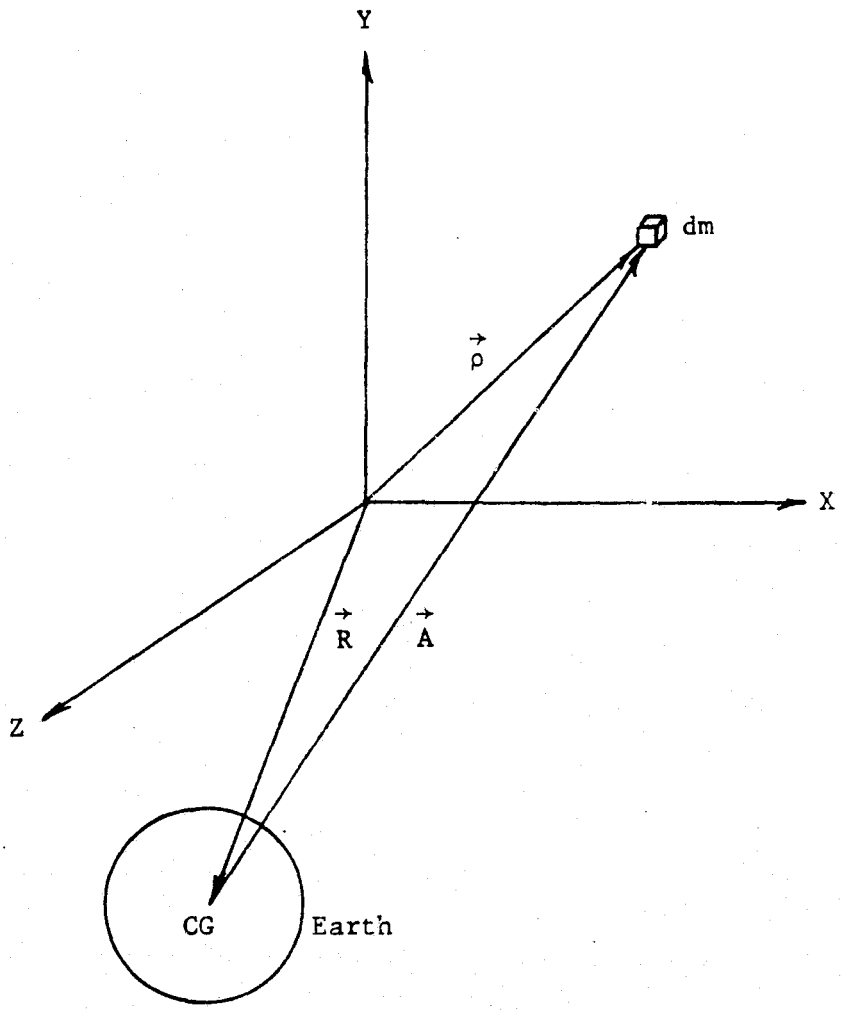

Figure A-1. Configuration Used In Determining Gravity Gradient Torque.

and,

$$\vec{R} = R_X\hat{i} + R_Y\hat{j} + R_Z\hat{k} \tag{A-4}$$

From Equations (A-3) and (A-4) the magnitude of $\vec{A}$ is determined to be

$$|\vec{A}| = |\vec{P}-\vec{R}| = \left[(X-R_X)^2 + (Y-R_Y)^2 + (Z-R_Z)^2\right]^{1/2} \tag{A-5}$$

Substituting this result into Equation (A-2) yields

$$\nabla\vec{B} = \frac{GM\left[(X-R_X)\hat{i} + (Y-R_Y)\hat{j} + (Z-R_Z)\hat{k}\right]}{\left[(X-R_X)^2 + (Y-R_Y)^2 + (Z-R_Z)^2\right]^{3/2}} \tag{A-6}$$

From Equations (A-3) and (A-6) the integrand of Equation (A-1) becomes

$$\vec{\rho} \times \nabla\vec{B} = GM\,\frac{(ZR_Y-YR_Z)\hat{i} + (XR_Z-ZR_X)\hat{j} + (YR_X-XR_Y)\hat{k}}{\left[(X-R_X)^2 + (Y-R_Y)^2 + (Z-R_Z)^2\right]^{3/2}} \tag{A-7}$$

assuming that $|\vec{\rho}| << |\vec{R}|$ call the denominator of Equation (A-7) $F(X,Y,Z)$.

$$F(X,Y,Z) = \left[(X-R_X)^2 + (Y-R_Y)^2 + (Z-R_Z)^2\right]^{-3/2} \tag{A-8}$$

The Taylor's series for $F(X,Y,Z)$ expanded about the point (0,0,0) is

$$F(X,Y,Z) = F(0,0,0) + XF_X(0,0,0) + YF_Y(0,0,0)$$

$$+ ZF_Z(0,0,0) + \text{higher order terms} \tag{A-9}$$

where

$$F_X = \frac{\partial F(X,Y,Z)}{\partial X}\Bigg|_{(0,0,0)}$$

$$F_Y = \frac{\partial F(X,Y,Z)}{\partial Y}\Bigg|_{(0,0,0)}$$

$$F_Z = \frac{\partial F(X,Y,Z)}{\partial Z}\Bigg|_{(0,0,0)}$$

Performing the indicated partial differentiation and substituting the results in Equation (A-9) with the higher order terms neglected yields

$$F(X,Y,Z) = \frac{1}{R^3}\left[1 + 3\left(\frac{XR_X + YR_Y + ZR_Z}{R^2}\right)\right] \qquad \text{(A-10)}$$

where

$$R = \sqrt{R_X^{\,2} + R_Y^{\,2} + R_Z^{\,2}}$$

Equation (A-1) now becomes

$$\vec{T}_{gg} = \int_{\text{volume}} (\vec{\rho} \times \nabla\vec{B})\,dm$$

$$= \frac{GM}{R^3}\int_{\text{volume}} \left[(ZR_Y - YR_Z)\hat{i} + (XR_Z - ZR_X)\hat{j} + (YR_X - XR_Y)\hat{k}\right]dm$$

$$+ \frac{3GM}{R^5}\int_{\text{volume}} \Big[(XZR_XR_Y - XYR_XR_Z + YZR_Y^{\,2} - Y^2R_YR_Z + Z^2R_YR_Z - YZR_Z^{\,2})\,\hat{i}$$

$$+ (X^2R_XR_Z - XZR_X^{\,2} + XYR_YR_Z - YZR_XR_Y + XZR_Z^{\,2} - Z^2R_XR_Z)\hat{j}$$

$$+ (XYR_X^{\,2} - X^2R_XR_Y + Y^2R_XR_Y - XYR_Y^{\,2} + XZR_XR_Z - XZR_YR_Z)\hat{k}\Big]\,dm \qquad \text{(A-11)}$$

Since the origin of the vehicle coordinate system is at the vehicle center of gravity and since the X,Y,Z axes are the principle vehicle axes, this symmetry gives the following results

$$\int_{volume} X dm = \int_{volume} Y dm = \int_{volume} Z dm = 0 \tag{A-12}$$

$$\int_{volume} XY dm = \int_{volume} XZ dm = \int_{volume} YZ dm = 0 \tag{A-13}$$

and

$$\int_{volume} X^2 dm = I_X \tag{A-14a}$$

$$\int_{volume} Y^2 dm = I_Y \tag{A-14b}$$

$$\int_{volume} Z^2 dm = I_Z \tag{A-14c}$$

Substituting Equations (A-12) through (A-14) into Equation (A-11) yields the gravity gradient torque as

$$\vec{T}_{gg} = -\frac{3GM}{R^5}\left[R_Y R_Z (I_Y - I_Z)\hat{i} + R_X R_Z (I_Z - I_X)\hat{j} + R_X R_Y (I_X - I_Y)\hat{k}\right]$$